1-1-2015

Cold In-Place Recycling Characterization Framework for Single or Multiple Component Binder Systems

Ben C. Cox

Cold in-place recycling characterization framework for single or multiple component binder systems

By

Benjamin C. Cox

A Dissertation
Submitted to the Faculty of
Mississippi State University
in Partial Fulfillment of the Requirements
for the Degree of Doctor of Philosophy
in Civil Engineering
in the Department of Civil and Environmental Engineering

Mississippi State, Mississippi

December 2015

Cold in-place recycling characterization framework for single

or multiple component binder systems

By

Benjamin C. Cox

Approved:

Isaac L. Howard
(Major Professor)

Janice DuBien
(Committee Member)

Randolph Charles Ahlrich
(Committee Member)

John Kent Newman
(Committee Member)

James L. Martin
(Graduate Coordinator)

Jason M. Keith
Dean
College of Engineering

Name: Benjamin C. Cox

Date of Degree: December 11, 2015

Insitution: Mississippi State University

Major Field: Civil Engineering

Major Professor: Isaac L. Howard

Title of Study: Cold in-place recycling characterization framework for single or multiple component binder systems

Pages in Study: 171

Candidate for Degree of Doctor of Philosophy

Cold in-place recycling (CIR) is a pavement rehabilitation technique which has gained momentum in recent years. This momentum is due partly to its economic and sustainability characteristics, which has led to CIR market expansion. When pavement network deterioration is considered alongside increasing material costs, it is not beyond reason to expect demands on CIR to continue to increase.

Historically, single component binder (SCB) systems, those with one stabilization binder (or two if the secondary binder dosage is 1% or less), have dominated the CIR market and could be considered the general state of practice. Common stabilization binders are either bituminous or cementitious. Two example SCB systems would be: 1) 3% portland cement, or 2) 3% asphalt emulsion with 1% hydrated lime.

While traditional SCB systems have demonstrated positive economic and sustainability impacts, this dissertation focuses on multiple component binder (MCB) systems (bituminous and cementitious combined) which exhibit the potential to provide better overall economics and performance. Use of MCBs has the potential to alleviate

SCB issues to some extent (e.g. cracking with cementitious SCBs, rutting with bituminous SCBs). Furthermore, to fairly represent both binders in an MCB system a universal design method which can accommodate multiple binder types is needed.

The main objectives of this dissertation are to develop a universal CIR design framework and, using this framework, characterize multiple SCB and MCB systems. Approximately 1500 CIR specimens were tested herein along with approximately 300 asphalt concrete specimens which serve as a reference data set for CIR characterization. A case study of a high-traffic Mississippi CIR project which included cement SCB and emulsion SCB sections is also presented to support laboratory efforts.

Individual components needed to comprise a universal design framework, such as curing protocols, were developed. SCB and MCB characterization indicated that cement SCBs yielded low cracking resistance, high rutting resistance, and lower costs. Emulsion SCBs yielded the opposite. MCBs demonstrated the ability to balance rutting, cracking, and economics. Overall, the universal framework presented appears promising as it could offer agencies flexibility and, in some cases, improved overall performance beyond that of current SCB design methods.

Keywords: Cold In-Place Recycling, Sustainability, Multiple Component Binders

DEDICATION

Firstly, I dedicate this dissertation to my Lord Jesus Christ for both enabling me to complete the doctoral program and considering me righteous despite my unrighteousness. Secondly, I would like to dedicate this to my family for their continual support and encouragement during the course of my doctoral program. Most notably, I dedicate this dissertation to my wife, Rachel, who patiently walked with me and tirelessly sought to care for me throughout the earning of this degree.

ACKNOWLEDGEMENTS

Thanks are due to many for the successful completion of this dissertation. First, the author's major professor, Dr. Isaac Howard, is owed an immense amount of gratitude for his patient and invaluable guidance and support. Thanks are due to Dr. Randy Ahlrich, Dr. Kent Newman, and Dr. Jan DuBien for serving as committee members. The Mississippi Department of Transportation (MDOT) provided financial support which made the research in this dissertation possible. Ergon Asphalt & Emulsions, Inc. (especially Baxter Burns and Mark Ishee) also provided financial support within the *Ergon Asphalt & Emulsions Distinguished Doctoral Fellowship in Construction Materials* held by the author while earning this degree.

Paragon Technical Services, Inc. (especially Gaylon Baumgardner, John Dumas, Paul Morris, Mike Hemsley, and Trey Jordan), Holcim (US), Inc. (especially Tim Cost), APAC Mississippi (especially Michael Bogue and Scott Glusenkamp), InstroTek, Inc. (especially Ali Regimand), and MDOT (especially Durwood Graham, Jonathan Dixon, Alex Middleton, Nan Mitchell, and Drew Parker) graciously provided materials, technical support, testing services, and project information and also facilitated field work. The University of Florida (UF) was very helpful and forthcoming regarding past experiences with cracking characterization testing. Key individuals at UF were Dr. Reynaldo Roque, Dr. Jian Zou, and George Lopp.

Thanks are due to the many undergraduate research assistants that worked on this research, providing assistance in areas such as material processing, specimen production and testing, and data organization and analysis. Thanks are due to Mr. Joe Ivy for his knowledge and assistance in maintaining laboratory equipment as well as designing and fabricating multiple pieces of equipment.

TABLE OF CONTENTS

LIST OF TABLES

LIST OF FIGURES

LIST OF SYMBOLS

AADT	Annual average daily traffic
AASHTO	American Association of State Highway and Transportation Officials
Abs	Aggregate absorption
AC	Asphalt concrete
ADC	Analog to digital counts
ANOVA	Analysis of variance
APA	Asphalt pavement analyzer
ASCE	American Society of Civil Engineers
ASTM	American Society for Testing and Materials
α	Empirical power parameter in the complex refractive index model
BBR	Bending beam rheometer
β	Fitted constant for GS3 temperature correction
c	Portland cement
CF	Correction factor
CI	Cracking index
C.I.	Confidence interval
CIR	Cold in-place recycling
COV	Coefficient of variation
CR	Laboratory-crushed RAP (Chapter 4) or curing room (Chapter 5 and 7)
CRIM	Complex refractive index model
D_{HMA}	HMA thickness
D_p	Pavement thickness
d_0	FWD deflection under center of loading
$d_{0\text{-}20}$	d_0 at 20 C
DCB	Density curve broke
DCSE	Dissipated creep strain energy
$DCSE_{min}$	Minimum required DCSE
DCT	Disc-shaped compact tension test
DDC	Deformation differential curve
DGA	Dense-graded asphalt
DNB	Density curve did not break
DO	Dry oven curing
DOT	Department of transportation
D(t)	Creep compliance
d2s	Difference two-sigma limit of ASTM C670
e	Asphalt emulsion
EC	Evaluation criteria

EE	Elastic energy
ER	Energy ratio
ERDC	Engineering Research and Development Center
ε_{air}	Air dielectric constant
ε_{bulk}	Bulk dielectric permittivity
ε_{CIR}	CIR dielectric constant
$\varepsilon_{H,f}$	Horizontal strain at fracture
ε_{ult}	Horizontal strain at peak stress
ε_{water}	Water dielectric constant
FAA	Fine aggregate angularity
FDR	Full-depth reclamation
FE	Fracture energy
FHWA	Federal Highway Administration
FWD	Falling weight deflectometer
G1 to G4	RAP gradation 1 to RAP gradation 4
G_b	Specific gravity of asphalt binder
G_{cm}	Specific gravity of portland cement
G_{HL}	Specific gravity of hydrated lime
G_{mb}	Bulk mixture specific gravity
G_{mm}	Maximum mixture specific gravity
$G_{mm,CIR}$	Estimated maximum specific gravity for the CIR mixture
$G_{mm,RAP}$	D6857 maximum specific gravity of RAP
$GS3_i$	Observed raw GS3 reading at time *i*
$GS3_{i,corrected}$	Temperature-corrected GS3 reading at time *i*
G_{sa}	Aggregate apparent specific gravity
G_{sb}	Aggregate bulk specific gravity
G_{se}	Effective specific gravity
G_w	Specific gravity of water
γ_d	Dry density
$\gamma_{d,max}$	Maximum dry density
HL	Hydrated lime
HLWT	Hamburg loaded wheel tester
HMA	Hot mix asphalt
HO	Humid oven curing
IDT	Indirect tensile
IL	Independent laboratory
JCP	Jointed concrete pavement
KA	Key area
LAC	Linear asphalt compactor
M_L	Cantabro mass loss percentage
M_R	Subgrade resilient modulus
M_r	IDT resilient modulus
$M_{r,total}$	Total IDT resilient modulus
$Max\ Range_{10}$	Maximum acceptable range of ten results of ASTM C670
MC	Moisture content
MCB	Multiple component binder

MDOT	Mississippi Department of Transportation
MLP	Multilaboratory precision
MRI	Mean roughness index
n	Number of replicates or number of tests
N_{design}	Design gyration level
N_{gyr}	Gyration level
NG	Nuclear gage
NMAS	Nominal maximum aggregate size
OD	Outdoor curing
OGFC	Open-graded friction course
OMC	Optimum moisture content
ω_{add}	Moisture content due to added water only
ω_{comp}	Compacted mixture moisture content
$\omega_{mix,target}$	Target mixture moisture content
$\omega_{mix,actual}$	Actual mixture moisture content
ω_{total}	Total moisture content
$P_{AC(T164)}$	Asphalt content determined by solvent extraction (AASHTO T164)
$P_{AC(T308)}$	Asphalt content determined by NCAT ignition oven (AASHTO T308)
P_b	Total asphalt content
$P_{ba,mix}$	Absorbed asphalt content on a mix mass basis
P_{be}	Effective asphalt content
P_{cm}	Percent of cement by mass of RAP
$P_{contact}$	Contact load in resilient modulus testing
$p_{critical}$	Significance level
P_{Em}	Percent of emulsion by mass of RAP
P_{HL}	Percent of hydrated lime by mass of RAP
P_{max}	Max load in resilient modulus testing
P_{Res}	Percent of asphalt residue by mass of emulsion
$P_{12.5}$	Passes to 12.5 mm rut
PCI	Pavement condition index
PCR	Pavement condition rating
PG	Performance grade
p-value	Observed significance level
PW	PURWheel
QA	Quality assurance
QC	Quality control
R_g	Range
R^2	Coefficient of determination
RAP	Reclaimed asphalt pavement
RD_{APA}	APA rut depth
R1 to R3	RAP material 1 to RAP material 3
SCB	Single component binder
SCBend	Semi-circular bend test
S.D.	Standard deviation (also St. Dev.)
SENB	Single-edge notched beam test
SGC	Superpave gyratory compactor

SIP	Stripping inflection point
SN_{eff}	Effective structural number
SOP	Single-operator precision
S.P.	Special provision
SSE	Error sum of squares
S_t	Indirect tensile strength
$S_{t,f}$	Fracture indirect tensile strength
$S_{t,ult}$	Ultimate indirect tensile strength
T_{crit}	Critical cracking temperature
T_i	Temperature at time *i*
T_r	Reference temperature
TRB	Transportation Research Board
$T209_{SSD}$	AASHTO T209 performed with supplemental dry-back procedure
UCS	Unconfined compressive strength
US-49	US Highway 49
UTM	Universal testing machine
V_a	Air voids
$V_{a(T166)}$	Air voids via AASHTO T166
$V_{a(T269)}$	Air voids via AASHTO T269
$V_{a(T331)}$	Air voids via AASHTO T331
V_{CIR}	CIR volume fraction
V_{water}	Water volume
VFA	Voids filled with asphalt
VMA	Voids in mineral aggregate
VMC	Volumetric moisture content
$w_{NE/cm}$	Non-evaporable water cement ratio
WMA	Warm mix asphalt
1s	One-sigma limit of ASTM C670

CHAPTER 1

INTRODUCTION

1.1 Introduction and Background

Cold in-place recycling (CIR) is a pavement rehabilitation technique which has been used for several decades, traditionally on low-volume roads. It is a process where existing asphalt concrete pavement layers are reclaimed, resized, stabilized, mixed, placed, and re-compacted at ambient temperatures. Relative to traditional reconstruction, CIR usually reduces emissions and costs because fewer virgin materials are required. Relative to other rehabilitation techniques such as thin overlays, CIR addresses many pavement distresses to a greater degree, often resulting in extended performance.

In recent years, CIR has gained momentum due partly to its economic and sustainability implications, and this momentum has expanded CIR markets into, for example, higher traffic routes. With pavement networks continually deteriorating and material costs increasing, it is not beyond reason to expect demands on CIR to continue to increase. As a result, CIR has garnered greater research interest.

Historically, single component binder (SCB) systems have dominated the CIR market. SCB systems are defined in this dissertation as those with one stabilization binder (or two if the secondary binder dosage is 1% or less). For example, SCB stabilization blends could be either 3% portland cement or 3% asphalt emulsion with 1% hydrated lime. In general, CIR stabilization blends are usually bituminous rather than cementitious,

although cementitious blends have been used to some extent. For example, the Mississippi Department of Transportation (MDOT) conducted a high-traffic CIR project on US Highway 49 and built cement SCB and emulsion SCB sections.

In contrast, this dissertation focuses on multiple component binder (MCB) systems where two or more binders are each utilized at greater than 1% dosages. Relative to SCB systems, MCBs could offer a better overall balance of economics and performance. For example, emulsion SCBs are generally crack resistant but are prone to rutting and are less economical, while cement SCBs are the opposite (crack prone, rutting resistant, and more economical). Use of MCBs has the potential to alleviate these issues to some extent, producing CIR materials which yield mid-range economics and are better balanced with respect to rutting and cracking.

Current mix design methods cannot fairly represent both binders in an MCB system since current methods are specific to one binder type. In order to consider MCB systems, a CIR design method is needed which can accommodate bituminous and cementitious binder types for fair side-by-side comparisons. At present, this type of universal design method does not exist to the author's knowledge. However, if one were developed, it could provide a vehicle through which advantages of MCBs could be more effectively realized while maintaining the flexibility to continue SCB use when warranted or desired.

1.2 Objectives and Scope

This dissertation focuses on testing of CIR using 100% reclaimed asphalt pavement (RAP) (i.e. no virgin aggregates added). Further, the Superpave design method

is a key consideration in this research as it is widely accepted and is well established for plant-mixed asphalt design. The two primary objectives of this dissertation are to:

1. Provide a universal CIR design framework, including specimen preparation, curing, and testing, which can be applied to any mixture irrespective of the stabilization materials used.
2. Conduct a detailed characterization of various SCB and MCB systems in order to provide guidance on potential advantages of MCB systems in the context of economics and performance, especially rutting and cracking.

Developing a design framework which is universal requires most aspects of previous SCB design methods to be evaluated. In doing so, consideration was given to developing a design framework which could more easily interface with construction quality control. Additionally, consideration was given to developing laboratory protocols which provide a better representation of field and construction environments, as this could be considered a more suitable approach in terms handling different binder types within a single design framework. Key components evaluated within the first objective were mixing and compaction moisture contents, laboratory curing protocols, density measurement methods, and performance tests. Key components evaluated within the second objective were wet and dry wheel tracking, permeability, resilient modulus, indirect tensile strength, and cracking characterization at intermediate and low temperatures. The second objective evaluated nine binder systems: three cement SCB systems, three emulsion SCB systems, and three MCB systems including cement and emulsion.

1.3 Organization of Study

This dissertation is organized into eight chapters. The first and last chapters are an introduction and conclusion. The remaining six chapters represent six peer-reviewed documents (some have been published, while others are in various stages as of the date of this document) which each provided a different contribution to the two main objectives of this dissertation. Chapters 2 through 5 relate to development of individual components of the presented design framework. Chapter 6 presents a case study of the US Highway 49 CIR project as it pertains to the overall study of SCB and MCB systems. Chapter 7 presents a full SCB and MCB characterization using recommendations of Chapters 2 through 5, which, collectively, comprise a universal CIR design framework.

As of the writing of this dissertation, Chapters 2 through 4 have been published as peer-reviewed papers, and Chapters 5 through 7 have been submitted to peer-reviewed journals and are currently in review. Minor non-technical modifications were required to each paper in order to align them with the dissertation format and create one cohesive document. Since the published papers are interrelated, mentions of companion research were common in the published versions but have been removed herein since the papers now form a single document.

CHAPTER 2

IN-PLACE RECYCLING MOISTURE-DENSITY RELATIONSHIPS FOR HIGH-TRAFFIC APPLICATIONS

This chapter has been previously published as a conference proceeding in the American Society of Civil Engineers (ASCE) proceedings of the International Foundations Congress and Equipment Expo 2015 (Geotechnical Special Publication No. 256). The original paper may be accessed at http://dx.doi.org/10.1061/9780784479087.035. With permission from ASCE, the paper (Cox et al. 2015a) has been reformatted and reproduced herein with minor modifications to suit the objectives of this dissertation.

2.1 Introduction and Background

In-place recycling has seen increased use rehabilitating low-volume, and some high-traffic, roads. These techniques (no heat) generally classify as cold in-place recycling (CIR) or full-depth reclamation (FDR). CIR often refers to recycling the majority of the existing asphalt layer(s); whereas, FDR also incorporates a significant amount of underlying layers. Higher moisture contents (*MC*) and binder dosages are generally required for FDR than CIR (e.g. average FDR mixing *MC* is 7.2% versus 3.5% for CIR) (Cox and Howard 2013). Because FDR typically has a finer gradation, includes aggregate base, and may have particles with plasticity, this trend seems reasonable.

The Mississippi Department of Transportation (MDOT) performed a high-traffic CIR project on US-49 in 2010 (Federal Aid Project No. NH-008-03(032)). Although CIR was performed, *MC*s were more representative of FDR. As a result, this chapter investigates CIR moisture-density relationships using Proctor and (Superpave Gyratory Compactor) SGC compaction. Although US-49 is high-traffic, this chapter is likely applicable for any traffic level.

This chapter has two objectives and two phases. The first objective is to investigate moisture-density relationships used in US-49 design and construction. To this end, Phase 1 describes the US-49 project and performs complementary laboratory testing focusing on Proctor compaction since it was a notable component in MDOT special provisions used during US-49. The second and primary objective is to present CIR moisture-density relationships using the SGC since MDOT has expressed interest in its use for future in-place recycling projects. Ideally, the SGC would be used for all binders (e.g. cement, emulsion, hydrated lime, and combinations) to standardize protocols (at least to some extent) as this was not done for US-49 but would be a CIR advancement. To this end, Phase 2 utilized 303 SGC specimens to evaluate SGC moisture-density relationships and compare them to Proctor compaction.

2.2 Abbreviated Literature Review

CIR and FDR were reviewed as some US-49 aspects are typical of FDR (e.g. higher *MC*s). Many CIR sources (e.g. Kim et al. 2011) appear to use a standardized *MC*. Other Marshall-based approaches select *MC* based on density and strength (e.g. Carter et al. 2010). Few use traditional moisture-density curves to select optimum *MC* (*OMC*) (e.g.

Martinez et al. 2007). FDR sources reporting a method for determining *OMC* mostly used Proctor curves (e.g. Lewis et al. 2006). Kim et al. (2007) studied CIR and found no discernible *OMC*; RAP's coarseness and few fines were deemed possible causes (*OMC* could have possibly been discernible if the fines content was higher). Ultimately, a *MC* of 4.0% was selected. Perforated SGC molds and base plates have been used to allow drainage during compaction (e.g. Mallick et al. 2002, Santagata et al. 2010). At high *OMC* values that occur in many Proctor tests (e.g. Mallick et al. 2002), notable water is often expelled during SGC compaction, which brings its necessity into question.

2.3 Phase 1: Efforts Related to US-49

2.3.1 US-49 Project Information

A 14.8 km section of four-lane US-49 (average annual daily traffic (AADT): 12,000) in Madison County, MS was in-place recycled in the summer of 2010 (bid price: ~$15,000,000). Table 2.1 provides project parameters. Original jointed concrete (JCP) and full-depth hot mix asphalt (HMA) sections were built in 1959 and 1980, respectively. The project called for mill and remove depths of 75 mm, with underlying materials left for in-place recycling. Recycling depths varied reaching 230 mm in full-depth HMA sections and 150 mm in JCP sections. During construction, subgrade stability issues in full-depth HMA sections resulted in a supplemental agreement to change most emulsion CIR to nominal 400 mm cement FDR (4.8% dosage); however, only CIR sections are discussed herein. Final project costs totaled approximately $16,500,000.

Pertinent MDOT special provisions during US-49 design and construction were S.P. 907-425-1 (emulsion) and S.P. 907-499-1 (cement). S.P. 907-425-1 (emulsion)

requires *OMC* be obtained by Proctor compaction. S.P. 907-499-1 (cement) requires use of Mississippi Test Method MT-25, which entails Proctor compaction of unstabilized and stabilized material (MT-8, MT-9) and compressive strength (MT-26). For US-49, 97% of standard Proctor density was required in place for 100% pay. Maximum dry density is denoted as $\gamma_{d,max}$, while dry density is generically denoted γ_d.

Table 2.1 US-49 CIR Information at Time of Bidding

	Northbound Lanes	**Southbound Lanes**
Nominal Existing Pavement Properties		
Cored Thickness (mm): Full-Depth HMA	290 to 380	305 to 405
Cored Thickness (mm): HMA over JCP	215 to 230	190 to 230
Recycled Layer Properties		
Nominal Recycling Depth (mm)	150 or 230	150 or 230
Binder	4% CSS-1H emulsion plus 1% hydrated lime	4.4% Type I portland cement
ω_{add} (%)	5	7.4
ω_{total} (%)	6.5	7.4
Curing Specification	<2.5 ω_{total}%	7-day (emulsion sealed)
As Designed Asphalt Concrete Properties Used to Overlay In-Place Recycling		
Base Course (76 mm thickness)	19 mm NMAS (PG 76-22)	19 mm NMAS (PG 76-22)
Surface Course (38 mm thickness)	9.5 mm NMAS (PG 76-22)	9.5 mm NMAS (PG 76-22)

-- Emulsion, hydrated lime, and portland cement dosage rates are a percentage of dry mass.
-- ω_{add} = moisture content due to added water only
-- ω_{total} = total moisture content including added water, water in the emulsion, and RAP moisture

Table 2.2 presents all feasibly obtainable Proctor data from design and construction. Table 2 *OMC* values are more closely representative of FDR than CIR. It is also noteworthy that single-point field Proctor *MC*s were, on average, 1.5% lower than the MDOT *OMC*, yet their densities were essentially identical (1980 versus 1970 kg/m^3).

CIR mix designs were performed by MDOT and two independent labs (IL-1 and IL-2). For the cement design, 140 mm tall specimens (150 mm diameter) were SGC-compacted to 35 gyrations at the MT-8 *OMC* (7.4%), moist-cured seven days, then tested

for unconfined compressive strength. The lowest cement content yielding 2068 kPa (300 psi) was selected (4.4%). For the emulsion design, IL-2 constructed 30-gyration SGC moisture-density curves for RAP with 1.5% cement and reported 6.7% *OMC* and 1866 kg/m^3 $\gamma_{d,max}$. A 4% emulsion content was selected based on air voids, dry and wet indirect tensile strength, percent coating by boil test, Marshall stability and flow, and dynamic modulus. Emulsion water was subtracted from 6.7% to obtain 5.2% ω_{add}, later rounded to 5%. Ultimately, 1% hydrated lime replaced the 1.5% cement to improve stripping performance (failure mode in lower layers prior to rehabilitation).

Table 2.2 US-49 Moisture-Density Curve Data

			***OMC* (%)**				**$\gamma_{d,max}$ (kg/m^3)**			
Binding Agent	**Description**	***n***	**Mean**	**S.D.**	**R_g**	**C.I.**	**Mean**	**S.D.**	**R_g**	**C.I.**
Results from Proctor Compaction Curves										
None	MDOT (design)	1	7.4	---	---	---	1968	---	---	---
5.5% Cement[a]	IL-1 (design) 7/14/10	1	8.4	---	---	---	1954	---	---	---
4.4% Cement	MDOT (field) 6/23/10 to 8/13/10	12	7.9	0.52	1.6	6.8 to 8.9	1970	17.5	49.7	1935 to 2006
4% Emulsion + 1% Hyd. Lime	MDOT (field) 6/26/10 to 8/17/10	9	8.7	0.62	1.8	7.4 to 9.9	1855	10.6	35.2	1834 to 1876
Results from QC/QA Single-Point Field Proctor Tests[b]										
4.4% Cement	IL-1 (field) 8/12/10 to 8/13/10	9	6.4	0.72	2.3	5.0 to 7.9	1980	39.2	110.5	1901 to 2058

a) A terminology discrepancy led to IL-1 using 5.5% cement by mass as opposed to 4.4% by mass.
b) For single-point field Proctor tests, OMC and $\gamma_{d,max}$ refer to in-place moisture content (MC) and γ_d.
-- S.D. = Standard Deviation -- R_g = Range -- n = number of tests -- C.I. = 95% Confidence Interval

2.3.2 Proctor Compaction Testing and Results

Proctor compaction tests were performed according to Mississippi Test Method MT-8 (unstabilized materials) and MT-9 (stabilized materials) in the laboratory with US-49 RAP (denoted R1) at the bulk gradation obtained from on-site sampling (denoted G1) and also with a second RAP source (denoted R2) sieved and batched to the G1 gradation.

Three binder dosage combinations were used; two of them were those used for US-49, and a third employed a balanced blend of portland cement and emulsion, which is being studied in some detail in MDOT State Study 250 as well as this dissertation.

Table 2.3 presents Proctor compaction results. R1G1 MT-8 $\gamma_{d,max}$ was 1974 kg/m^3, similar to the corresponding Table 2.2 value of 1968 kg/m^3. *OMC*, however, was lower by 1.2%. This is similar to the previously-mentioned 4.4% cement behavior in Table 2.2. This 4.4% cement behavior was consistent when Table 2.3 data for R1 (i.e. US-49) at 4.4% cement was incorporated. The *OMC* range increased from 1.5 to 2%, while the $\gamma_{d,max}$ range only increased from 10 kg/m^3 to 25 kg/m^3. Dry densities differing by 25 kg/m^3 (1.6 lb/ft^3) on a recycled material between three laboratories is very manageable. On the other hand, *OMC* values differing 2% is less manageable and brings to question the usefulness of Proctor-measured *OMC* for 100% RAP materials.

Testing the US-49 gradation with a different RAP source proved problematic across a wide range of binders, especially with emulsion included. Dry density continued to increase even at *MC*s where water was splattering and draining from the mold's base. Fine particles (i.e. high bitumen content particles) could have been escaping with the water, or some other behavior could have led to these results. Regardless, R2 data indicates an alternate compaction protocol (i.e. SGC) could be useful. A key Phase 2 question based on Tables 2.2 and 2.3 is what is moisture's role during SGC compaction for 100% RAP with varying binders and dosages.

Table 2.3 Laboratory Proctor Compaction Results

Material	c (%)	e (%)	HL (%)	Method	*OMC* (%)	$\gamma_{d,max}$ (kg/m^3)	Curve Description
R1G1[a]	0	0	0	MT-8	6.2	1974	DCB - Typically shaped
	4.4	0	0	MT-9	5.9	1995	DCB - Oddly shaped
	2.3	2	0	MT-9	6.6	1974	DCB - Poorly shaped
	0	4	1	MT-9	4.9	1799[e]	DCB - Very slight break
R2G1[b]	0	0	0	MT-8	7.8	1894	DCB - Very slight break
	4.6	0	0	MT-9	7.3	1914	DCB - Some scatter in data
	2.4	2	0	MT-9	8.7	1869	DNB
	2.4	2	0	MT-9a[c]	9.7	1859	DNB
	2.4	2	0	MT-9b[d]	9.3	1800	DNB
	0	4	1	MT-9	8.6	1844	DNB

a) RAP sampled from US-49 during construction further described in Table 5.
b) RAP sampled from asphalt producer's stockpile further described in Table 5.
c) Stabilized RAP re-used for each point on the Proctor curve.
d) Similar to (c) except compacted with automatic Texas hammer.
e) A new emulsion sample was used which was not used for all other Proctor data. This drastically decreased $\gamma_{d,max}$ for two replicates. Therefore, additional single-point Proctors were conducted with the new emulsion sample for R1G1 cement and cement/emulsion blends with 6% moisture. Relative to the original emulsion sample, γ_d decreased 5.7% for the cement/emulsion blend and was unaffected for the cement blend. Further, 30-gyration SGC γ_d changes were less than 1% between original and new emulsion samples. SGC γ_d's at 6% moisture with the new emulsion sample were 2038, 2002, and 1984 kg/m^3 for cement, cement/emulsion, and emulsion blends, respectively. Unlike SGC compaction, Proctor compaction appeared sensitive to a different emulsion sample.
-- Cement (c), emulsion (e), and hydrated lime (HL) dosed as a percentage of dry RAP mass.
-- DCB = density curve broke; DNB = density curve did not break, reported max density achieved

2.4 Phase 2: SGC Moisture-Density Relationships

2.4.1 Materials Tested

R1 was field-sampled from the US-49 project and tested at its as-received bulk gradation (denoted G1). R2, obtained from an asphalt producer stockpile in Lowndes County, MS, was blended to three gradations denoted G1, G2, and G3. Three gradations were tested to investigate gradation effects (if any) to moisture-density relationships. G2 (fine) and G3 (coarse) were constructed to approximate outer bands of literature gradations in Cox and Howard (2013). Properties are shown in Table 2.4.

CIR binders used were Type I portland cement, CSS-1H emulsion (63.5% residue), and hydrated lime. Three blends (Table 2.4) were tested, targeting the US-49 cement and emulsion blends (B1 and B3) and a balanced blend of cement and emulsion (B2 – laboratory-tested only). Mixing and compaction water was calculated as a percentage of dry solid material (i.e. RAP, emulsion residue, cement, and hydrated lime).

Table 2.4 Properties of Bituminous Materials Tested

Material ID	R1			R2								
Gradation	G1			G1			G2			G3		
NMAS	12.5			9.5			9.5			9.5		
$P_{AC(T308)}$[a] **(%)**	5.1			6.2			6.5			5.7		
$P_{AC(T164)}$[b] **(%)**	4.8			5.6			6.2			4.9		
-9.5 mm[c]	85			85			91			65		
-2.36 mm	38			38			49			21		
-0.075 mm	1.5			1.5			2.3			0.8		
Blend[d]	B1	B2	B3	B1	B2	B3	B1	B2	B3	B1	B2	B3
***Cement* (%)**	4.4	2.3	0	4.6	2.4	0	4.6	2.4	0	4.6	2.4	0
***Emulsion* (%)**	0	2	4	0	2	4	0	2	4	0	2	4
***Hydrated Lime* (%)**	0	0	1	0	0	1	0	0	1	0	0	1

a) NCAT Ignition oven: no aggregate correction factor was used.
b) Solvent Extraction: an 85%/15% blend of toluene/ethanol was used for extraction.
c) Gradation shown is bulk RAP gradation.
d) Binders dosed as a percentage of dry RAP mass.

2.4.2 Test Methods

The goal of testing was to evaluate the role of water during compaction of CIR mixtures with similar binder dosages as US-49. This was accomplished by monitoring dry density and moisture content of 288 SGC-compacted specimens (100 mm diameter) at multiple gyration levels (N_{gyr}) and target moisture contents.

Phase 2 terms are: 1) target and actual moisture contents of an uncompacted mixture ($\omega_{mix,target}$ & $\omega_{mix,actual}$); 2) post-compaction SGC specimen moisture content

(ω_{comp}). They are expressed as a dry solids percentage. Three $\omega_{mix,target}$ values (6, 8, & 10%) were chosen to reasonably bracket all observed *OMC* values in Tables 2.2 and 2.3.

Two groups of specimens, *SGC-1* and *SGC-2*, were compacted to differing N_{gyr} numbers. *SGC-1* was used to establish SGC moisture-density relationships, and *SGC-2* was used to verify them for additional materials. *SGC-1* evaluated R2G1, all binder blends, 3 $\omega_{mix,target}$ values, and 12 N_{gyr} levels (5, 10, 15 and 15-150 in increments of 15). At one replicate, this yielded 108 *SGC-1* specimens. *SGC-2* evaluated all other materials (R1G1, R2G2, and R2G3), all binder blends, 3 $\omega_{mix,target}$ values, and 4 N_{gyr} levels (15, 30, 75, and 135). At one replicate, this yielded 108 *SGC-2* specimens.

RAP and water were mixed two minutes before binder addition and two minutes after binder addition. After mixing, $\omega_{mix,actual}$ was obtained, and SGC specimens were compacted (unmodified molds). Immediately after compaction, mass and volume were recorded. The entire specimen was used to obtain ω_{comp} for γ_d calculation.

To evaluate variability, two variability sets, *VS-1* and *VS-2*, were compacted to 30 gyrations. Based on *SGC-1* and *SGC-2* results, there appeared to be no added value in further testing 10% moisture. *VS-1* evaluated R1G1, all binder blends, and 6% and 8% $\omega_{mix,target}$; at six replicates, this yielded 36 *VS-1* specimens. *VS-2* was identical to *VS-1* except R2G1 was used instead of R1G1.

2.4.3 SGC Compaction Results

Figure 2.1 shows *SGC-1* results. R2G1 γ_d increased with N_{gyr} relatively consistently between $\omega_{mix,target}$ values. As N_{gyr} increased, ω_{comp} decreased and converged between $\omega_{mix,target}$ values. For high $\omega_{mix,target}$ values, moisture was reduced considerably

by 30 gyrations, which is a commonly documented N_{gyr} for CIR (e.g. Cross 2002), and moisture forced out of the gyratory mold was unavailable to aid in compaction. Furthermore, all $\omega_{mix,target}$ values yielded similar γ_d at any N_{gyr}. The findings indicate γ_d for *SGC-1* is essentially independent of moisture content in the range of moisture which encompasses the unstabilized Proctor-determined *OMC* of 7.8%.

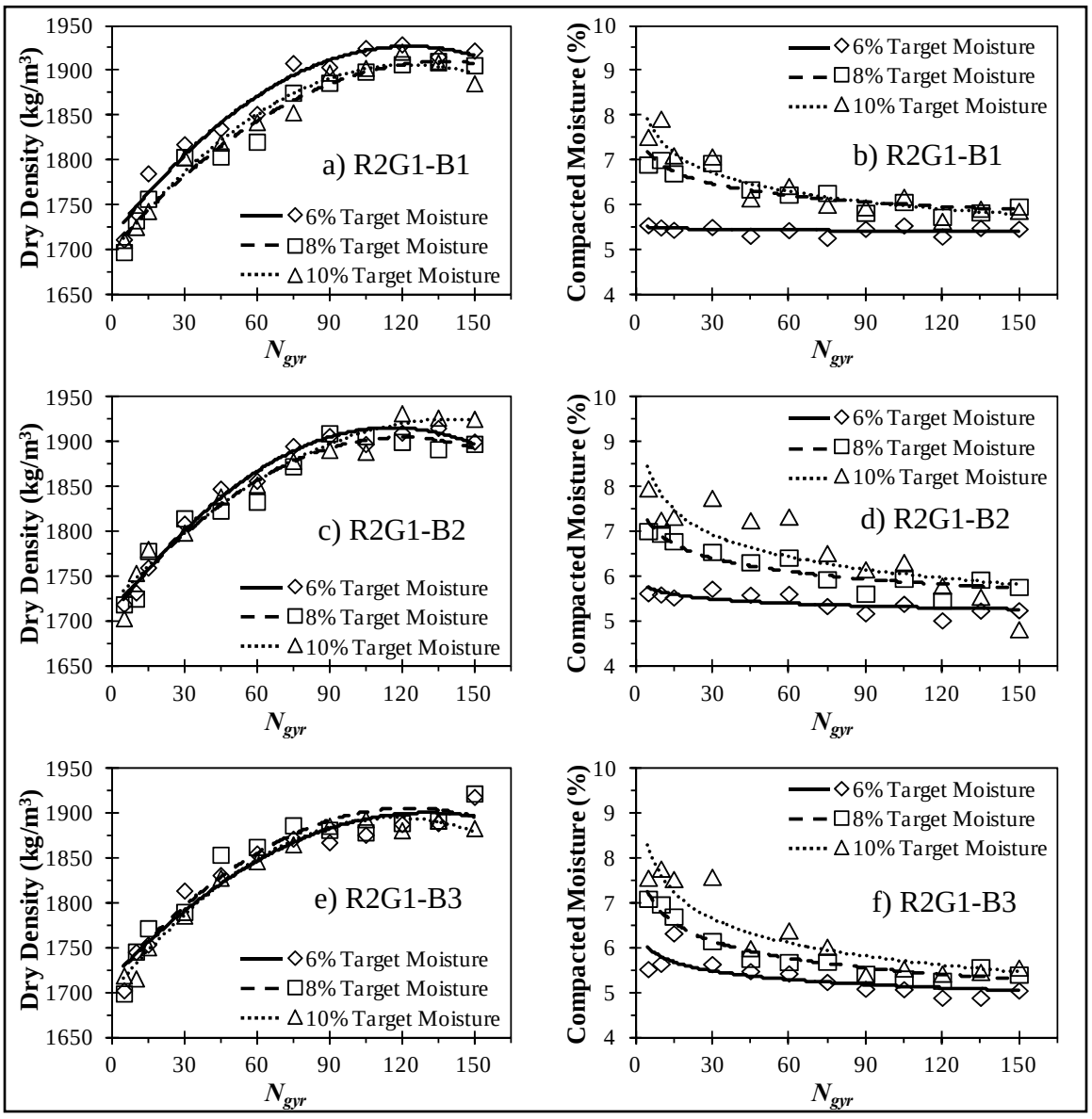

Figure 2.1 Dry Density and Compacted Moisture versus N_{gyr} for *SGC-1*

Dry density and ω_{comp} curves were fit with regression lines of the general form of Equations 2.1 and 2.2, respectively. Regression constants for *SGC-1* are shown in Table 2.5 as well as summary statistics to evaluate quality of fit.

$$\gamma_d = C_1\left(N_{gyr}\right)^2 + C_2\left(N_{gyr}\right) + C_3 \quad (2.1)$$

$$\omega_{comp} = C_4 N_{gyr}^{\ C_5} \quad (2.2)$$

Where,

γ_d = dry density (kg/m^3)

ω_{comp} = moisture content after compaction (%)

N_{gyr} = number of gyrations

C_1, C_2, C_3, C_4, C_5 = regression constants

Table 2.5 Dry Density and Compacted Moisture Results for *SGC-1*

			2nd Order Polynomial Fit Dry Density vs. N_{gyr} (Eq. 1)					**Power Fit ω_{comp} vs. N_{gyr} (Eq. 2)**			
Mixture	$\omega_{mix,\ target}$	**Avg** $\omega_{mix,\ actual}$	C_1	C_2	C_3	R^2	*SSE*	C_4	C_5	R^2	*SSE*
R2G1-B1	6	5.9	-14.1	3.47	1713	0.97	1869	5.55	-5	0.11[a]	0.09
	8	8.3	-11.0	3.03	1701	0.97	1696	7.91	-59	0.81	0.46
	10	9.9	-13.8	3.41	1696	0.98	1214	9.20	-93	0.87	0.83
R2G1-B2	6	6.1	-15.5	3.61	1706	0.99	758	6.01	-27	0.52	0.26
	8	7.5	-13.5	3.23	1711	0.96	2232	8.10	-69	0.84	0.46
	10	10.4	-10.1	2.89	1719	0.96	2163	10.08	-110	0.65	3.71
R2G1-B3	6	6.0	-10.9	2.84	1715	0.95	2718	6.52	-51	0.59	0.82
	8	8.0	-12.7	3.12	1713	0.93	3627	8.43	-93	0.95	0.23
	10	10.8	-14.2	3.33	1699	0.99	542	10.11	-123	0.84	1.96

a) R^2 misrepresentative of fit quality due to shallow slope. SSE *indicates good fit as shown in Fig. 2.1b.*
-- SSE = sum of squared errors of prediction -- R^2 = coefficient of determination

Table 2.6 shows density, moisture, and regression data for *SGC-2*. As in *SGC-1*, each material exhibited similar γ_d regardless of $\omega_{mix,target}$ and similar trends for $\omega_{mix,target}$ versus N_{gyr}. For R1G1-B1, γ_d ranges from 1978 to 2030 kg/m^3 at 30 gyrations which is comparable to corresponding Table 2.2 and 2.3 $\gamma_{d,max}$ values. This is notable as it supports use of 30 design gyrations (N_{design}) as recommended by others (e.g. Cross 2002). However, N_{design} recommendations are not the purpose of this work.

Figure 2.2 provides equality plots comparing γ_d at various $\omega_{mix,target}$ values for *SGC-1*, *SGC-2*, *VS-1*, and *VS-2*. Standard Deviation (S.D.) and coefficient of variation (COV) are relatively small for both variability sets. *VS-2* data was used to construct 95% confidence interval (C.I.) bands because *VS-2* had the lower S.D. which would provide a tighter confidence band. Most data lies within these bands. This indicates scatter around the equality line was due largely to RAP variability not differing *MC*s.

As an independent check, 15 specimens of this experiment's 288 were selected in a stratified random approach by another researcher uninvested in this project. These were compacted on a different SGC (different model as well), and a paired *t*-test was conducted on the results. At a 5% significance level, the mean difference (3.8 kg/m^3) was not significant (*p-value* = 0.6190). All data collected concludes that moisture content within the range tested is irrelevant regarding γ_d.

Table 2.6 Dry Density and Compacted Moisture Results for *SGC-2*

Mixture	$\omega_{mix,target}$	Avg $\omega_{mix,actual}$	Dry Density (kg/m^3) at N_{gyr} (15, 30, 75, 135)	2nd Order Polynomial Fit C_1	C_2	C_3	R^2	*SSE*	ω_{comp} (%) at N_{gyr} (15, 30, 75, 135)	Power Fit C_4	C_5	R^2	*SSE*
R1G1-B1	6	6.03	(1976, 2030, 2078, 2093)	-12.6	2.78	1946	0.97	251	(5.3, 4.9, 4.2, 4.1)	7.45	-127	0.98	0.016
	8	7.94	(1948, 1978, 2070, 2106)	-11.6	3.10	1900	0.99	43	(5.8, 5.5, 4.3, 4.0)	9.74	-181	0.96	0.099
	10	9.71	(1932, 1995, 2059, 2108)	-11.4	3.08	1898	0.98	348	(6.0, 5.6, 4.5, 4.0)	10.17	-187	0.98	0.058
R1G1-B2	6	6.23	(1986, 2017, 2065, 2115)	-4.4	1.70	1965	0.99	42	(5.1, 4.8, 3.9, 3.7)	8.06	-162	0.98	0.036
	8	8.85	(1949, 1997, 2059, 2108)	-9.0	2.62	1917	0.99	127	(5.6, 5.3, 4.1, 3.7)	10.10	-205	0.96	0.130
	10	10.26	(1953, 1994, 2060, 2101)	-9.4	2.60	1919	0.99	37	(6.0, 5.3, 4.2, 3.8)	10.75	-214	0.99	0.017
R1G1-B3	6	6.29	(1959, 1991, 2060, 2094)	-9.4	2.54	1923	0.99	1	(4.7, 4.3, 3.6, 3.2)	7.90	-182	0.99	0.015
	8	8.37	(1943, 2001, 2059, 2094)	-11.8	2.95	1910	0.98	268	(5.6, 4.6, 3.7, 3.3)	10.47	-237	0.99	0.020
	10	9.95	(1949, 2001, 2056, 2110)	-7.9	2.45	1923	0.98	257	(5.7, 4.7, 3.9, 3.2)	11.20	-250	0.99	0.017
R2G2-B1	6	5.92	(1765, 1818, 1873, 1888)	-13.4	2.97	1730	0.98	190	(5.7, 5.9, 5.6, 5.9)	5.62	6	0.06[a]	0.051
	8	7.96	(1779, 1830, 1870, 1888)	-10.7	2.43	1754	0.96	293	(7.7, 7.3, 6.8, 6.4)	9.65	-82	0.99	0.004
	10	9.98	(1757, 1797, 1841, 1879)	-7.0	2.00	1734	0.98	141	(8.2, 7.6, 6.5, 6.1)	12.16	-142	0.99	0.024
R2G2-B2	6	6.18	(1801, 1821, 1872, 1908)	-4.7	1.61	1778	0.99	1	(5.5, 5.7, 5.7, 5.3)	5.84	-14	0.16[a]	0.090
	8	7.89	(1767, 1802, 1868, 1915)	-7.7	2.37	1735	0.99	16	(7.3, 7.3, 6.6, 5.9)	9.80	-96	0.87	0.179
	10	9.38	(1747, 1785, 1839, 1875)	-8.0	2.22	1720	0.99	68	(8.4, 8.0, 6.9, 6.7)	11.51	-112	0.98	0.046
R2G2-B3	6	5.96	(1790, 1826, 1893, 1913)	-11.4	2.72	1753	0.99	3	(5.8, 5.9, 4.7, 4.5)	8.69	-135	0.87	0.228
	8	7.91	(1774, 1825, 1887, 1921)	-11.5	2.89	1739	0.99	141	(7.1, 7.0, 5.5, 5.2)	11.43	-163	0.92	0.297
	10	9.53	(1778, 1815, 1885, 1917)	-10.6	2.73	1741	0.99	6	(8.0, 7.4, 6.0, 5.4)	13.56	-188	0.98	0.107
R2G3-B1	6	5.53	(1695, 1754, 1810, 1875)	-7.5	2.52	1669	0.98	401	(5.1, 5.4, 5.2, 5.1)	5.32	-7	0.04[a]	0.080
	8	7.68	(1670, 1763, 1788, 1837)	-11.0	2.82	1653	0.87	1985	(6.1, 6.3, 5.1, 5.2)	8.12	-95	0.76	0.281
	10	9.87	(1659, 1698, 1815, 1825)	-19.8	4.41	1592	0.99	117	(6.9, 6.1, 5.6, 5.3)	9.23	-115	0.98	0.037
R2G3-B2	6	5.58	(1709, 1754, 1828, 1875)	-10.2	2.88	1672	0.99	51	(5.4, 5.4, 5.4, 4.9)	6.18	-41	0.56[a]	0.100
	8	6.85	(1716, 1756, 1818, 1842)	-11.0	2.67	1682	0.99	27	(6.8, 6.3, 5.8, 5.2)	9.31	-114	0.97	0.038
	10	9.89	(1692, 1753, 1824, 1857)	-14.3	3.44	1652	0.99	213	(6.6, 6.3, 6.0, 5.7)	7.84	-63	0.98	0.007
R2G3-B3	6	5.87	(1737, 1774, 1846, 1907[b])	-6.7	2.40	1705	0.99	19	(5.4, 5.1, 4.1, 3.8)	8.77	-169	0.97	0.067
	8	7.95	(1764, 1769, 1837, 1851)	-7.6	1.94	1729	0.96	216	(6.1, 5.6, 5.1, 5.1)	7.58	-85	0.90	0.064
	10	8.79	(1744, 1719, 1836, 1852)	-9.1	2.48	1687	0.86	1849	(6.4, 5.4, 4.8, 4.8)	8.77	-131	0.92	0.121

a) R^2 value not representative of fit quality due to shallow slope. SSE *indicates good fit.* *b) Data point questionable*

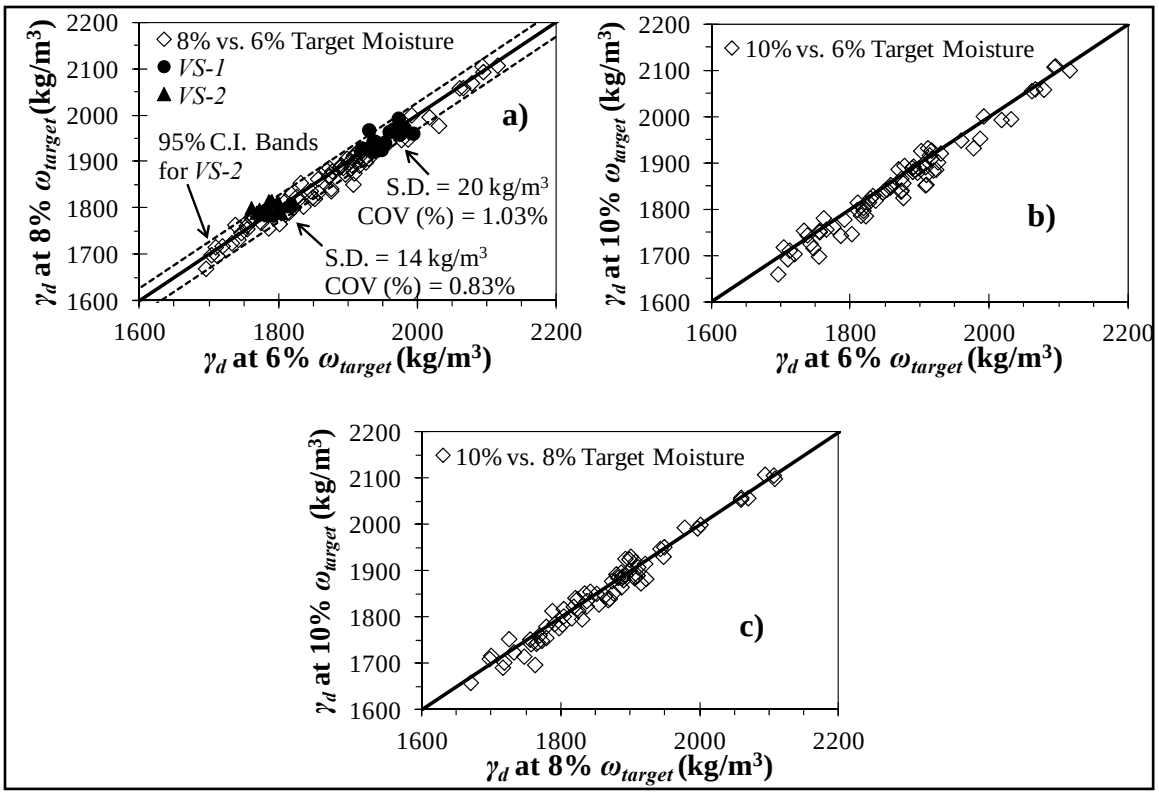

Figure 2.2 Dry Density Equality Plots for All Specimens

2.5 Conclusions

Compaction of multiple materials at multiple gradations with various binding agent blends revealed no interaction between initial moisture content and dry density, at least in the range of moisture contents where Proctor compaction detected an *OMC*. From this chapter, the following conclusions are made.

- Because SGC dry density was indifferent to modest changes in moisture content, Proctor *OMC* does not appear as informative for CIR as for soil or crushed stone. Therefore, the SGC is recommended for future use with CIR.

- For R1G1, the only material for which typically-shaped Proctor curves were obtained, 30 N_{gyr} generally resulted in dry densities similar to standard Proctor values.
- When using the SGC for CIR compaction, more than 6% moisture content adds no value in terms of density gain for the mixtures tested. Because a wide variety of combinations was tested, it is likely that 6% maximum moisture is relevant to most CIR mixtures and is recommended. Additional work paralleling this work at lower than 6% moisture could be useful.

CHAPTER 3

MERITS OF ASPHALT CONCRETE DURABILITY AND PERFORMANCE TESTS WHEN APPLIED TO COLD IN-PLACE RECYCLING

This chapter has been previously published as a conference proceeding in the American Society of Civil Engineers (ASCE) proceedings of the International Foundations Congress and Equipment Expo 2015 (Geotechnical Special Publication No. 256). The original paper may be accessed at http://dx.doi.org/10.1061/9780784479087.037. With permission from ASCE, the paper (Cox and Howard 2015b) has been reformatted and reproduced herein with minor modifications to suit the objectives of this dissertation.

3.1 Introduction and Background

Within the pavement industry, there exists a continually growing sustainability emphasis. CIR is one pavement rehabilitation technique with potential sustainability benefits. However, CIR processes have yet to be soundly established on a large scale. Further, CIR is not fully distinguished in terms of performance relative to other recycling options such as traditional asphalt mixtures incorporating high percentages of reclaimed asphalt pavement (RAP). Traditional plant recycling aligns more closely with that of traditional asphalt and, consequently, is reasonably established. Conversely, CIR introduces factors not present in plant recycling or traditional asphalt such as binders with

vastly differing properties (e.g. portland cement and asphalt emulsion), cold mixing temperatures, use of mixing water, and similar. Therefore, while currently established design and testing procedures for traditional asphalt mixtures provide a logical starting point, they need to be evaluated and possibly modified to accommodate CIR differences relative to traditional asphalt.

The objective of this chapter is to evaluate CIR using several available durability and performance tests originally developed for asphalt concrete and, thus, assess their capability of characterizing CIR specifically for a diverse array of binding agents. The screening of these performance tests is part of a larger study focusing on development of a universal CIR design method capable of accommodating multiple binder types as this does not seem to currently exist but would be an advancement for CIR technology. Current design methods are binder-type specific (i.e. chemical or bituminous); a universal method could accommodate both types as well as hybrid blends of the two (e.g. a balanced amount of cement and emulsion).

Tests evaluated herein are the Cantabro durability test, the bending beam rheometer (BBR) flexural stiffness test for mixture beams, wheel tracking tests in the Hamburg Loaded Wheel Tester (HLWT) and Asphalt Pavement Analyzer (APA), a loaded wheel fatigue test, and a cracking characterization test conducted in the indirect tensile (IDT) mode. Following the materials tested section, each test is discussed individually under six major headings. Tests were conducted on CIR utilizing 100% RAP (i.e. no virgin aggregate) with three binding agent blends consisting of cement, emulsion, and a hybrid of both. Unless otherwise stated, all specimens were gyratory-compacted to 30 gyrations and cured in a 40 °C oven at 30 to 40% relative humidity. Curing conditions

were chosen to approximate Mississippi field conditions (hot with some humidity) rather than to produce specimens exhibiting ultimate-cure properties (e.g. dry oven curing of emulsion specimens). This chapter in no way endorses or recommends the binder blends or compaction and curing protocols utilized herein; they were selected solely to establish a reasonable framework in which these performance tests could be evaluated. In all, approximately 100 specimens were tested in this chapter.

3.2 Performance Test Evaluation Criteria

Given the overall focus of this chapter, four evaluation criteria (EC) were established as shown below to aid in systematic screening of the six performance tests evaluated. Tests which do not satisfy all criteria may not be optimal for further consideration in the context of a universal CIR design method.

EC1) Specimens must be feasibly producible. If specimens cannot be successfully fabricated, the corresponding performance test cannot be properly conducted.

EC2) The test must not be so harsh that all binder blends behave poorly. CIR mixtures with cement or emulsion binders have demonstrated satisfactory field performance in some applications. The goal of this evaluation is largely to characterize behavior of these current CIR designs, and a test that quickly destroys all specimens regardless of binder/dosage is not useful for this goal.

EC3) If reasonable results are achieved, the test must be capable of differentiating between cement and emulsion. In general, cement provides

strength but is brittle, and emulsion provides flexibility but is less stable. Behavior of cement and emulsion blends are of secondary concern regarding EC3 since they were arbitrarily selected dosages. EC3 largely focuses on single binders (cement or emulsion [sometimes with a small amount of hydrated lime]).

EC4) The resulting information gained from a test should be worth the testing effort. If a test provides a marginal result but requires intensive time, financial, and material resources to conduct, it may not be optimal for further consideration. It should be noted that EC4 is more of an indirect consideration rather than a strict criteria.

3.3 Materials Tested

Table 3.1 presents material properties. R1 was field-sampled from a CIR project on US-49 in Madison County, MS and tested at its as-received bulk gradation (denoted G1). R2, obtained from an asphalt producer stockpile in Lowndes County, MS, was blended to gradation G1 as well as a coarser gradation (denoted G3) which is typical of many CIR gradations observed in literature (Cox and Howard 2013). R3 was milled from the surface of I-55 near Grenada, MS and was obtained from an asphalt producer stockpile. R3 was tested at its as-received bulk gradation (G4). Testing was conducted primarily with R1 and R2.

CIR binders used were Type I portland cement, CSS-1H emulsion (63.5% residue), and hydrated lime. For R1 and R2, three blends (Table 3.1) were tested, targeting the US-49 cement and emulsion blends (B1 and B3) as well as a balanced blend

of cement and emulsion (B2). It should be noted that B2 was arbitrarily selected by halving the dosages of B1 and B3; it was selected solely to incorporate a hybrid cement-emulsion binder into the text matrix and should be evaluated in that context. Moisture for mixing and compaction was fixed at 6% (includes water in emulsion) based on Chapter 2 recommendations. Additionally, bulk dry density measurements were obtained via AASHTO T269. For R3, the only binder considered was emulsion at three dosages, and no additional water was added during mixing.

Table 3.1 Properties of Bituminous Materials Tested

Material ID	R1			R2			R2			R3		
Gradation	G1			G1			G3			G4		
NMAS	12.5			9.5			9.5			9.5		
$P_{AC(T308)}$[a] **(%)**	5.1			6.2			5.7			---		
$P_{AC(T164)}$[b] **(%)**	4.8			5.6			4.9			5.5		
-9.5 mm[c]	85			85			65			81		
-2.36 mm	38			38			21			30		
-0.075 mm	1.5			1.5			0.8			0.3		
Blend[d]	B1	B2	B3	B1	B2	B3	B1	B2	B3	B1	B2	B3
Cement (%)	4.4	2.3	0	4.6	2.4	0	4.6	2.4	0	0	0	0
Emulsion (%)	0	2	4	0	2	4	0	2	4	3	4	5
Hydrated Lime	0	0	1	0	0	1	0	0	1	0	0	0

a) NCAT Ignition oven: no aggregate correction factor was used.
b) Solvent Extraction: an 85%/15% blend of toluene/ethanol was used for extraction.
c) Gradation shown is bulk RAP gradation. d) Binders dosed as a percentage of dry RAP mass.

3.4 Cantabro Testing

Cantabro abrasion loss test is often used to evaluate relative durability (i.e. aggregate loss) for open-graded friction course (OGFC) where an upper limit mass loss (M_L) criteria of 20% has been recommended (Watson et al. 2004). More recently, the Cantabro test has also been used to evaluate dense-graded asphalt (DGA) (e.g. Doyle and Howard 2011). Doyle and Howard (2014) assessed the suitability of a DGA Cantabro

durability test and recommended three replicates be tested for SGC specimens. No documented case of CIR Cantabro testing was found by the author.

An initial CIR Cantabro investigation tested R2G1. Three replicate specimens (150 mm diameter by 115 mm tall) were cured 7 days. Then, Cantabro testing was conducted in an LA Abrasion drum absent steel spheres for 300 revolutions at a specimen temperature of 25 ± 1 °C. For B1, B2, and B3, respectively, average bulk dry densities were 1.79, 1.74, and 1.74 g/cm^3, and M_L values were 99, 99, and 97%.

In attempts to further evaluate the Cantabro test, R3G4 was also tested. Prior to compaction, R3G2 was heated to 38 °C to assess temperature effects on M_L. Compaction effort was increased to 50 gyrations; average bulk dry densities (AASHTO T331) for B1, B2, and B3, respectively, were 1.94, 1.97, and 2.00 g/cm^3. Specimens were cured at room temperature and humidity until constant mass was achieved (37 days). Average M_L values were 99, 95, and 84% for B1, B2, and B3, respectively. For comparison, Howard et al. (2013) cites typical M_L values for traditional Mississippi DOT asphalt which range from 6 to 16%. Even with 5% emulsion and higher compaction temperature and effort, M_L was not informative; therefore, R1G1 and R2G3 testing was not conducted. Based on these results, the Cantabro test does not satisfy EC2.

3.5 Bending Beam Rheometer Testing

BBR testing of asphalt mixture beams, in contrast to asphalt binder beams, is a fairly recent development. Others have demonstrated its practical feasibility, controllable variability, and theoretical validity (e.g. Zofka et al. 2005, Marasteanu et al. 2009). BBR mixture beam testing has been used to evaluate stiffness and *m-value* responses of high-

RAP mixtures (Doyle and Howard 2013) and seal treatment rejuvenated pavements (Braham et al. 2014); however, no documented case of CIR BBR mixture beam testing was found by the author.

Typically, beams are sawn from 150 mm diameter specimens as illustrated in Figure 3.1a and 3.1b. Sawing procedures were attempted on R2G1 specimens (115 mm tall) for all three binder blends and two cure times (7 and 28 days). Bulk dry densities ranged from 1.71 to 1.81 g/cm^3. Vertical saw cuts were extremely difficult and usually unsuccessful, and horizontal saw cuts were never successful (Figure 3.1c). Beams broke into multiple pieces during sawing regardless of binder or cure time. Based on ineffective attempts to further Cantabro testing with R3G2, it was elected to conclude the BBR investigation after testing R2G1 only. Based on these results, BBR specimen preparation (and thus testing) of CIR mixture beams does not satisfy EC1.

a) Traditional Asphalt Slices *b) Traditional Asphalt Beam* *c) CIR Slice & Broken Beam*

Figure 3.1 Example BBR Specimen Preparation for Traditional Asphalt and CIR

3.6 Hamburg Loaded Wheel Testing

The HLWT is commonly used to evaluate asphalt mixture rutting potential and moisture susceptibility. At 20,000 passes, maximum rut depth criteria of 4 (Hamburg, Germany) and 10 (Colorado DOT) mm have been documented (Aschenbrener 1995). Additionally, well-performing pavements generally exhibit stripping inflection points

(SIP) at ≥10,000 passes. The Texas DOT specifies a minimum 10,000 and 15,000 passes to 12.5 mm rut depth for PG (performance grade) 64 and 70 binders, respectively (Rand 2006). No documented case of CIR Hamburg testing was found by the author.

Hamburg testing was conducted according to typical protocols for asphalt mixtures (i.e. 20,000 passes at 50 °C with a 705 N vertical load applied by solid metal wheels contacting the specimen). R1G1, R2G1, and R2G3 were tested at all three binder blends. Specimens targeted 63 mm height and were cured 7 days. Two specimens comprise one replicate test, and only one replicate was tested for each combination of material and binder blend. Average bulk dry densities for B1, B2, and B3, respectively, were as follows: (R1G1) 2.01, 1.99, and 1.98 g/cm^3; (R2G1) 1.83, 1.84, and 1.82 g/cm^3; and (R2G3) 1.71, 1.73, and 1.75 g/cm^3.

Test results are shown in Figure 3.2. It should be noted that R2G1-B1 terminated prematurely for unknown reasons, but this does not have a major impact on overall findings. Nearly all specimens failed quickly (i.e. approximately 14 mm rut depth). For comparison, all specimens (except for R2G1-B2) fell considerably short of the Texas DOT criteria. Based on these results, Hamburg testing does not satisfy EC2.

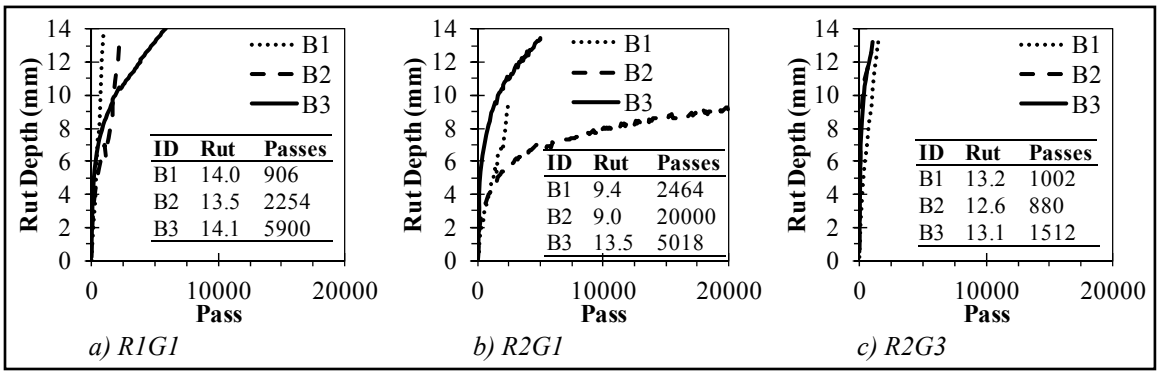

Figure 3.2 Hamburg Test Results

3.7 Loaded Wheel Fatigue Testing

Fatigue testing is relatively common for asphalt mixtures. Most commonly, strain-controlled flexural beam fatigue tests are used. Little documentation exists regarding loaded wheel fatigue testing. Howard et al. (2013) conducted loaded wheel fatigue testing in the APA as a general comparison of conventional asphalt and high-RAP warm mix asphalt. Both control and high-RAP mixtures at typical air void levels generally lasted 50,000 cycles without failing (i.e. 1 mm deflection change in one pass). Wu et al. (2014) conducted APA fatigue tests but different from that of Howard et al. (2013). Instrumentation was used for stress and strain measurements allowing for a more traditional theoretical analysis approach. Cycles to failure (50% stiffness reduction criteria) ranged from approximately 30,000 to 120,000. Fatigue testing of CIR in the IDT mode has been documented in a few cases (e.g. Modarres et al. 2011), but CIR loaded wheel fatigue testing does not appear to be documented in literature.

Fatigue beam specimens were sawn from slabs produced in the linear asphalt compactor described in Howard et al. (2012). Sawn dimensions were nominally 29 by 12.5 by 7.6 cm. Because of slab compaction material demands, only R2G1 was initially considered. Bulk dry densities for B1, B2, and B3, respectively, were 1.88, 1.84, and 1.75 g/cm^3. Two replicates of all binder blends were tested at two cure times (7 and 56 days) and two loads. Tests were conducted at 20 °C and 2 Hz (2 passes per second) for 50,000 cycles (100,000 passes) with solid metal wheels contacting simply supported specimens. Figure 3.3 depicts representative fatigue beams.

Test results are shown in Figure 3.4 in which several general trends can be observed. For example, the 1100 N load was largely uninformative. Generally, 56-day

fatigue data is more informative than 7-day data, which is not surprising considering fatigue is typically considered a longer-term performance issue. For the 445 N load at 56 days, B2 failed after very few cycles in comparison to B1 and B3.

a) Traditional Asphalt *b) Tested R2G1-B1* *c) Tested R2G1-B3*

Figure 3.3 Loaded Wheel Fatigue Testing

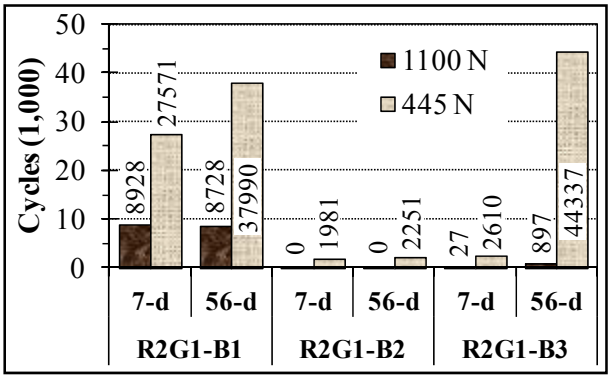

Figure 3.4 Average Fatigue Test Results

Although shorter fatigue life is plausible with B2, the overwhelming differences between B2 and B1 or B3 bring several items to question. First, strains induced by the applied loads are not explicitly considered. Appropriate CIR strain levels are not well-established and are also modulus-dependent (and to some extent application-dependent), which is not currently known for these materials. Using loads which induce realistic strain levels may, but also may not, result in reasonable comparisons for all binder

blends. Second, fatigue resistance at a given load likely requires some threshold minimum strength. IDT results presented later suggest B2 strength may be a concern at early cure times (recall the B2 blend of cement and emulsion was arbitrarily selected). At present, loaded wheel fatigue results appear somewhat inconclusive but not greatly promising. Given the marginal acceptance of loaded wheel fatigue tests for traditional asphalt combined with these results and labor intensive specimen preparation, CIR loaded wheel fatigue testing is not believed to be optimal based on EC4.

3.8 APA Loaded Wheel Testing

The APA has been used for several years by multiple DOTs to evaluate asphalt mixture rutting potential. Typically, pass/fail rut depth criteria is used. Cited criteria are 4 to 6 mm, 6 mm for high traffic in MS, 12 mm for standard and medium MS traffic (Buchanan et al. 2004), and 8 mm (Brown et al. 2001). Du and Cross (2007) performed CIR APA testing with 1.5% CMS-1 emulsion, 1.5% CMS-1 plus 1.5% hydrated lime, and 1.5% CMS-1 plus 1.14% quick lime. Rut depths at 8,000 cycles ranged from 3.7 to 6.7 mm.

APA testing was conducted according to typical Mississippi protocols for asphalt mixtures (i.e. 8,000 cycles at 64 °C with a 445 N vertical load applied by pressurized rubber hoses (689 kPa) contacting the specimen). R1G1, R2G1, and R2G3 were tested at all three binder blends. Specimens targeted 75 mm height and were cured 7 days. Two specimens compose one replicate test, and only one replicate was tested for each combination of material and binder blend. Average bulk dry densities for B1, B2, and B3,

respectively, were as follows: (R1G1) 2.02, 2.01, and 1.99 g/cm^3; (R2G1) 1.88, 1.87, and 1.85 g/cm^3; and (R2G3) 1.77, 1.77, and 1.76 g/cm^3.

Test results are shown in Figure 3.5. B1 exhibits negligible rutting, while B3 exhibits moderate rutting. B2 exhibits rutting closer to that of B1. Depending on the pass/fail criteria used, B3 may be borderline unacceptable in terms of rutting. Figure 3.5 demonstrates the ability of cement to improve rutting resistance, which is a common reason for its use. Based on these results, the APA satisfies EC1 through EC4.

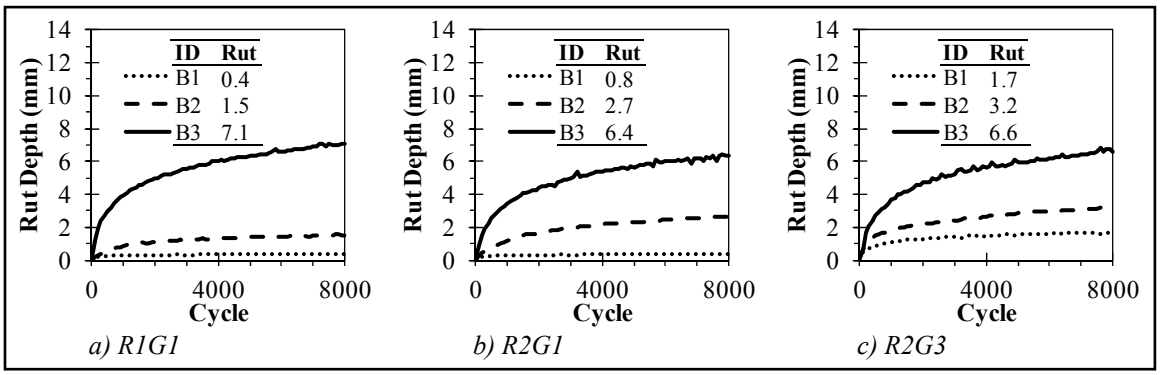

Figure 3.5 APA Test Results

A small experiment was conducted on R1G1-B3 at 60 and 80% of the full 445 N load to account for pavement depth within a typical pavement structure (CIR overlaid with asphalt concrete). The average bulk dry density of the four specimens tested was 2.01 g/cm^3. Figure 3.6 shows rut depths were 7.0 and 7.6 mm, which were not meaningfully different from the 7.1 mm full-load rut depth.

Based on Figure 3.6, the final rut depth appears to be indifferent to the load applied, which was somewhat unexpected. However, it should be noted that 55 to 65% of the total rut depth occurred by 1,000 cycles, and 0.32 mm rut per 1,000 cycles, on

average, was accumulated between 2,000 and 8,000 cycles. This suggests that initial mixture densification, perhaps due to higher air voids than asphalt concrete, drives the final rut depth more than mixture rutting (defined as mixture shear failure). Further, all loads tested appeared comparable in terms of their effect on mixture densification.

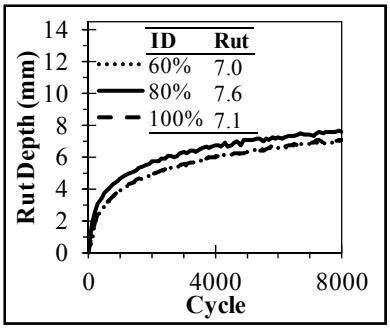

Figure 3.6 Reduced and Full Load APA Test Results for R1G1-B3

3.9 Indirect Tensile Testing

Cracking characterization can be performed with various tests such as the single-edge notched beam test, disc-shaped compact tension test (DCT), semi-circular bend test (SCBend), and IDT tests. For CIR, Charmot et al. (2010, 2013) conducted DCT and SCBend testing. No other documentation of CIR cracking characterization appeared readily available. The approach used in this chapter is based on IDT protocols developed largely by Roque and Buttlar (1992). The area under an IDT stress-strain curve, commonly referred to as the fracture energy (FE), has been used by several researchers to characterize cracking behaviors of asphalt mixtures (e.g. Birgisson et al. 2007, Koh and Roque 2010). Their work has demonstrated FE is a fundamental mixture property and can be indicative of mixture cracking potential.

Instrumented IDT testing (Figure 3.7a) was conducted at 25 °C with a load rate of 50 mm/min. Typically, traditional asphalt specimens are sliced from the center of tall gyratory specimens so that two sawn faces are achieved. It was suspected from laboratory experiences with CIR (e.g. BBR work previously presented) that slicing CIR specimens might damage them considerably; therefore, specimens were instead compacted to the desired height and not sawn. To obtain a solid mounting surface for extensometer gage points, a high-speed drill press and small grinding stone attachment were used to polish specimen surfaces as shown in Figure 3.7b.

a) Testing Configuration *b) Polished Mounting Points* *c) Example Stress-Strain Plot*

Figure 3.7 IDT Testing

R1G1, R2G1, and R2G3 were tested at all three binder blends. Specimens targeted 63 mm height and were cured 7 days. Three replicates were tested for each combination of material and binder blend. Average bulk dry densities for B1, B2, and B3, respectively, were as follows: (R1G1) 2.05, 2.01, and 1.99 g/cm^3; (R2G1) 1.85, 1.83, and 1.84 g/cm^3; and (R2G3) 1.75, 1.76, and 1.76 g/cm^3.

Three parameters thought to be informative for this chapter were derived from IDT testing (Table 3.2). These were tensile strength at fracture ($S_{t,f}$), horizontal strain at fracture ($\varepsilon_{H,f}$), and area under the stress-strain curve which is referred to herein as a

cracking index (*CI*) (Figure 3.7c). The instant of fracture was determined by plotting vertical minus horizontal strain versus time; the peak of this curve was taken as the instant of fracture (Koh and Roque 2010). *CI* is distinguished from FE primarily because of the slight differences in CIR testing protocols used herein relative to traditional asphalt (e.g. polished mounting points). Conceptually, *CI* and FE are identical, but the author chose to distinguish between them at present until further research and protocol refinement is conducted. The area under the stress-strain curve (*CI*) was calculated by numerical integration using Simpson's trapezoidal rule.

Table 3.2 Average IDT Results

	R1G1			**R2G1**			**R2G3**		
	B1	**B2**	**B3**	**B1**	**B2**	**B3**	**B1**	**B2**	**B3**
No. Replicates	6	6	6	6	5	6	2	5	6
$S_{t,f}$ **(kPa)**	476	293	354	433	221	339	221	154	303
$\varepsilon_{H,f}$ **(με)**	190	719	4289	248	1005	3068	1022	1069	4477
CI **(kJ/m^3)**	0.06	0.17	1.32	0.07	0.18	0.83	0.21	0.14	1.17

-- 3 replicates were tested with 2 instrumented faces totaling 6 data points absent any testing errors.
-- For R2G3-B1, one specimen (two data points) broke prior to testing.
-- Testing errors occurred with R2G1-B1 (1), R2G3-B1 (2), and R2G3-B2 (1). Review of data collected from these tests suggests one or more gage points may have become unbonded during testing. This incident occurred primarily with B1 blends (cement only), was generally a result of cemented material flaking off specimen faces, and should be further investigated to rectify the issue for future testing.
-- R2G3-B1 average results may be misleading given only two data points were available.

Results show that B1, with the exception of R2G3-B1 $S_{t,f}$ and *CI*, exhibited the highest $S_{t,f}$ and lowest $\varepsilon_{H,f}$ (i.e. flexibility) and *CI*. B3 was the opposite of B1. B2 $\varepsilon_{H,f}$ and *CI* generally fall between that of B1 and B3 but closer to that of B1; interestingly, B2 exhibited the lowest $S_{t,f}$. Perhaps the same issue presented in the fatigue section is occurring where there is an insufficient amount of either cement or emulsion and the whole system suffers. It is likely that, with additional curing, B1 $S_{t,f}$ would continue

increasing to undesirable levels (i.e. producing a stiff, crack-prone material), B3 $S_{t,f}$ would remain relatively unchanged, and B2 $S_{t,f}$ would increase slightly, perhaps near that of B3. Based on these findings, this form of IDT testing satisfies EC1 through EC4. It appears promising for CIR with multiple binder types and warrants further consideration at longer test times and with a wider range of cement and emulsion combinations.

3.10 Discussion of Results

Table 3.3 presents a summary of the six performance tests currently available for traditional asphalt mixtures which were evaluated for use with CIR in this chapter. For a test to be considered appealing, it must reasonably satisfy the four evaluation criteria established herein. For CIR testing conducted herein, Cantabro, BBR, and HLWT testing were least optimal, while APA and IDT testing appeared most optimal.

Table 3.3 Summary of Performance Test Evaluation

	Test					
Criteria	**Cantabro**	**BBR**	**HLWT**	**Fatigue**	**APA**	**IDT**
EC1	✓	×	✓	✓	✓	✓
EC2	×	n/a	×	●	✓	✓
EC3	n/a	n/a	n/a	●	✓	✓
EC4	n/a	n/a	n/a	×	✓	✓

n/a = not applicable ✓ *= Good* ● *= Moderate* × *= Bad*

In addition, it must be understood that CIR mixtures are not developed to possess the strength and stiffness of asphalt concrete mixtures. One reason is that CIR is rarely used as a pavement surface but, rather, is used as a base layer. Therefore, stresses and loads applied in traditional asphalt concrete tests may be irrelevant when testing CIR. In

light of this issue, reduced loads were considered for fatigue and APA testing. Fatigue results were more informative with the reduced 445 N load; however, CIR loaded wheel fatigue testing is not believed to be optimal based on EC4.

APA results were not distinguishably different at 60 and 80% of the standard 445 N load. As stated previously, initial densification under load due to typically higher air voids than asphalt concrete appears to be a larger factor in the overall APA rut depth than shear failure of the mixture (i.e. rutting). Therefore, reduced load protocols do not appear more informative than current APA test protocols. Instead, establishing alternative maximum rut depth criteria for CIR could be more useful than reduced load protocols as this would allow CIR rut depths to be directly compared to asphalt concrete rut depths.

3.11 Conclusions and Recommendations

APA testing satisfied all criteria and can be informative for CIR in its current state (i.e. 445 N load at 689 kPa hose pressure). IDT testing satisfied all criteria and should be further studied for CIR. Testing specimens at later cure times as well as additional combinations of cement and emulsion is recommended to aid in refining test protocols.

CHAPTER 4

VACUUM SEALING BASED VOLUMETRIC DENSITY MEASUREMENT APPROACH FOR COLD IN-PLACE RECYCLING

This chapter has been previously published as a journal article in Issue 2444 of the Transportation Research Record: Journal of the Transportation Research Board (TRB). The original paper may be accessed at http://dx.doi.org/10.3141/2444-02. With permission from TRB, the paper (Cox and Howard 2014) has been reformatted and reproduced herein with minor modifications to suit the objectives of this dissertation.

4.1 Introduction

Due to current economic pressures, state departments of transportation (DOT's) are finding it difficult to adequately maintain pavement networks. Therefore, DOT's have sought effective rehabilitation methods as viable alternatives to complete reconstruction. Cold in-place recycling (CIR) is one method which invokes mixed DOT responses. A recently-accessed FHWA survey (FHWA) where 42 DOT's responded revealed 22 states use CIR to some degree, and of those, 17 claimed to use CIR routinely or have a special provision or standard specification. Seventeen DOT's indicated they had no interest or enough concerns to prevent CIR use in the near future.

Survey results indicate CIR has merit within certain areas of pavement rehabilitation and that gaps within mix design and quality control procedures are what led

to the majority of the observed criticism. This is evidenced by approximately one-third of surveyed DOT's reporting successful CIR use, but their success appears to depend largely on experience or within-state methods, not standard methods. Of the issues mentioned, density control method variability was of particular interest herein. Responses included 100% of AASHTO T180 maximum dry density, 98% density, 94% of lab-compacted dry density, 98% of test strip density, 96% of Marshall briquette density, and 95% of Marshall density measured by vacuum sealing. Also, there were variations of these methods (e.g. 96% to 98% of test strip density). Some entities used a method-based specification, and others had no means of controlling density. While other factors also lead to CIR criticism, density control likely lends to reduced variability, improved performance, and agency acceptance. At present, agencies would benefit both in mix design and quality control/assurance from a consistent standard for controlling density.

This chapter's objective is to present a method for controlling CIR density that is derived from volumetrics (i.e. maximum and bulk specific gravity, G_{mm} and G_{mb}) and uses vacuum sealing (i.e. CoreLok®). Vacuum sealing's simplicity, quickness, and reliability, alongside its ability to alleviate key testing issues, were the basis for its central role in the method presented. Also, vacuum sealing, with nominal effort, could be implemented in quality control/assurance programs. G_{mm} is a well-accepted asphalt reference property that is independent of compaction procedures (unlike other CIR density methods). Herein, reclaimed asphalt pavement (RAP) G_{mm} measured by ASTM D6857 (vacuum sealing method) is evaluated against AASHTO T209 (traditional method, also termed Rice gravity). An equation was developed to estimate CIR G_{mm} (i.e. post binder(s) addition) using RAP G_{mm} (i.e. pre binder(s) addition) and binder specific

gravities (e.g. emulsion and cement) to further simplify the process. CIR G_{mb} is measured by a modified version of AASHTO T331 (vacuum sealing method) and evaluated against AASHTO T166 (saturated surface dry, or SSD, method) and T269 (dimensional measurement method).

RAP G_{mm} is more difficult to accurately obtain relative to conventional asphalt. This chapter aims to demonstrate the induced error is tolerable for CIR and the G_{mm}/G_{mb} method (even with some error) would be an improvement over the current abundance of methods used. One should note that Superpave ideology was shaped over a period of approximately 20 years (TRB Superpave Committee 2005). This method, while not necessarily fully refined, seeks to demonstrate feasibility of concept at a laboratory scale. The approach presented is currently only applicable to CIR using 100% RAP.

4.2 Literature Review

4.2.1 Maximum Specific Gravity of Asphalt

A study of four Ohio asphalt mixes (33 total replicates) found no statistical differences between D6857 and T209 at a 5% significance level (Rajagopal and Crago 2007). Sholar et al. (2005) conducted a larger investigation evaluating D6857 and FM 1-T209 (equivalent to T209 and further referred to as T209). Five hot-mixed asphalt (HMA) mixes were tested (ten replicates each) with varying nominal maximum aggregate size (NMAS), gradation, aggregate type, and aggregate water absorption. For T209, the SSD dryback procedure (denoted $T209_{SSD}$) was also performed.

D6857 and $T209_{SSD}$ produced similar results (difference of 0.001) for very low absorption granite (<1%). Test results for all four limestone mixtures with medium (2-

3%) to high (5-6%) absorption aggregates were statistically different (5% significance level) with D6857 values being greater than $T209_{SSD}$ values by 0.011, 0.002, 0.004, and 0.033. D6857 standard deviations were significantly greater (5% significance level) than those of $T209_{SSD}$ for all mixes indicating greater variability with D6857. It was suggested the higher variability may be due to operator unfamiliarity. D6857 and T209 results were, for all practical purposes, similar, but Sholar et al. (2005) stated a dryback procedure for D6857 may be necessary with high-absorption aggregates as they cannot be accurately characterized otherwise.

Doyle et al. (2012) compiled a database of all Mississippi DOT (MDOT) asphalt mix designs from 2005-2010. Since all materials tested herein were from Mississippi and were at one time a new mixture, the Figure 4.1 G_{mm} histograms are useful for evaluating test results. Results outside the 95% confidence interval (C.I.) indicate a questionable test result or method.

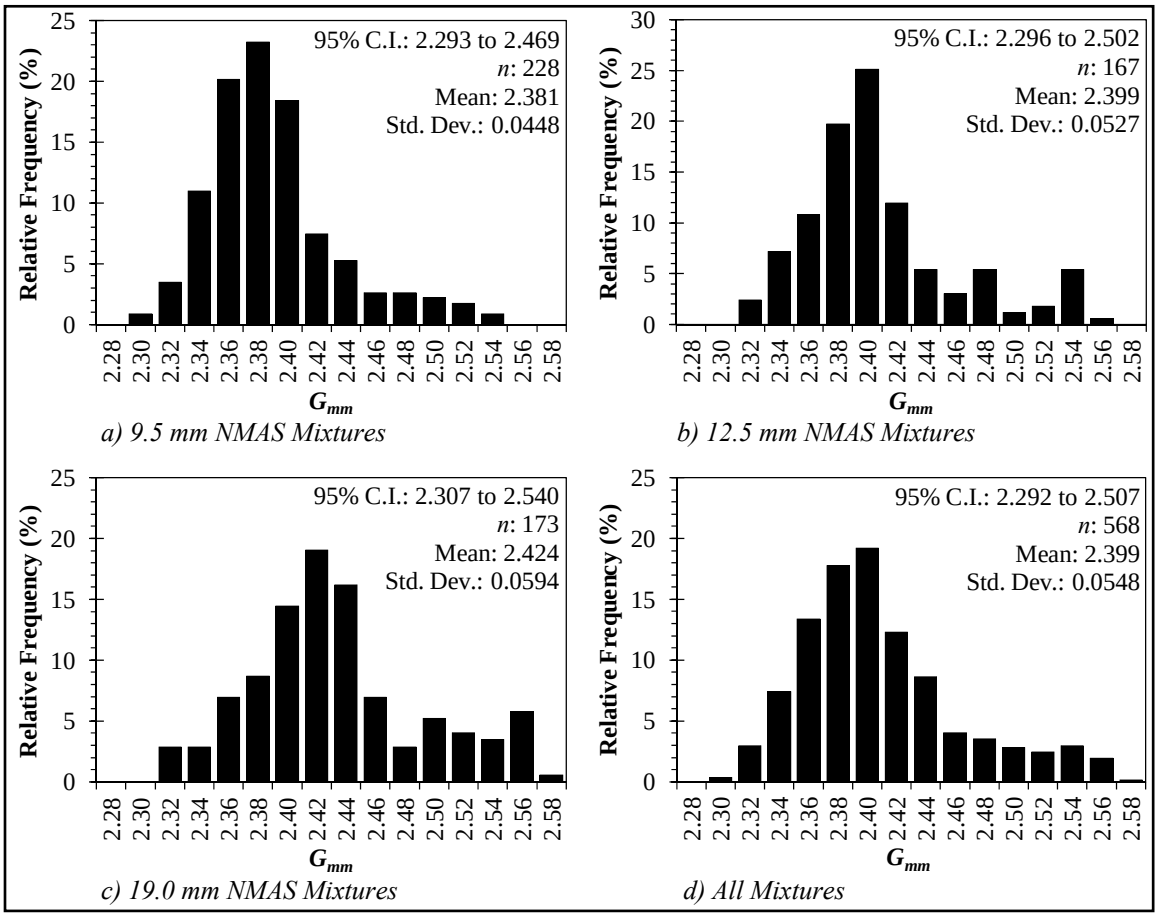

Figure 4.1 Relative Frequency Histogram of G_{mm} from MDOT Database

4.2.2 Maximum Specific Gravity of RAP and CIR

Sholar et al. (2005) evaluated a low-absorption (1-2%) limestone RAP with D6857 and T209. The difference between D6857 and T209 and also D6857 and $T209_{SSD}$ G_{mm} values was 0.002. Closeness between these methods (difference of 0.002) was attributed to the low-absorption aggregate. D6857 standard deviations were again slightly greater than T209 and $T209_{SSD}$. Bang et al. (2011) used D6857 to test full-depth reclamation (FDR) which, for all meaningful purposes, is similar to CIR in relation to

G_{mm} measurement. However, motives for using D6857 over T209 were not provided, and results were not compared to any other method.

4.2.3 Bulk Specific Gravity of Asphalt

Approximately 2,500 data points coupled with an in-depth literature review of asphalt G_{mb} measurement methods found that T331 was evaluated favorably against T166 and T269 (Howard and Doyle 2014). For typical mixtures, the 2.0% water absorption limit for T166 can easily be exceeded at air void (V_a) levels of 8-9%. T166 correlations of the form of Equation 4.1 were developed to predict T331 V_a at typical mix design (V_a = 4%), performance testing (V_a = 7%), and moderately high construction acceptance (V_a = 10%) levels.

$$V_{a(i)} = C_1\left(V_{a(T166)}\right) + C_2 \tag{4.1}$$

Where,

$V_{a(i)}$ = percent air voids measured by method i (e.g. $V_{a(T269)}$, $V_{a(T331)}$)

$V_{a(T166)}$ = percent air voids measured by AASHTO T166

C_1, C_2 = regression constants

Predicted $V_{a(T331)}$ was dependent on NMAS and gradation (fine vs. coarse), but predicted $V_{a(T331)}$ was almost always greater than $V_{a(T166)}$. On average, T331 yielded higher air voids relative to T166 as follows: 0.8% at mix design levels, 1.2% at performance testing levels, and 1.2-1.6% at construction acceptance levels.

4.2.4 Bulk Specific Gravity of CIR

Literature review reveals that, for those sources which measure and specify G_{mb} as opposed to dry density (γ_d), one of three measurement methods is typically used: T166 (Cross 2002, Cross 2003, Skok et al. 2008), T269 (Kim and Lee 2006, Kim and Lee 2007, Kim and Lee 2008, Kim et al. 2008, Kim et al. 2009, Kim and Lee 2011) or T331 (Cross 2002, Mallick et al. 2002, Cross 2003, Bang et al. 2011). In addition, some sources report G_{mb} yet do not specify how the value was determined (Carter et al. 2010, Chan et al. 2010, Schwartz and Khosravifar 2013). Several sources referenced in this portion of the literature review researched FDR; however, CIR and FDR are closely related in the context that G_{mb} determination for either is similar.

Mallick et al. (2002) began using vacuum sealing to determine G_{mb} on freshly compacted FDR specimens because it was suspected the specimens would break down underwater if tested by T166. Cross (2002, 2003), who researched CIR, and NCHRP Synthesis 421 on in-place recycling (Stroup-Gardiner 2011) expressed concerns that T166 may not be suitable due to water absorption issues caused by typically high air voids in recycling mixtures. CIR V_a levels found in literature are often higher than the 8-9% value previously mentioned by Howard and Doyle (2014). Literature reports V_a levels of 2-14% (Mallick et al. 2002), 8.9-14.4% (Carter et al. 2010), 13.7-16.4% (Schwartz and Khosravifar 2013), 6-10% (Kim and Lee 2006, Kim and Lee 2008), 9.7-14.2% (Cross 2002), 8-17% (Kim et al. 2007), 9.2-17.9% (Kim et al. 2008), 5.8-10% (Kim and Lee 2011), and 6.3-22.4% (Bang et al. 2011). Data presented later in this chapter shows V_a levels ranging from 17.1-26.9% (G_{mb} and G_{mm} measured via vacuum sealing). While different measurement methods used in these citations may provide somewhat differing

V_a results, the majority of the V_a levels reported were well above the range at which 2% water absorption can occur with T166. Therefore, T166 use for determining G_{mb} of CIR is discouraged.

4.3 Experimental Program

4.3.1 Materials Tested

Four bituminous materials were tested (Table 4.1). R1 was sampled from an in-place recycling project and tested at the as-received bulk gradation (denoted G1). R2 was blended to G1 and also G2 and G3. G2 and G3 were constructed based on 28 observed gradations from literature review (Cox and Howard 2013) to approximate the finest and coarsest gradations documented. R1 and R2 were air-dried to less than 0.25% moisture before sieving into multiple size fractions. Test specimens were batched from these fractions to improve precision and allow multiple gradations to be batched from one material source.

Hwy 45 and Hwy 41 materials were used to create typical HMA loose mixes and a laboratory-crushed RAP material (denoted CR) to evaluate the difference in G_{mm} as a function of physical state. Slabs were processed in the laboratory to create: 1) loose mix (denoted HMA) by heating slabs until just workable, then removing saw-cut edges and separating slabs; and 2) a simulated, crushed RAP (denoted CR) by freezing slabs overnight (saw-cut edges intact), then using a jaw crusher. CR was sieved into multiple sizes for batching. RAP millings (denoted RAP) were also obtained from Highway 41 and processed in the laboratory similar to R1 and R2.

Table 4.1 Properties of Bituminous Materials Tested

Material ID	R1	R2			Hwy 45		Hwy 41		
Denoted	G1	G1	G2	G3	HMA	CR	HMA	CR	RAP
NMAS	12.5	9.5	9.5	9.5	9.5	9.5	9.5	9.5	9.5
$P_{AC\text{-}T308}$[a] **(%)**	5.1	6.2	6.5	5.7	---	---	7.6	7.6	5.7
$P_{AC\text{-}T164}$[b] **(%)**	4.8	5.6	6.2	4.9	6.8	6.8	6.8	6.8	5.4
-25.0 mm[c]	100	100	100	100	---	100	---	100	100
-19.0 mm	99	100	100	93	---	---	---	---	---
-12.5 mm	94	94	97	78	---	67	---	58	89
-9.5 mm	85	85	91	65	---	---	---	---	---
-4.75 mm	55	55	68	34	---	24	---	22	48
-2.36 mm	38	38	49	21	---	11	---	12	27
-1.18 mm	28	23	30	13	---	---	---	---	---
-0.60 mm	19	15	20	8	---	---	---	---	---
-0.30 mm	8	8	10	4	---	---	---	---	---
-0.15 mm	3	3	5	2	---	---	---	---	---
-0.075 mm	1.5	1.5	2.3	0.8	---	---	---	---	---

a) No aggregate correction factor was used
b) An 85%/15% blend of toluene/ethanol was used for extraction
c) Bulk gradation of RAP material (i.e. not aggregates post extraction)
--- Data not obtained
--- Origin of materials

- R1: sampled during CIR project on US-49 in Madison County, MS
- R2: milled RAP sampled from asphalt producer stockpile in Columbus, MS
- Hwy 45: slabs were cut from surface lift of an abandoned portion of US-45 in Crawford, MS
- Hwy 41: slabs were cut from surface lift of MS-41 near Okolona, MS
- Hwy 41: milled RAP from surface lift sampled near same location as slabs from MS-41 near Okolona, MS

Hwy 41 RAP was sampled directly from the milling machine near the slab-cutting site to minimize material differences. As evidenced by the large asphalt content (P_{AC}) discrepancy, Hwy 41 RAP greatly differed from Hwy 41 HMA or CR (also affirmed by differences in G_{mm}). Segregation within the milling drum is a likely explanation as there were several issues with the machine during the sampling period. The machine was repeatedly stopped and started because of mechanical issues, yet timing constraints prevented sampling postponement.

CIR binders used were Type I portland cement, CSS-1H emulsion (63.5% residue), and hydrated lime with specific gravities of 3.15, 1.03, and 2.32 g/cm^3, respectively. Three binder blends (Table 4.2) were developed targeting an entirely cement blend, a hybrid blend of cement and emulsion, and an entirely emulsion blend (plus 1% hydrated lime). B1 and B3 were used on US-49 (source of R1), and B2 was chosen as a balanced blend of emulsion and cement.

Table 4.2 Dosage Rates for CIR Blends

Material	R1			R2		
Blend	B1	B2	B3	B1	B2	B3
***Cement* (%)**	4.4	2.3	0	4.6	2.4	0
***Emulsion* (%)**	0	2	4	0	2	4
***Hydrated Lime* (%)**	0	0	1	0	0	1

Note: Binders dosed as a percentage of dry RAP mass.

4.3.2 Test Methods

G_{mm} RAP samples and water were mixed (6% moisture) two minutes before binder addition and two minutes following binder addition. Mixing moisture includes batch and, where applicable, emulsion water. Samples were air-dried under fans approximately seven days before testing.

G_{mm} testing was performed using T209 and D6857. For T209, the dry-back procedure is denoted $T209_{SSD}$. For D6857, testing complied with the manufacturer's operating manual and D6857. All testing was performed with a 300-second vacuum dwell setting.

T209 and D6857 precision statements (Table 4.3) were used as an acceptability reference. The one-sigma limit (1*s*) is the maximum allowable standard deviation of a

group of results, and the difference two-sigma limit (d2*s*) is the maximum allowable difference between two test results. The maximum acceptable range of individual measurements when ten results are averaged (*Max Range*$_{10}$) is 14.1 times 1*s*. ASTM C670 (standard practice for preparing precision and bias statements) only reports a 1*s* multiplier up to ten replicates. Although these precision statements were not used according to their intended purpose, they do provide reasonable comparison boundaries for subjective assessment.

Table 4.3 AASHTO and ASTM Precision Statements

	AASHTO T209-05			**AASHTO T209-11**			**ASTM D6857-03**		
Test & Type Index	**1*s***	**d2*s***	***Max Range*$_{10}$**	**1*s***	**d2*s***	***Max Range*$_{10}$**	**1*s***	**d2*s***	***Max Range*$_{10}$**
Single-operator Precision (*SOP*)	0.0040	0.011	0.056	0.0051	0.014	0.072	0.0070	0.020	0.099
Multilaboratory Precision (*MLP*)	0.0064	0.019	0.090	0.0084	0.024	0.118	---	---	---

G_{mb} specimens were mixed identically to G_{mm} samples (6%, 8%, or 10% moisture), compacted to 30 or 75 gyrations in a Superpave Gyratory Compactor (SGC), and cured using various protocols. While these variables could noticeably affect G_{mb}, the measurement methods of interest can measure G_{mb} irrespective of the curing protocol employed.

G_{mb} testing was performed using T269 and T331. For T269, wet G_{mb} was calculated immediately after mold extrusion using dimensions and mass. Moisture content (*MC*) was used to convert to dry G_{mb}. To keep specimens intact, *MC* was estimated from *MC* vs. gyration curves which were constructed by compacting specimens

(216 total) to gyration levels from 5-150 and then measuring *MC*. A curve corresponding to each unique CIR mixture was constructed for completeness. This data set was not shown for brevity.

For T331, specimens were tested post-curing. Depending on curing type and length, residual moisture was likely present in the specimen, resulting in a moist G_{mb}. Its *MC* was then measured directly to convert to dry G_{mb} and obtain V_a. The goal of this research component was to investigate potential T331 use for moist specimens. Specimens could be moist vacuum sealed, tested if desired (e.g. indirect tensile), and then used to obtain *MC*.

4.3.3 Test Plan

Testing was divided into three components: 1) T209 (including $T209_{SSD}$) and D6857 testing to assess D6857, 2) D6857 testing to develop and refine a CIR G_{mm} estimation equation, and 3) G_{mb} testing to assess T331 use for moist CIR specimens. In all, 396 tests were conducted: 168 for Component 1 (i.e. pre binder(s) addition); 56 (plus 16 tests at additional cement dosages) for Component 2 (i.e. post binder(s) addition); and 156 for Component 3 (Table 4.4).

Table 4.4 Summary of Test Plan

ID	R1	R2			Hwy 45		Hwy 41		
Binder	G1	G1	G2	G3	HMA	CR	HMA	CR	RAP
None	✓	✓	×	×	✓	✓	✓	✓	✓
B1	×	×, ❖	×	×	---	---	---	---	---
B2	×	×, ❖	×	×	---	---	---	---	---
B3	×	×, ❖	×	×	---	---	---	---	---

✓ *T209 and D6857 conducted (12 replicates)* × *D6857 conducted (4 replicates)*
❖ *T269 and T331 conducted* *--- No test conducted*

4.4 Test Results

4.4.1 RAP G_{mm} Test Results

Figure 4.2 displays G_{mm} test results. For T209/D6857 and $T209_{SSD}$/D6857, results from two respective data sets are combined and analyzed (e.g. 12 T209 replicates and 12 D6857 replicates). Practically, T209 and D6857 result in similar mean G_{mm} values for each material (Figure 4.2a). $T209_{SSD}$ generally provides the lowest mean G_{mm}. For T209/D6857, G_{mm} increases 0.012 and 0.010 when going from HMA to CR for Hwy 45 and 41, respectively; however, $T209_{SSD}$ results remain practically the same.

Hwy 41 HMA and CR have very low G_{mm} values with respect to the Figure 4.1 MDOT database. However, G_{mm} values for all 7 materials are within the 95% confidence interval. The database is useful in showing that such low G_{mm} values exist in Mississippi which demonstrates the Hwy 41 HMA and CR results are possible.

Regarding Table 4.3, $T209_{SSD}$ and $T209_{SSD}$/D6857 are the only test categories that violate multilaboratory 1*s* limits in some way (Figure 4.2b). The current T209-11 *MLP* 1*s* is violated in only two cases. It is not surprising, though, to find more variability within dry-back procedures.

In Figure 4.2c, all violations of multilaboratory d2*s* limits occur with $T209_{SSD}$ or $T209_{SSD}$/D6857 except for one case with T209/D6857 for R1G1 (which still does not violate the current T209-11 limit). It should be noted again that d2*s* limits correspond to the maximum allowable difference in two results; both twelve and twenty-four results are analyzed here. For those cases which do exceed d2*s* limits, the $Max\ Range_{10}$ limits were still comfortably satisfied.

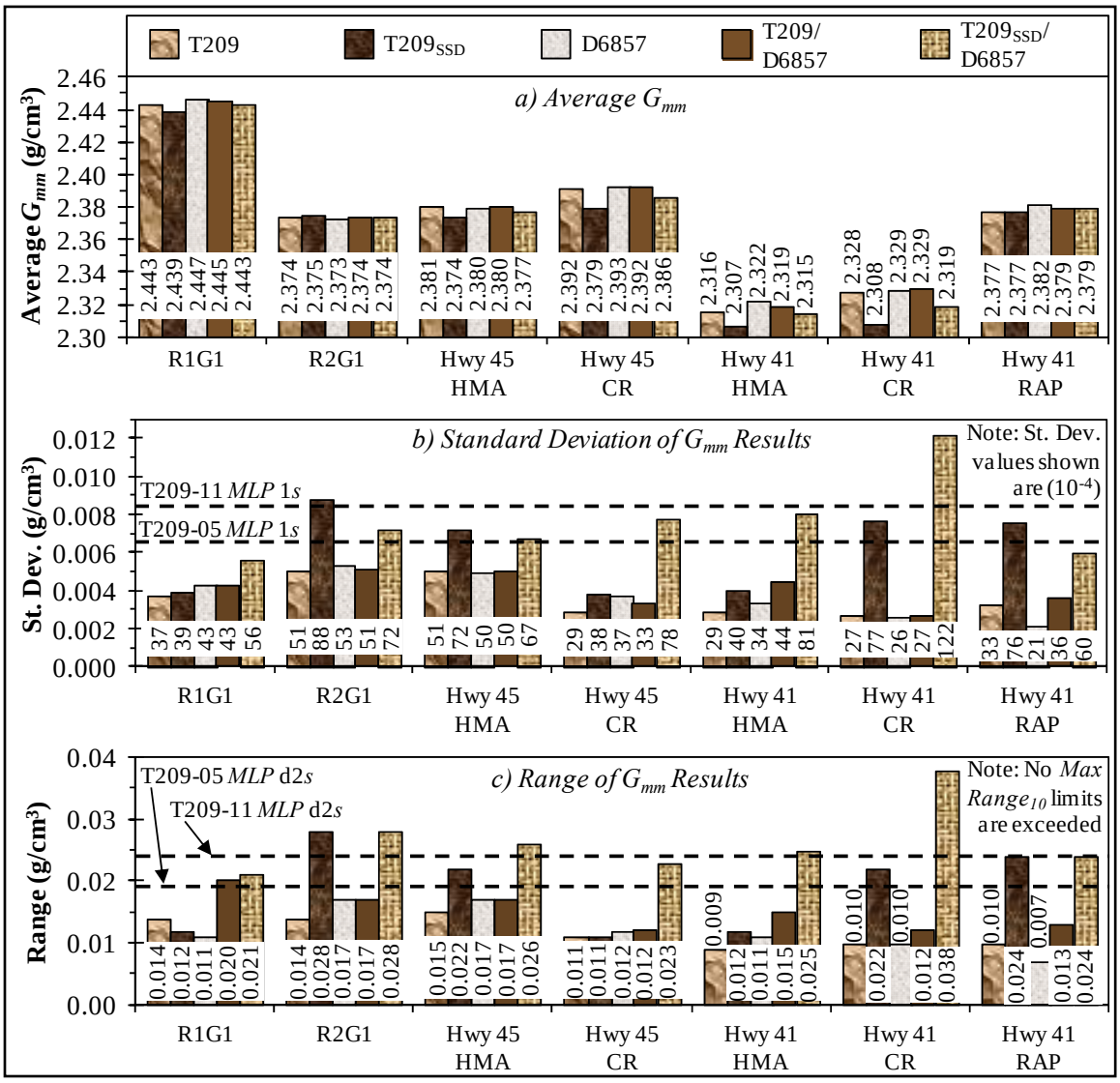

Figure 4.2 G_{mm} Test Results

Statistical analysis is shown in Table 4.5. T209 and D6857 were not significantly different, except for Hwy 41 HMA. $T209_{SSD}$ and D6857 were significantly different for all materials except R2G1. For Hwy 41 and 45, going from HMA to CR yielded significantly different results via T209 and D6857. This did not occur for Hwy 41 $T209_{SSD}$. Hwy 45 $T209_{SSD}$ was statistically but not practically different between HMA

and CR. Overall, there were some differences in measuring RAP and HMA G_{mm} between and sometimes within test methods.

Table 4.5 Two-Sample *t*-test Comparison of G_{mm} Results

Material	Comparison	*n*	Mean	Std. Dev. (10^{-3})	*p*-value	Variances Equal?[a]	Sig. Different?[b]
R1G1	T209	12	2.443	3.7	0.0502	Yes	No
	D6857	12	2.447	4.3			
	$T209_{SSD}$	12	2.439	3.9	0.0001	Yes	Yes
	D6857	12	2.447	4.3			
R2G1	T209	12	2.374	5.1	0.7381	Yes	No
	D6857	12	2.373	5.3			
	$T209_{SSD}$	12	2.375	8.8	0.6997	No	No
	D6857	12	2.373	5.3			
Hwy 45 HMA	T209	12	2.381	5.1	0.7196	Yes	No
	D6857	12	2.380	5.0			
	$T209_{SSD}$	12	2.374	7.2	0.0342	No	Yes
	D6857	12	2.380	5.0			
Hwy 45 CR	T209	12	2.392	2.9	0.4302	Yes	No
	D6857	12	2.393	3.7			
	$T209_{SSD}$	12	2.379	3.8	<0.0001	Yes	Yes
	D6857	12	2.393	3.7			
Hwy 41 HMA	T209	12	2.316	2.9	0.0001	Yes	Yes
	D6857	12	2.322	3.4			
	$T209_{SSD}$	12	2.307	4.0	<0.0001	Yes	Yes
	D6857	12	2.322	3.4			
Hwy 41 CR	T209	12	2.328	2.7	0.2291	Yes	No
	D6857	12	2.329	2.6			
	$T209_{SSD}$	12	2.308	7.7	<0.0001	No	Yes
	D6857	12	2.329	2.6			
Hwy 41 RAP	T209	12	2.377	3.3	0.0007	No	No
	D6857	12	2.382	2.1			
	$T209_{SSD}$	12	2.377	7.6	0.0570	No	Yes
	D6857	12	2.382	2.1			
Hwy 45	T209 HMA	12	2.381	5.1	<0.0001	No	Yes
	T209 CR	12	2.392	2.9			
	D6857 HMA	12	2.380	5.0	<0.0001	No	Yes
	D6857 CR	12	2.393	3.7			
	$T209_{SSD}$ HMA	12	2.374	7.2	0.0392	No	Yes
	$T209_{SSD}$ CR	12	2.379	3.8			
Hwy 41	T209 HMA	12	2.316	2.9	<0.0001	Yes	Yes
	T209 CR	12	2.328	2.7			
	T209 HMA	12	2.316	2.9	<0.0001	Yes	Yes
	T209 RAP	12	2.377	3.3			
	T209 CR	12	2.328	2.7	<0.0001	Yes	Yes
	T209 RAP	12	2.377	3.3			
	D6857 HMA	12	2.322	3.4	<0.0001	No	Yes
	D6857 CR	12	2.329	2.6			
	D6857 HMA	12	2.322	3.4	<0.0001	No	Yes
	D6857 RAP	12	2.382	2.1			
	D6857 CR	12	2.329	2.6	<0.0001	Yes	Yes
	D6857 RAP	12	2.382	2.1			
	$T209_{SSD}$ HMA	12	2.307	4.0	0.8443	Yes	No
	$T209_{SSD}$ CR	12	2.308	7.7			
	$T209_{SSD}$ HMA	12	2.307	4.0	<0.0001	Yes	Yes
	$T209_{SSD}$ RAP	12	2.377	7.6			
	$T209_{SSD}$ CR	12	2.308	7.7	<0.0001	Yes	Yes
	$T209_{SSD}$ RAP	12	2.377	7.6			

a) Homogeneity of variances tested at the 95% confidence level. --- $p_{critical} = 0.05$

b) Significance testing performed at the 95% confidence level.

4.4.2 CIR G_{mm} Test Results

Table 4.6 shows D6857 CIR results. CIR differs from RAP materials discussed in the previous section in that binders (cement, emulsion, or a combination) have been applied. The St. Dev. and range of all results are within T209-05 multilaboratory and single-operator precision. Because of the time required to obtain G_{mm} for a single CIR mixture (approximately one week), a simple but accurate estimation of G_{mm} would be useful. The approach used herein parallels parts of Superpave (AI 2001). Equation 4.2 is the Superpave aggregate blending equation in general form, and Equation 4.3 was developed for determination of CIR G_{mm}. Equation 4.3 takes on a similar form to Equation 4.2 but was adapted to accommodate binders. In order to estimate G_{mm} of a dry CIR mix, the emulsion water is treated as evaporated (only emulsion residue was included in the estimation). Conversely, some portion of mixing water is devoted to cement hydration; therefore, it permanently adds mixture mass and volume, reducing G_{mm}. For example, Feldman (Feldman 1972) reported a specific gravity of 2.35 for fully hydrated cement. Specific gravity decrease due to hydrated water is accounted for in Equation 4.3 by the term non-evaporable water cement ratio (w_{NE}/cm).

An experiment was conducted where Type I portland cement paste (water-cement ratio of 0.5) was sealed in containers and cured on a lab bench for 1, 3, and 7 days. After curing, the container was placed in an oven overnight to determine the amount of non-evaporable water. Average w_{NE}/cm for 1-, 3-, and 7-day cures (4 replicates each) was 0.13, 0.14, and 0.16, respectively. These numbers are likely higher than for CIR mixtures since CIR is not cured in a sealed container with this much free water. A w_{NE}/cm of 0.10 worked well for the mixtures tested. Figure 4.3 is an equality plot of predicted vs.

measured (Table 4.6) G_{mm}, where sum of squares error (SSE) and coefficient of determination (R^2) values indicate good correlation.

Table 4.6 ASTM D6857 G_{mm} Results for CIR Mixtures

Material	D6857 RAP G_{mm}	Mean	*n*	Std. Dev.	Range
R1G1-B1	2.447	2.451	4	0.0040	0.009
R1G1-B2		2.414	4	0.0029	0.006
R1G1-B3		2.369	4	0.0050	0.011
R2G1-B1	2.373	2.386	4	0.0028	0.006
R2G1-B2		2.344	4	0.0045	0.010
R2G1-B3		2.303	4	0.0042	0.010
R2G2-B1	2.367	2.378	4	0.0018	0.004
R2G2-B2		2.330	4	0.0033	0.007
R2G2-B3		2.295	4	0.0050	0.010
R2G3-B1	2.383	2.395	4	0.0051	0.011
R2G3-B2		2.354	4	0.0051	0.010
R2G3-B3		2.314	4	0.0020	0.005

$$G_{sb} = \frac{P_1 + P_2 + \cdots + P_N}{\frac{P_1}{G_1} + \frac{P_2}{G_2} + \cdots + \frac{P_N}{G_N}} \tag{4.2}$$

Where,

G_{sb} = bulk specific gravity for the total aggregate

P_1, P_2, P_N = individual percentages by mass of aggregate

G_1, G_2, G_N = individual (e.g. coarse, fine) bulk specific gravity of aggregate

A second experiment was conducted to validate Equation 4.3 and the 0.10 w_{NE}/cm value for a wide range of cement contents. Four replicates of R1G1 with P_{cm} of 1, 3, 5, and 7% were tested by D6857. The average predicted minus measured G_{mm} values for

the 1, 3, 5, and 7% cement mixtures were 0.005, 0.007, 0.011, and 0.014, respectively. The w_{NE}/cm component of this chapter likely has room for improvement, but the concept is promising, reasonable, and appears implementable based on Figure 4.3.

$$G_{mm,CIR} = \frac{1 + \left[P_{cm} + w_{NE/cm} P_{cm}\right] + P_{HL} + P_{Em} P_{Res}}{\frac{1}{G_{mm,RAP}} + \left[\frac{P_{cm}}{G_{cm}} + \frac{w_{NE/cm} P_{cm}}{G_w}\right] + \frac{P_{HL}}{G_{HL}} + \frac{P_{Em} P_{Res}}{G_b}} \quad (4.3)$$

Where,

$G_{mm,CIR}$ = estimated maximum specific gravity for the CIR mixture

P_{cm} = percent of cement by mass of RAP

w_{NE}/cm = non-evaporable water-cement ratio

P_{HL} = percent of hydrated lime by mass of RAP

P_{Em} = percent of emulsion by mass of RAP

P_{Res} = percent of asphalt residue by mass of emulsion

$G_{mm,RAP}$ = D6857 maximum specific gravity of RAP

G_{cm} = specific gravity of portland cement

G_w = specific gravity of water = 0.997 g/cm^3 at 25 °C

G_{HL} = specific gravity of hydrated lime

G_b = specific gravity of asphalt binder

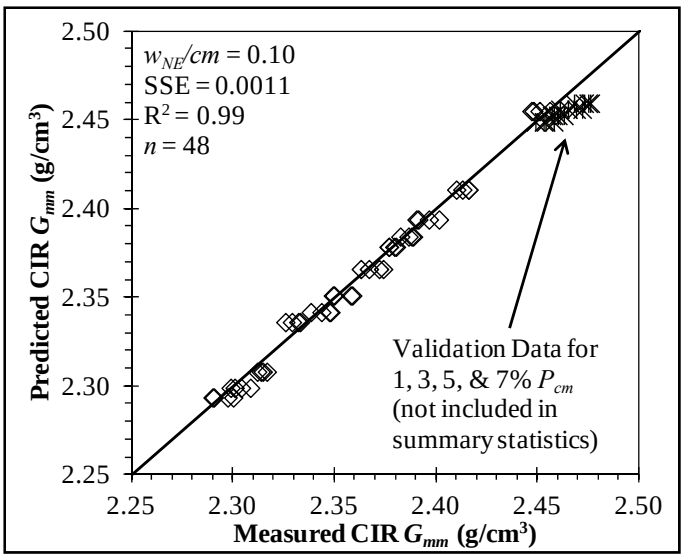

Figure 4.3 Predicted vs. Measured CIR G_{mm}

4.4.3 CIR G_{mb} Test Results

Figure 4.4a shows that, on average, T269 air voids were 1.1% greater than T331. Howard and Doyle (2014) found that $V_{a(T269)}$ minus $V_{a(T331)}$ ranged from 0.9-2.6% for air voids of 4-10%. CIR $V_{a(T269)}$ minus $V_{a(T331)}$ was on the lower end of this range despite air voids ranging from approximately 18-28%. Bang et al. (2011) noted the SGC typically produced smooth sides on CIR specimens; reducing surface texture reduces the difference between $V_{a(T269)}$ and $V_{a(T331)}$. Figure 4.4a indicates T269 and T331 have relationships on the order of those observed by Howard and Doyle (2014) when measured in a moist condition (*MC* ranged 0.1-6.9%) and converted to dry G_{mb} values. Figure 4.4b demonstrates that the relationship between T269 and T331 is similar regardless of gyration level.

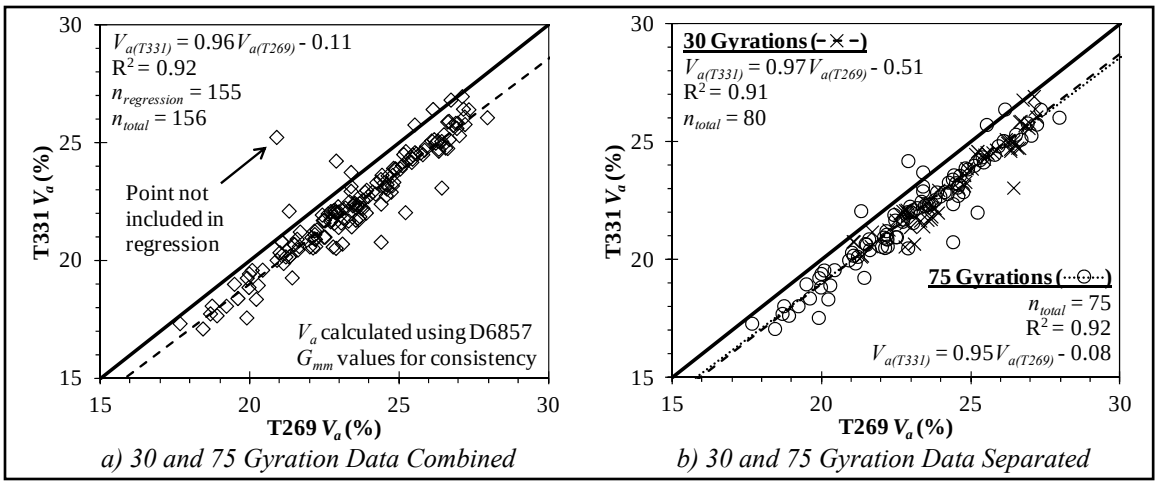

Figure 4.4 Air Voids Equality Plot Using T331 and T269 G_{mb} Data

4.5 Discussion of Results

RAP G_{mm} test data indicates T209 and D6857 yield practically and statistically similar results. This is supported by AASHTO and ASTM precision statements (Table 4.3). Hwy 45 and 41 results confirm there are significant differences between G_{mm} of HMA and CR. As recommended by Sholar et al. (2005), data indicates a dry-back procedure alleviates this difference. Obtaining dry-back results for D6857, however, is likely problematic. It is difficult to remove all material from a vacuum sealing bag, though it is a critical aspect of the dry-back procedure. Even though the dry-back procedure cannot be easily performed with D6857, it still has advantages over T209 in that it requires ~17 fewer minutes per test, and fines loss in the water bath is more easily controlled.

Additionally, the error caused by not performing the dry-back procedure for CR or RAP is small relative to other variability factors currently within CIR. For Hwy 45 D6857 results, the change in G_{mm} from HMA to CR is 0.012. For Hwy 41 D6857 results,

the change in G_{mm} from HMA to CR (HMA to RAP is not discussed due to G_{mm} discrepancies) is 0.010. The inherent difference in G_{mm} when testing RAP instead of HMA would result in increased air voids for a compacted mixture with a fixed G_{mb}. For a G_{mb} of 1.937 (corresponding G_{mb} for lowest Figure 4.3 V_a value), an increase in RAP G_{mm} of 0.012 from 2.380 to 2.392 (CIR G_{mm} increase would be slightly less than 0.012) yields a V_a increase of 0.41%. Likewise, evaluating 127 data points from (Bang et al. 2011) indicates a similar 0.012 G_{mm} increase yields a V_a increase of 0.35-0.50%. This difference in V_a as a consequence of measuring G_{mm} of RAP instead of HMA appears manageable for CIR density control, especially since it seems to consistently increase calculated air voids.

Equation 4.3 provides reasonable CIR G_{mm} predictions based on data presented herein. Equation 4.3 assumes RAP does not absorb any of the virgin binders into its pores and that the cement hydration process does not create inaccessible pore space (i.e. the volume considered in G_{mm} measurement remains constant). It also assumes that no cement paste volume change occurs during hydration. All of these assumptions are probably violated to some extent, but none of the data indicates that use of these assumptions meaningfully affects results. Validation data indicates w_{NE}/cm may not be constant for all cement dosages. Errors due to an incorrect w_{NE}/cm appear manageable but improvable with additional study.

Based on literature, T166 use for CIR is difficult to justify. However, both T269 and T331 appear to be feasible for high V_a mixtures (e.g. some CIR mixtures). The ability to vacuum seal moist specimens would allow for both G_{mb} and another property (e.g. indirect tensile or unconfined compression strength) to be measured on one specimen.

4.6 Summary and Conclusions

Currently, CIR variability appears at least partly due to lack of standard and reliable density control methods. G_{mm} and G_{mb} have remained largely undisputed as reliable means of determining asphalt density. Based on the data presented, CIR would also benefit from their use as G_{mm} provides a consistent reference density and G_{mb} encompasses the intent of other common bulk density properties in use (e.g. γ_d). G_{mm} differences for asphalt (e.g. HMA) and RAP do not appear significant enough to discourage the use of RAP G_{mm} as a reference density.

Vacuum sealing is recommended for determination of CIR G_{mm} where 100% RAP is used. For RAP G_{mm}, it provides at least as reliable measurements as T209 but with greater ease and less time. Differences between asphalt and RAP G_{mm} are consistent between D6857 and T209. Directly measuring G_{mm} of loose CIR mixtures (as opposed to compacted then broken up mixtures) is most reliable but is more difficult. The proposed CIR G_{mm} estimation equation appears reasonable and efficient, though the w_{NE}/cm concept should be investigated further.

Given the typically high CIR V_a levels from literature, G_{mb} measurement with T269 or T331 is more appropriate than T166. While T331 is recommended for most accurate results, T269 is more efficient and cost-effective and, because of the relatively consistent offset between the two methods, could be used almost interchangeably with T331. This chapter's findings indicate determining CIR G_{mm} and G_{mb}, as determined by the CoreLok® and Equation 4.3, comprise a reliable, convenient, and implementable approach to controlling density and likely reducing performance variability. This approach's ease could accommodate more frequent field testing to better control density

longitudinally as material change in the direction of traffic has been a notable hindrance to previous density control measures.

CHAPTER 5

COLD IN-PLACE RECYCLING MOISTURE-RELATED DESIGN AND CONSTRUCTION CONSIDERATIONS FOR SINGLE OR MULTIPLE COMPONENT BINDER SYSTEMS

This chapter has been submitted as a paper to a peer-reviewed journal. At the time of writing of this dissertation, the paper is in peer review.

5.1 Introduction

In recent years, cold in-place recycling (CIR) has gained momentum due to its economic, performance, and sustainability characteristics, and this momentum is likely to expand the market into, for example, higher traffic routes. To further understand how to continue improving CIR for existing applications, and expand to new applications, better techniques are needed with regard to interfacing design and construction. Moisture is one key area where design and construction are often disconnected. To this end, this chapter's objective is to evaluate moisture (and associated early-age strength/stability) aspects of CIR with the intention of better representing actual construction conditions during design within a framework that can consider hydraulic cement, bituminous emulsion, or combinations of both binders. A universal CIR design framework that can accommodate any binder or combination of binders while representing early-age field conditions has advantages for an agency, not only in its reasonable characterization of the construction

process, but also in facilitating competition and creativity in the process of selecting materials and proportions.

This chapter is part of a larger research effort to develop a universal CIR design and characterization framework which interfaces with construction. A major component of this framework is its provision for both single component binder (SCB) systems (cementitious *or* bituminous) and multiple component binder (MCB) systems (cementitious *and* bituminous). Herein, an MCB system is defined as two or more binders at >1% dosage each (by mass). Within this framework, specimens would be handled independently of binder type. In a universal framework like the one envisioned, moisture must be more carefully considered since moisture effects on performance properties are ordinarily different between cementitious and bituminous binders. Generally, laboratory design protocols favor either binder's performance with respect to moisture considerations. In the context of universal design, more appropriate moisture-related laboratory procedures may perhaps be those which represent field conditions (i.e. moisture conditions not necessarily optimal for any binder type). In light of the larger research goal, a secondary objective of this chapter is to evaluate CIR moisture from a balanced perspective considering both cementitious and bituminous binders.

To satisfy the objective, results herein are presented in three phases. Phase 1 details a Mississippi Department of Transportation (MDOT) cement CIR project on US Hwy 45 Alt (*Hwy 45Alt*) where moisture instrumentation was installed before compaction. Field and laboratory data supplemented instrumentation data collected during compaction and throughout the 14-day curing period. Phase 2 evaluates moisture's role during compaction using *Hwy 45Alt* data to provide guidance on laboratory moisture

content (*MC*) selection methods, particularly those which traditionally yield high *MC*s (e.g. Proctor methods). Phase 3 evaluates moisture during curing using *Hwy 45Alt* field data alongside laboratory evaluation of multiple curing protocols using materials from two CIR projects (*Hwy 45Alt* and *Hwy 49*).

5.2 Literature Review

5.2.1 CIR Moisture Instrumentation

Presently, CIR pavement layer instrumentation appears to be documented by only one group, University of Iowa Department of Civil and Environmental Engineering (Lee et al. 2009, Kim and Lee 2011, Woods et al. 2012). In all, five foamed asphalt and two emulsion CIR projects were instrumented with moisture and temperature sensors at various depths. ECH_2O sensors were used in Lee et al. (2009) and Kim and Lee (2011) while Woods et al. (2012) does not specify. Though not specifically documented, discussion with the corresponding author revealed sensors were installed after compaction with the factory calibration reporting volumetric *MC* (*VMC*). Laboratory experiments later correlated *VMC* to *MC* (gravimetric), which was reported.

Generally, the objective of Lee et al. (2009), Kim and Lee (2011), and Woods et al. (2012) was to evaluate CIR *MC* during curing for overlay timing purposes relative to the common 1.5% maximum moisture criteria. Sensor outputs were generally fairly constant throughout curing for all projects except for rainfall events. Sensors were sensitive to rainfall with *MC* after rainfall generally ranging from 8 to 16% with several observations near 22%. Generally, *MC* gradually decreased back to a baseline *MC* (2 to

6% varying by project), and all but one project remained above 2% moisture when overlaid.

5.2.2 Moisture as Related to Compaction

Several methods exist for selecting CIR design *MC*s: standardized *MC*s generally ranging from 2 to 5% (e.g. Mamlouk and Ayoub 1983, Khosla and Bienvenu 1996, Kim et al. 2011); Marshall methods yielding density- and strength-optimized *MC*s (e.g. Lee et al. 2001, Carter et al. 2010); and Proctor-based moisture-density relationships (e.g. Martinez et al. 2001, Kim and Lee 2006). MDOT selects design *MC* via Proctor compaction for both cement and asphalt emulsion CIR according to MDOT special provisions S.P. No. 907-425-1 (emulsion) and S.P. No. 907-499-1 (cement).

Figure 5.1 presents a CIR *MC* distribution using 108 data points from 43 references summarized in Cox and Howard (2013). Although most values are 4% or less, *MC*s up to 8% are observed. Generally, Proctor compaction yields high *MC*s as in the MDOT *Hwy 49* CIR project where optimum *MC* (*OMC*) in Chapter 2 ranged from 7.4 to 8.7%. Likewise, *Hwy 45Alt*'s Proctor-designed *OMC* was 10.9%. At these *MC*s in Chapter 2, water was expelled from Proctor and Superpave Gyratory Compactor (SGC) specimens bringing into question its necessity (Cox et al. 2015).

Chapter 2 presents laboratory concepts which this chapter seeks to validate with field demonstration. In Chapter 2, approximately 300 SGC specimens were compacted at 6 to 10% moisture (selected to bracket Proctor-determined *OMC*s) and 5 to 150 gyrations for multiple reclaimed asphalt pavement (RAP) materials and gradations stabilized with various SCB and MCB systems. SGC densities were indifferent to *MC* between 6 and

10%, and *MC*s were approximately 5.5 to 6.5% by 30 gyrations regardless of the initial *MC*. Ultimately, Chapter 2 concluded more than 6% moisture added no value to laboratory compaction.

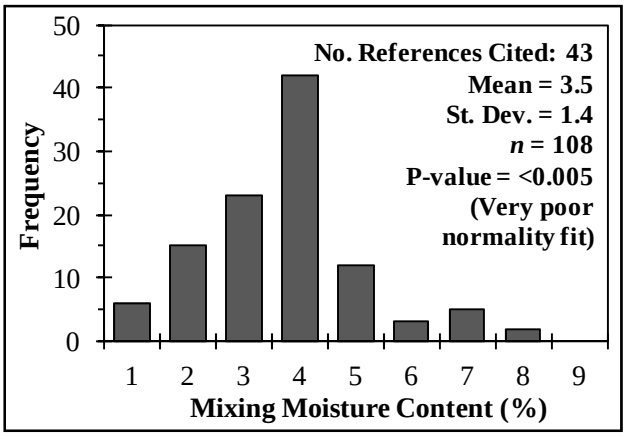

Figure 5.1 Moisture Content Values Observed in Literature

5.2.3 Moisture as Related to Curing

The key interest regarding curing is the difference in curing protocols between cementitious and bituminous binders. Bituminous-stabilized mixtures are generally cured in a dry oven at 60 °C (most common) (e.g. Mamlouk and Ayoub 1983, Lee et al. 2001, Salomon and Newcomb 2000, Cross 2002) or 40 °C (e.g. Kandhal and Koehler 1987, Lee and Kim 2003). Often, specimens are cured to constant mass to remove nearly all moisture. Cementitious-stabilized mixtures are commonly moist-cured at 23 °C (e.g. Lewis et al. 2006, Berthelot et al. 2010). Both mixtures have also been cured at room temperature and humidity, but in general, the most prevalent curing protocols represent a favorable environment for one binder and an unfavorable for the other. For a universal design approach, curing protocols would need to be standardized so that performance

properties of SCB (cementitious or bituminous) or MCB systems can be directly compared.

5.3 Materials Tested

Table 5.1 presents properties of RAP materials field-sampled from MDOT *Hwy 45Alt* and *Hwy 49* CIR projects. *Hwy 49* project details are provided in Cox et al. (2015) while *Hwy 45Alt* is discussed herein. Three binder blends were tested with each RAP using combinations of Type I portland cement, CSS-1H engineered emulsion (63.5% residue), and hydrated lime. MDOT design blends were tested as well as several arbitrary blends so that each RAP source was tested with a predominantly cement blend (SCB), predominantly emulsion blend (SCB), and a balanced blend of cement and emulsion (MCB).

Table 5.1 RAP Properties

Material ID	*Hwy 45Alt*				*Hwy 49*		
Source	Monroe Co., MS				Madison Co., MS		
$P_{AC\text{-}T164}$ (%)	5.1				4.8		
RAP G_{mm}	2.374				2.447		
Percent Passing (Bulk RAP)							
25.0 mm	100				100		
19.0 mm	99				100		
12.5 mm	89				94		
9.5 mm	73				85		
4.75 mm	41				55		
2.36 mm	25				38		
1.16 mm	18				29		
0.6 mm	13				20		
0.3 mm	8				8		
0.15 mm	6				3		
0.075 mm	4.9				1.5		
Blend	B1	B1*	B2	B3	B1	B2	B3
Cement (%)	4.2	4.2	2.1	0	4.4	2.5	0
Emulsion (%)	0	0	2	4	0	2	4
Hydrated Lime (%)	0	0	0	1	0	0	1
Water (%)	8.2	8.2	8.2	8.2	6.0	6.0	6.0
CIR G_{mm}	2.384	2.384	2.342	2.300	2.455	2.411	2.366
Prime Coat Applied?	---	Yes	---	---	---	---	---
Blend Type	D	D	A	A	D	A	D

-- $P_{AC\text{-}T164}$: Asphalt content by extraction (AASHTO T164). A blend of 85% toluene and 15% ethanol was used.
-- G_{mm}: maximum theoretical specific gravity determined via vacuum sealing (ASTM D6857) as described in Chapter 4.
-- Bulk RAP gradation is the as-received gradation. All RAP was tested at the as-received gradation.
-- Binders dosed as a percentage of dry RAP mass. Water dosed as a percentage of solids (i.e. RAP, emulsion residue, cement, and/or hydrated lime).
-- Blend B1 was tested in order to replicate Hwy 45Alt where an AE-P prime coat (0.91 L/m^2) was applied.*
-- Blend Type: "D" indicates a design blend used in the corresponding MDOT CIR project while "A" indicates a blend that was arbitrarily selected for comparison with design blends.

5.4 Experimental Program

The experimental program is divided into three subsections. Figure 5.2 illustrates key items in the overall experimental program discussed in detail in each subsection. Table 5.2 provides weather data for field and laboratory outdoor 14-day curing experiments.

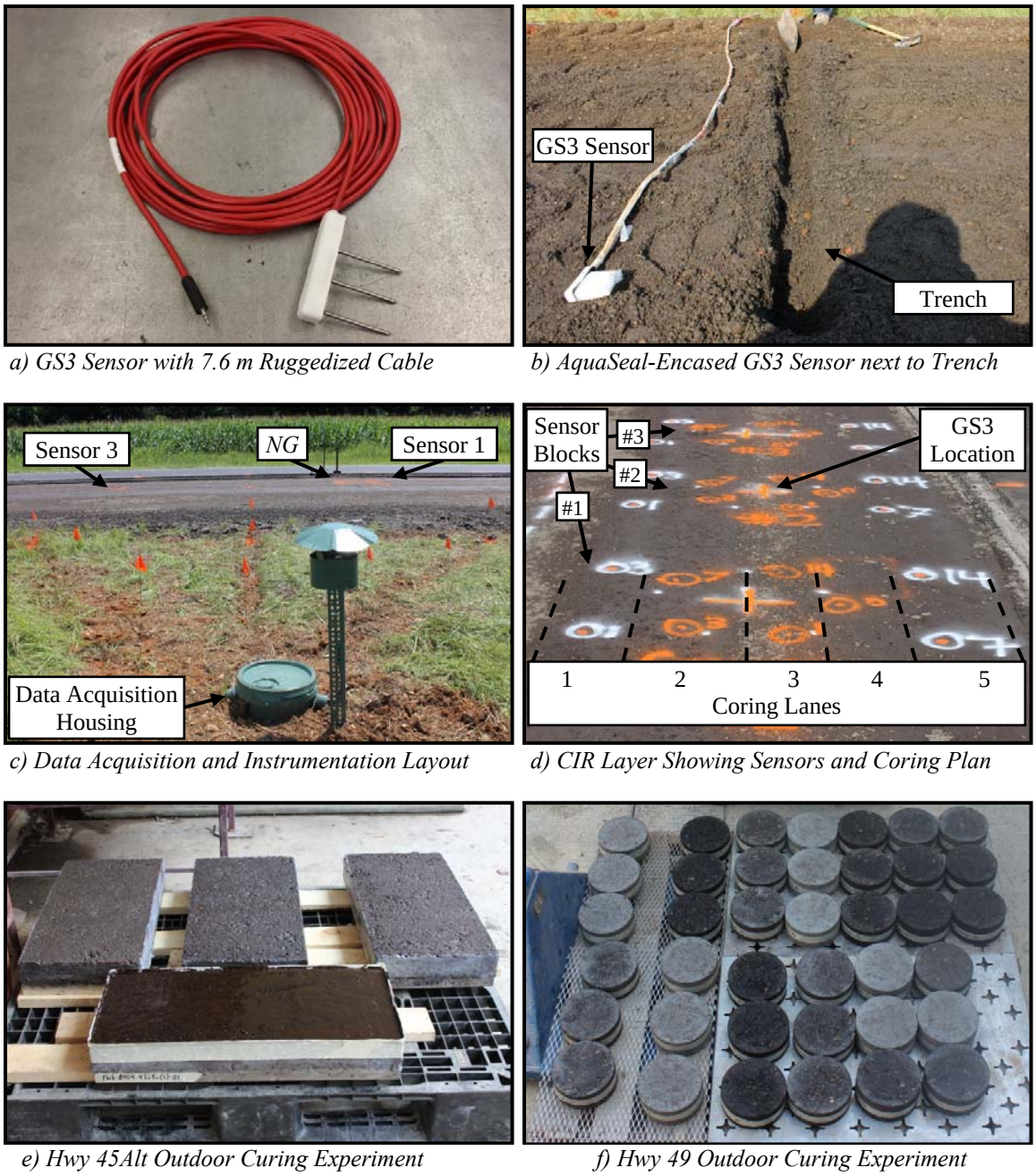

a) GS3 Sensor with 7.6 m Ruggedized Cable

b) AquaSeal-Encased GS3 Sensor next to Trench

c) Data Acquisition and Instrumentation Layout

d) CIR Layer Showing Sensors and Coring Plan

e) Hwy 45Alt Outdoor Curing Experiment

f) Hwy 49 Outdoor Curing Experiment

Figure 5.2 Photos of Field and Laboratory Testing

Table 5.2 Weather Data Summary for 14-Day Outdoor Curing

Variable			*Hwy 45Alt* - Field			*Hwy 45Alt* - Lab		*Hwy 49* - Lab	
			Weather Station	Omega HH314A	Decagon Em50	Weather Station	Omega HH314A	Weather Station	Omega HH314A
Daily Temp (°C)	Avg	Mean	24.8	27.2	36.3	24.5	27.8	24.9	27.3
		St. Dev.	2.0	2.9	2.2	2.2	0.8	1.9	3.2
	High	Mean	30.9	36.4	43.3	30.6	38.8	30.1	37.2
		St. Dev.	2.2	3.2	2.7	3.0	5.5	3.0	9.2
	Low	Mean	19.1	19.9	30.5	19.6	23.4	20.2	22.7
		St. Dev.	2.1	3.4	1.8	2.0	0.8	1.8	1.9
Daily Relative Humidity (%)	Avg	Mean	76.2	73.6	---	79.6	67.5	81.1	83.9
		St. Dev.	5.3	5.2	---	4.5	6.1	4.7	12.7
	High	Mean	98.3	99.6	---	99.2	84.7	99.6	98.0
		St. Dev.	3.1	1.0	---	2.1	3.7	1.6	3.9
	Low	Mean	46.4	40.6	---	52.4	48.0	57.8	51.3
		St. Dev.	6.5	6.4	---	9.7	11.8	9.6	28.1
Daily Wind Speed (mph)	Avg	Mean	3.8	---	---	2.4	---	2.4	---
		St. Dev.	2.0	---	---	1.3	---	0.8	---
	High	Mean	10.8	---	---	8.7	---	9.0	---
		St. Dev.	3.3	---	---	2.4	---	2.6	---
	Low	Mean	0.7	---	---	0.5	---	0.5	---
		St. Dev.	0.5	---	---	0.0	---	0.0	---
Total Precipitation (cm)			0.15	---	---	0.79	---	12.42	---

-- Weather station data is that of the nearest available weather station relative to each project location. Hwy 45Alt-Field weather station data was recorded approximately 16 miles ESE of the project. Hwy 45Alt-Lab and Hwy 49-Lab weather station data was recorded 3.6 miles WSW of the project.
-- Omega HH314A and Decagon Em50 data recorded at 30-minute intervals.
-- For Hwy 45 Alt, Omega HH314A temperatures were average of the onboard temperature probe and an additional K-type thermocouple.
-- Omega HH314A data was not available for some days due to device malfunctions. All available data is reported, and data was only considered available if data was available for the entire day.
-- Dates for outdoor curing periods: 7/24/14 to 8/7/14 (Hwy 45Alt – Field), 9/1/14 to 9/15/14 (Hwy 45Alt – Laboratory), 6/22/15 to 7/6/15 (Hwy 49 – Laboratory).

5.4.1 *Hwy 45Alt* Field Construction and Instrumentation

MDOT conducted a 9.8 km cement CIR project on *Hwy 45Alt* (9,200 ADT) in the summer of 2014. Full project details are provided in the MDOT State Study 250 report (Cox and Howard 2015a); only information pertinent to this chapter is provided herein. The existing 15 cm of asphalt over concrete pavement was recycled with 4.2% cement at 10.9% *OMC*. Compaction targeted 97% of standard Proctor dry density (1937 kg/m^3)

measured by nuclear gage (*NG*). Compacted CIR thicknesses targeted 20 cm. An AE-P emulsion prime coat was applied (0.91 L/m^2). A 14-day minimum cure was specified, which was followed by an 8.8 cm asphalt mixture overlay.

Three GS3 Ruggedized sensors with 7.6 m cables manufactured by Decagon Devices, Inc. (Figure 5.2a) were used to measure *MC* (frequency domain sensor) and temperature (thermistor) in the CIR layer. GS3 sensors use electromagnetic fields to measure the surrounding medium dielectric permittivity. Sensors are calibrated to relate signal voltage to dielectric permittivity. GS3 sensors are typically used in mineral soil applications and are shipped with a generic dielectric-to-*VMC* calibration based on a wide variety of soil types.

Given potential differences between mineral soil and CIR, GS3 sensors used herein were acquired with no calibration (i.e. sensor output was raw data which could be later calibrated). Each GS3 cable was encased in Kearney AquaSeal in attempts to seal potential moisture flow paths along the cable as well as add additional protection to the cable. Once cement and water were mixed with RAP but prior to compaction, trenches (spaced 2 m longitudinally) were dug (Figure 5.2b) then sensors were buried near the mid-depth of the loose CIR layer.

GS3 data was collected via Decagon's Em50 data logger during compaction (1 minute intervals) and curing (30 minute intervals). Ambient temperature and humidity were recorded with an Omega HH314A data logger at identical intervals. GS3 cables were buried and routed to a partially-buried 20 L plastic bucket housing both data loggers (Figure 5.2c).

During construction, loose *MC* samples were obtained at multiple points. Immediately after compaction, three 150 mm diameter cores were dry-cut (loose mixture was recovered because intact cores were not feasible) for compacted *MC*. Six cores were dry-cut at 1, 3, 7, and 14 days (24 total). Properties measured on cores were density (according to the modified AASHTO T331 protocol outlined in (*20*)), unconfined compressive strength (UCS), indirect tensile (IDT) strength (S_t) and *MC*. Figure 5.2d illustrates the coring layout relative to GS3 locations. *Hwy 45Alt* fieldwork data is used throughout Phases 1 to 3.

5.4.2 *Hwy 45Alt* Laboratory Testing

Hwy 45Alt slabs (6.3 by 29.3 by 62.4 cm) were compacted in the Linear Asphalt Compactor (LAC) (Doyle and Howard 2014) with 30 roller passes at a 2930 kPa hydraulic system pressure. Four slabs per Table 5.1 binder blend were compacted at 8.2% moisture (field *MC* immediately prior to compaction). Slab bottoms and sides were sealed with petroleum jelly to limit water evaporation to the surface.

One slab per binder blend was cured in four environments: outdoors exposed to sunlight but not rain (Figure 5.2e), 40 °C oven at approximately 35 to 50% humidity, 40 °C dry oven, and 23 °C moist curing room. These curing environments are referred to herein as outdoors (OD), humid oven (HO), dry oven (DO), and curing room (CR), respectively. One core (150 mm diameter) was dry-cut from each slab at 1, 3, 7, and 14 days (four cores can be cut from one slab) and tested for *MC*, density, and S_t. Results are presented in Phase 3.

5.4.3 *Hwy 49* Laboratory Testing

A second curing experiment was conducted with *Hwy 49* at three binder blends (Table 5.1). Specimens (150 mm diameter) were compacted 30 gyrations with 6% *MC* as recommended by Cox et al. (2015). Specimens were cured 3, 7, and 14 days with the OD, HO, and DO protocols. CR and 1-day curing were not considered based on *Hwy 45Alt* results presented later. Timing was coordinated so that *Hwy 49* and *Hwy 45Alt* OD curing conditions were similar. *Hwy 49* differed in that specimens were not sealed but were cured traditionally with all sides exposed to air.

Specimens were tested for *MC*, density, and S_t as with *Hwy 45Alt*. APA rut testing was also conducted as well as instrumented IDT testing to obtain strain measurements for fracture energy (FE) calculation (area under stress-strain curve). APA tests were conducted according to AASHTO T340 where all specimens were conditioned 6 hours (T340 allows 6 to 24 hours). FE protocols were similar, but slightly refined, relative to those in Chapter 3 (Cox and Howard 2015b) where FE's potential usefulness in distinguishing CIR cracking characteristics across a wide array of binders. Results are presented in Phase 3.

5.5 Results

5.5.1 Phase 1: *Hwy 45Alt*

Figure 5.3 presents unprocessed GS3 data (analog-to-digital counts, ADC). Figure 5.3a plots vertical lines for each roller pass crossing GS3 sensors. In all, 46 roller passes were required to attain 1879 kg/m^3 dry density by *NG* (for comparison, laboratory SGC compaction required 43 gyrations, on average, to reach field densities). Densities were

recorded after each roller pass except for some cases where consecutive passes were insufficiently spaced to facilitate a reading.

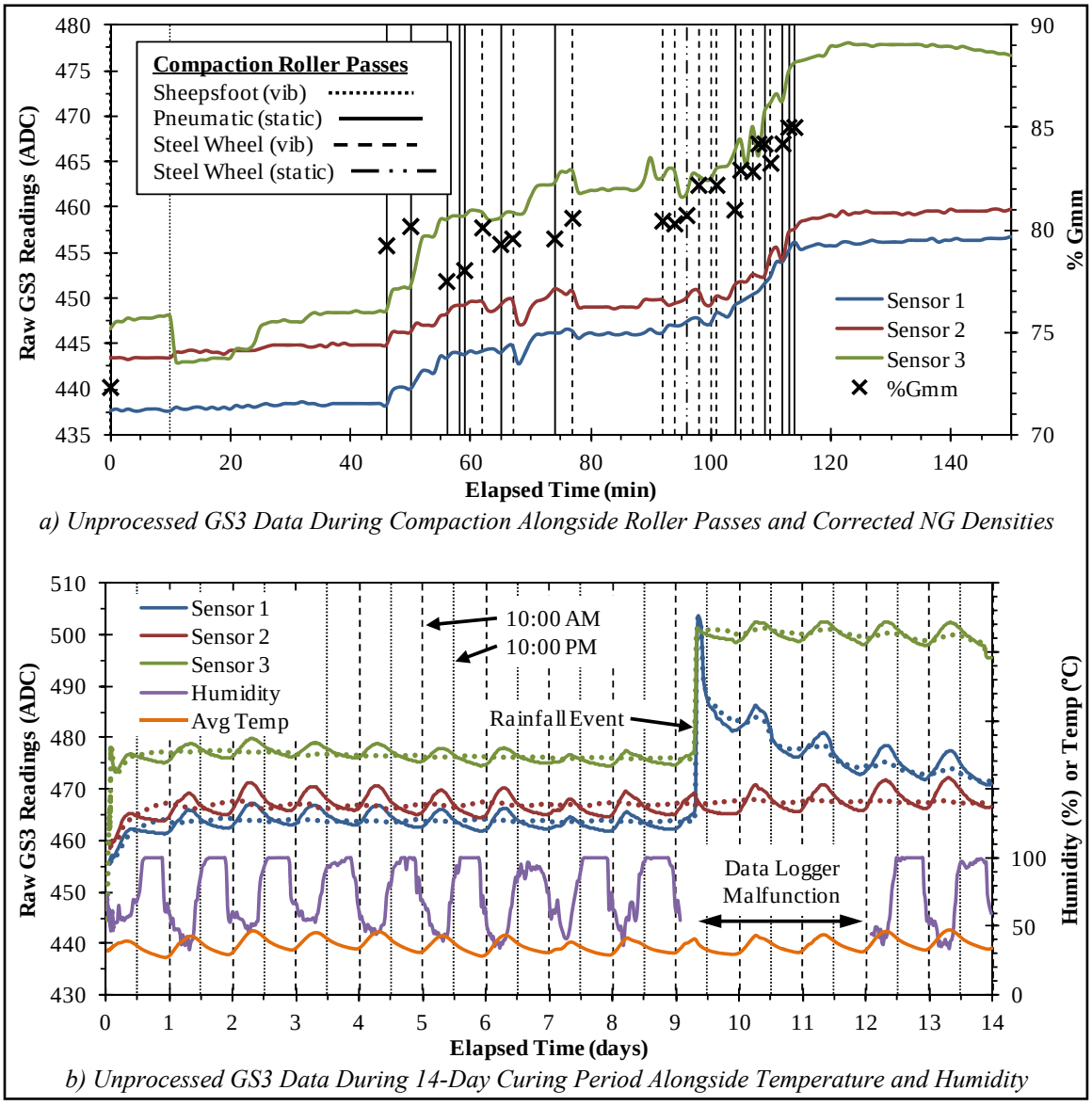

Figure 5.3 Unprocessed GS3 Moisture Data from *Hwy 45Alt*

The final *NG* density was 1885 kg/m^3; however, laboratory-measured dry density of cores averaged 2026 kg/m^3. Therefore, all *NG* densities were corrected by a simple

offset factor of 141 kg/m^3. Corrected densities are plotted in Figure 5.3a as a percentage of G_{mm}. Final densities were 85% of G_{mm}, or 15% air voids (V_a). Figure 5.3a shows GS3 readings are directly proportional to roller passes and density changes.

Figure 5.3b presents GS3 raw data and temperature as well as ambient humidity throughout the first 14 days of curing. Oscillations corresponding to daily temperature fluctuations are observed in GS3 data (also observed in Lee et al. (2009), Kim and Lee (2011), and Woods et al. (2012)). Temperature corrections were applied according to Equation 5.1 which is similar to electrical conductivity temperature corrections in Kizito et al. (2008). Attempts were made to systematically determine β, but no trends were observed. Instead, β was adjusted for each sensor until smoothing of the oscillations was visually optimized. Figure 5.3b dotted lines are temperature-corrected readings.

$$GS3_{i,corrected} = GS3_i + \beta(T_r - T_i) \tag{5.1}$$

Where,

$GS3_{i,corrected}$ = temperature-corrected GS3 reading at time i, ADC

$GS3_i$ = observed raw GS3 reading at time i, ADC

β = fitted constant (0.31, 0.40, and 0.24 for sensors 1, 2, and 3, respectively)

T_r = reference temperature, °C (14-day average GS3 temperature = 35.8 °C)

T_i = temperature at time i, °C

As in Lee et al. (2009), Kim and Lee (2011), and Woods et al. (2012), GS3 sensors detected rainfall. Sensor 2's location did not appear infiltrated by water based on

Figure 5.3b. Water appeared to infiltrate sensor 1's location but was able to drain over time. Water appeared to infiltrate sensor 3's location but was not able to drain well. Aside from rainfall, the most notable change in GS3 readings occurred within 24 hours after construction and is thought to be related to cement setting reactions.

To calibrate raw GS3 output to *MC*, raw GS3 readings were converted to bulk dielectric permittivity (ε_{bulk}) using calibration data supplied by Decagon. Observed GS3 readings ranged from 430 to 510; in this range, a second-order polynomial describes the ADC-to-dielectric relationship (Equation 5.2) satisfactorily ($R^2 = 0.999$).

$$\varepsilon_{bulk} = 8.8\times10^{-5}\left(GS3_{i,corrected}\right)^2 - 2.4\times10^{-2}\left(GS3_{i,corrected}\right) - 1.68 \tag{5.2}$$

The complex refractive index model (CRIM) (Leng 2011) was used to derive *MC* from ε_{bulk}. Essentially, CRIM (Equation 5.3) calculates weighted averages of a certain power of constituent material dielectric constants based on volume proportions. Volumetric equations (discussed further in Phase 2) were substituted to obtain Equation 5.4. Rearranging for *MC* yields Equation 5.5.

$$\varepsilon_{bulk}^{\,1/\alpha} = \varepsilon_{CIR}^{\,1/\alpha} V_{CIR} + \varepsilon_{water}^{\,1/\alpha} V_{water} + \varepsilon_{air}^{\,1/\alpha} V_{air} \tag{5.3}$$

$$\varepsilon_{bulk}^{\,1/\alpha} = \varepsilon_{CIR}^{\,1/\alpha} \frac{G_{mb}}{G_{mm}} + \varepsilon_{water}^{\,1/\alpha} \frac{G_{mb}\omega}{G_w} + \varepsilon_{air}^{\,1/\alpha}\left(1 - \frac{G_{mb}}{G_{mm}} - \frac{G_{mb}\omega}{G_w}\right) \tag{5.4}$$

$$\omega = \frac{G_w\left(\varepsilon_{bulk}^{1/\alpha} - \varepsilon_{CIR}^{1/\alpha}\frac{G_{mb}}{G_{mm}} - \varepsilon_{air}^{1/\alpha}\left(1-\frac{G_{mb}}{G_{mm}}\right)\right)}{G_{mb}\left(\varepsilon_{water}^{1/\alpha} - \varepsilon_{air}^{1/\alpha}\right)} \quad (5.5)$$

Where,

α = empirical power parameter equal to 2 in CRIM

ε_{CIR} = CIR dielectric constant

V_{CIR} = CIR volume fraction

ε_{water} = dielectric constant of water (74.7 at T_r)

V_{water} = water volume

ε_{air} = dielectric constant of air (1)

V_{air} = air volume (equal to V_a if V_{water} is zero)

G_{mb} = bulk mixture specific gravity

ω = gravimetric moisture content (also, MC)

G_w = water specific gravity (0.994 at T_r)

In Equation 5.5, ε_{CIR} is unknown; however, since MC and G_{mb} are known where direct MCs were obtained, ε_{CIR} can be iteratively estimated. Excel's Solver function was used to calculate ε_{CIR} for each GS3 (note that, because ε_{water} and G_w are temperature-dependent, their values at T_r were used). For sensors 1 to 3, ε_{CIR} was 2.77, 2.88, and 3.53, respectively. Although ε_{CIR} would generally be constant, using best-fit ε_{CIR} values was deemed reasonable since ε_{CIR} for each sensor was fit to average direct MC measurements. With ε_{CIR} estimated, MC was calculated where G_{mb} was known.

Figure 5.4 presents processed GS3 data. Figure 5.4a shows GS3 *MC* was, for all meaningful purposes, constant during compaction despite *MC* immediately before compaction being 8.2%. Figure 5.3a unprocessed data appeared to increase during compaction, but Figure 5.4a indicates these increases were related to density changes (accounted for in Equation 5.5) not *MC* changes.

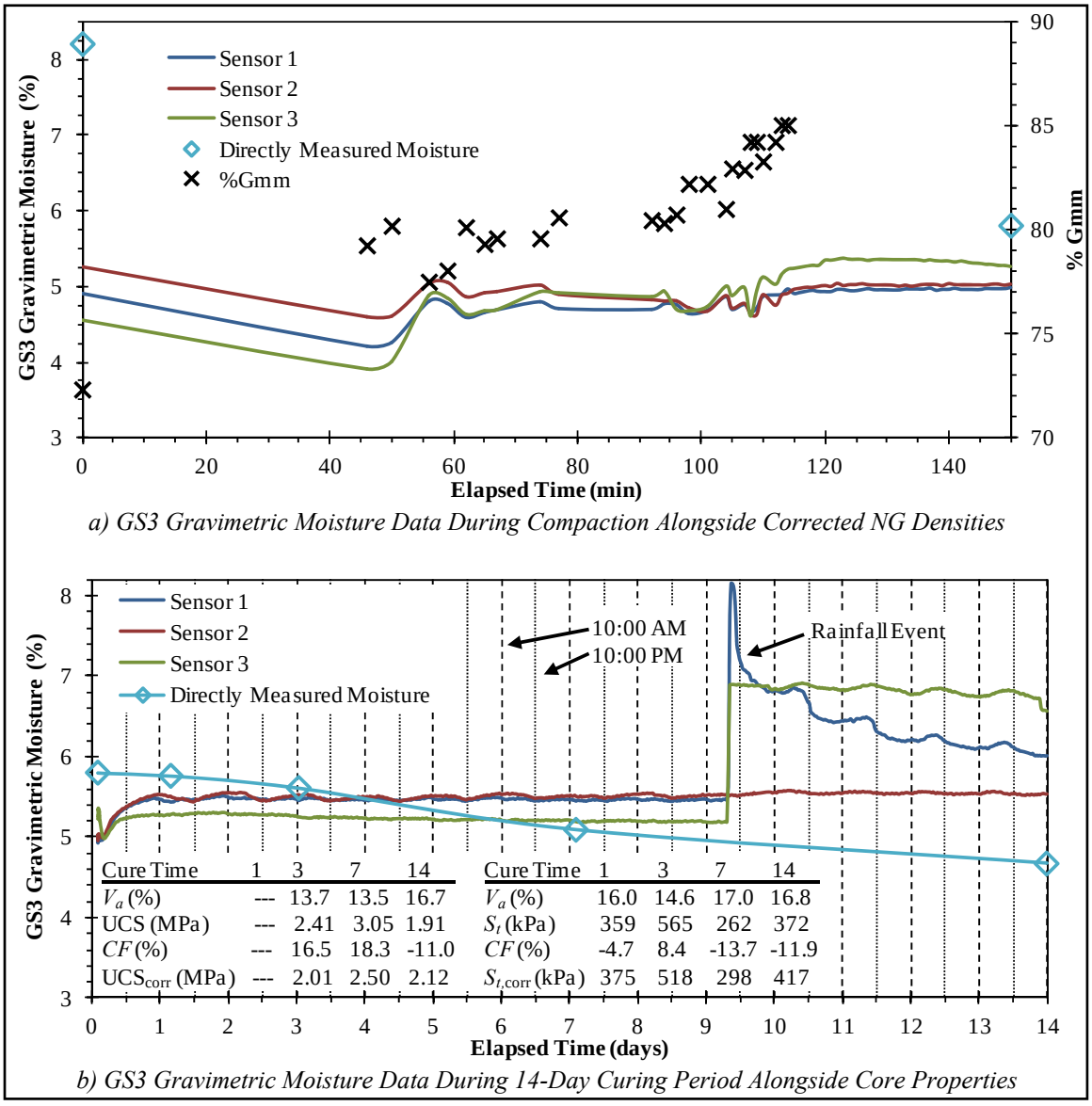

Figure 5.4 Processed GS3 Moisture Data from *Hwy 45Alt*

Figure 5.4b shows GS3 *MC* and directly-measured core properties. GS3 *MC* was mostly constant through curing (excluding exceptions previously mentioned) and did not follow directly-measured *MC*s. GS3 measurement radius is approximately 2 cm, meaning GS3 data represents the middle 4 cm of the 20 cm layer; whereas, directly-measured *MC*s nearly represented the entire layer. Therefore, directly-measured *MC*s may have been affected by drying near the layer's surface which was outside GS3 measurement range.

Note that intact 0-day cores for *MC* were not successfully obtained. Coring attempts broke the freshly-compacted layer into loose mix, and heat produced in coring appeared to dry the mix yielding an average 4.8% *MC*, on the order of *MC* measured at 14 days. Alternatively, a third-order polynomial was fit to 1- to 14-day *MC*s ($R^2 > 0.99$), and the 0-day *MC* (0.079 days actual) was calculated to be 5.8%. Given the small change in *MC* over 14 days, omitting the 0-day *MC* affected GS3 *MC* by 0.1 to 0.2%; therefore, this approach seemed reasonable.

UC strength (UCS) and S_t did not progressively increase with time, which appears partly due to V_a variability. An analysis of variance (ANOVA) determined V_a's were statistically different between coring lanes (transverse direction, Figure 5.2d). Therefore, SGC-compacted UCS versus V_a data (summarized by Equation 5.6, $R^2 = 0.99$) was used to normalize V_a effects. Relative correction factors (*CF*) were determined based on the difference between Figure 5.4b V_a's and the *Hwy 45Alt* 15.5% average V_a. Although fairly approximate, S_t values were corrected using the same procedure since no laboratory IDT testing was available to perform corrections.

$$UCS_{MPa} = 0.0243 \times V_a^{\,2} - 1.004 \times V_a + 12.394 \qquad (5.6)$$

5.5.2 Phase 2: Moisture Considerations during Compaction

Figure 5.4a shows directly-measured *MC* dropped from 8.2% to 5.8% during compaction. This agrees with findings in Chapter 2. For example, *MC* dropped from 7.9% to 5.5% for *Hwy 49*-B1 when SGC-compacted 30 gyrations.

For practical purposes, GS3 *MC*s did not change during compaction and were around 5%, which is slightly low compared to directly-measured *MC*s. Regardless, GS3 *MC* slopes are flat, suggesting a considerable amount of moisture is expelled early during compaction. GS3 data aligns with findings in Chapter 2 that *MC* was greatly reduced early in SGC compaction, suggesting this trend is also applicable to field compaction.

Figure 5.5 presents an idealized phase diagram to volumetrically investigate compactibility as a function of *MC*. Consider *Hwy 45Alt*'s initial 8.2% *MC*. Suppose W_{CIR} is 100 g (41.9 cm^3 with 2.384 G_{mm}), then W_w equals 8.2 g (approximately 8.2 cm^3). If 100% saturation is assumed during compaction (i.e. all voids between CIR particles are water-filled), 16.4% of V_{total} would be water, which, from a dry density perspective, would correspond to 16.4% V_{air}. Therefore, the minimum achievable V_a is 16.4% if *MC* truly remains at 8.2% throughout compaction and 100% saturation is assumed. However, *Hwy 45Alt* V_a's averaged 15.5% and were as low as 13.5%, which would not be possible unless water was expelled during compaction.

From a different perspective, the maximum allowable *MC* to permit 15.5% average V_a would be 7.7% (6.5% for the lowest-observed 13.5% value) under the ideal 100% saturation assumption. As a reference, additional analysis of data used in Chapter 2 showed saturation values immediately following SGC compaction generally ranged from 50 to 60%. Although field and laboratory saturation levels likely differ, the exercise

provides insight to reasonable degrees of saturation to be expected. Therefore, with saturation values likely closer to 50 to 60% rather than 100%, the 5.8% directly-measured *MC* after compaction does not appear unreasonable.

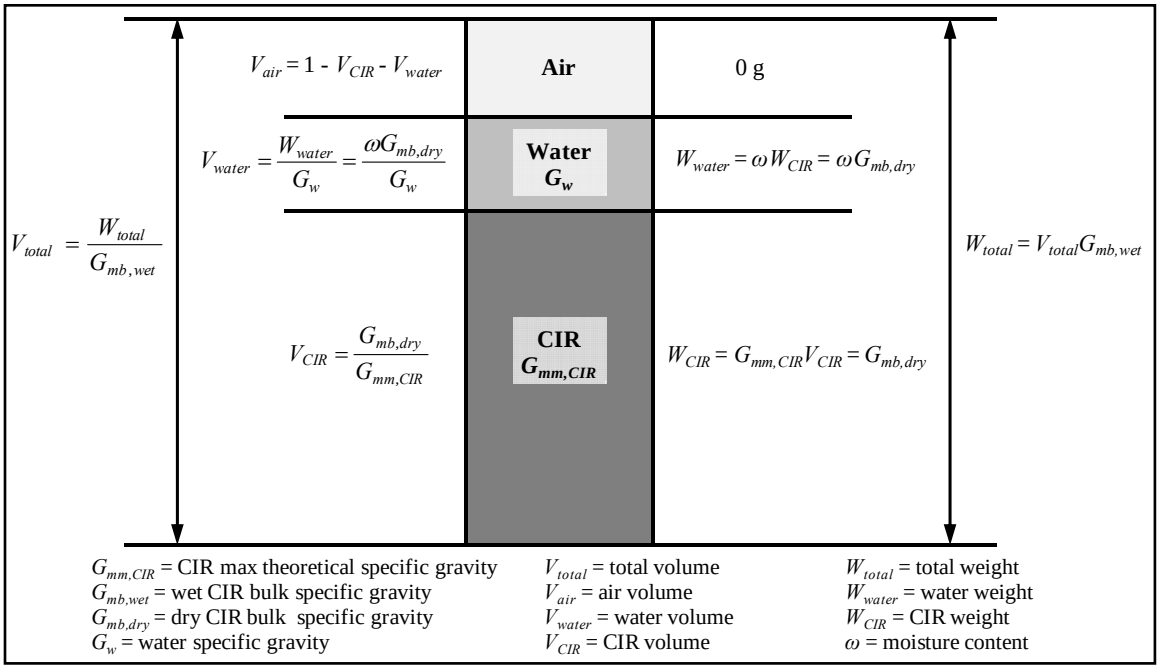

Figure 5.5 CIR Phase Diagram

Other caveats must also be considered. For example, it is almost certain some moisture would be present in the pavement prior to reclamation. Most of this moisture would exist in the void structure, but some may be absorbed into RAP pores (i.e. volume considered within G_{mm}). This would effectively open voids in the mixture, potentially allowing it to take on slightly more water for a given V_{air} than volumetrics might indicate. Effects of these factors are likely small and, for the calculations herein, would be offset by errors with the 100% saturation assumption, suggesting the phase diagram remains a useful theoretical or estimation tool. Ultimately, phase diagram and *Hwy 45Alt* findings

generally agree with Chapter 2 in discouraging the need for Proctor-level *MC*s for CIR compaction, consequently supporting standardized-*MC* practices as in Mamlouk and Ayoub (1983), Khosla and Bienvenu (1996), and Kim et al. (2011).

5.5.3 Moisture Considerations during Curing

Figure 5.6 presents *Hwy 45Alt* laboratory curing experiment results. Average V_a's for B1, B1*, B2, and B3 were 15.6%, 15.2%, 14.2%, and 13.2%, respectively. B1 and B1* slab V_a's were similar to field V_a's. Figure 5.6 dashed bars represent values from *Hwy 45Alt* field cores. Figure 5.6 shows *MC* decreased and S_t increased over time for nearly all curing environments and binder blends.

Figure 5.7 presents *Hwy 49* laboratory curing experiment results. Figure 5.7a displays similar *MC* trends as Figure 5.6a except Figure 5.7a *MC*s are approximately five times lower on average, likely because moisture loss was not restricted to the top surface. However, *MC*s were not expected to be as low as those in Figure 5.7a when developing this experiment.

Figure 5.7b shows B1 S_t change over time was not as pronounced as in Figure 5.6b, likely because less moisture was available throughout curing for cement hydration. Overall, OD and DO curing appeared closely related while HO curing generally yielded lower S_t values.

Figure 5.7c and 5.7d show FE and APA rut depth increase considerably from B1 to B3 as in Chapter 3 (Cox and Howard 2015b). Curing protocol differences with respect to FE and APA results are difficult to identify visually. Overall, *Hwy 49 MC*s were low

regardless of curing time or protocol resulting in few meaningful differences in performance properties.

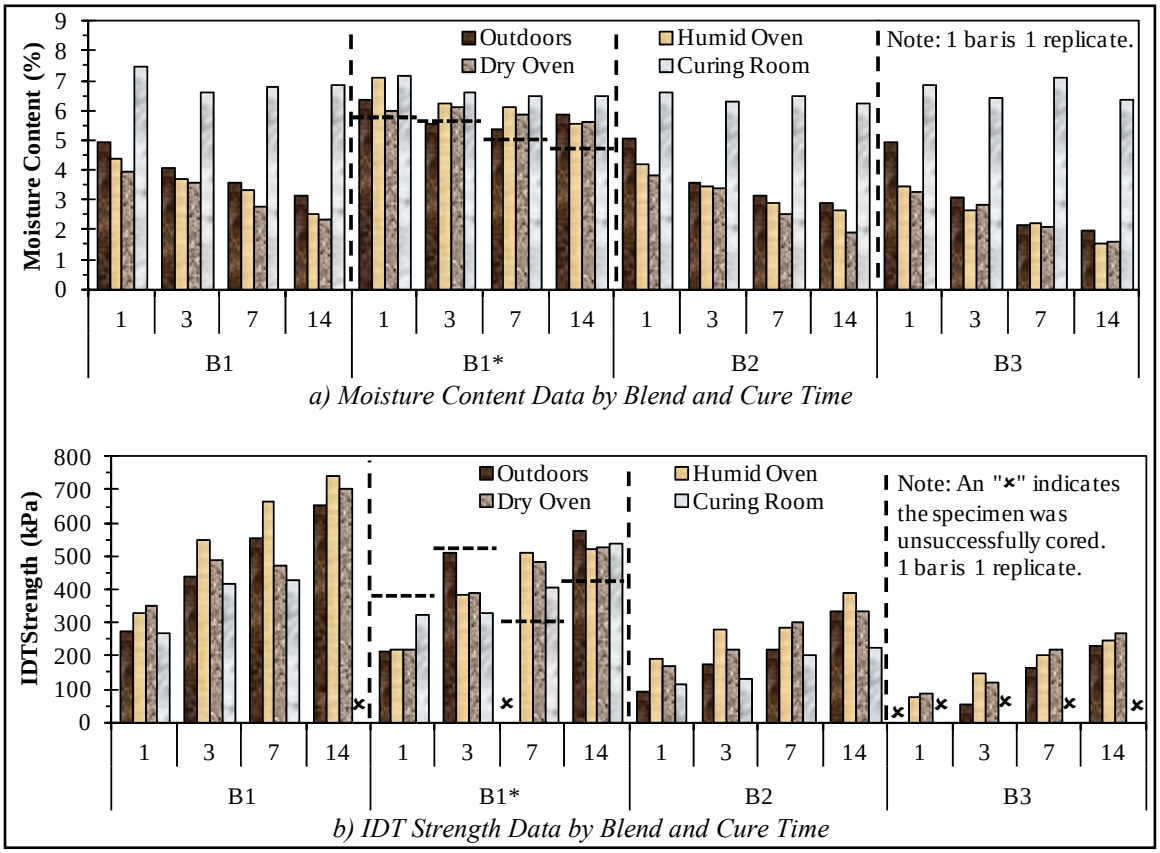

Figure 5.6 *Hwy 45Alt* Laboratory Curing Experiment Results

Figure 5.8 compares curing protocols studied to OD curing using Figure 5.6 and 5.7 data. Figures 5.8a and 5.8b discourage CR curing in the context of a universal design framework. Note that the CR S_t trendline is misleading because all B3 CR cores were not able to be successfully obtained and are therefore not represented. Aside from CR, Figure 5.8 suggests HO and DO curing reasonably approximate OD curing and are not greatly different from each other.

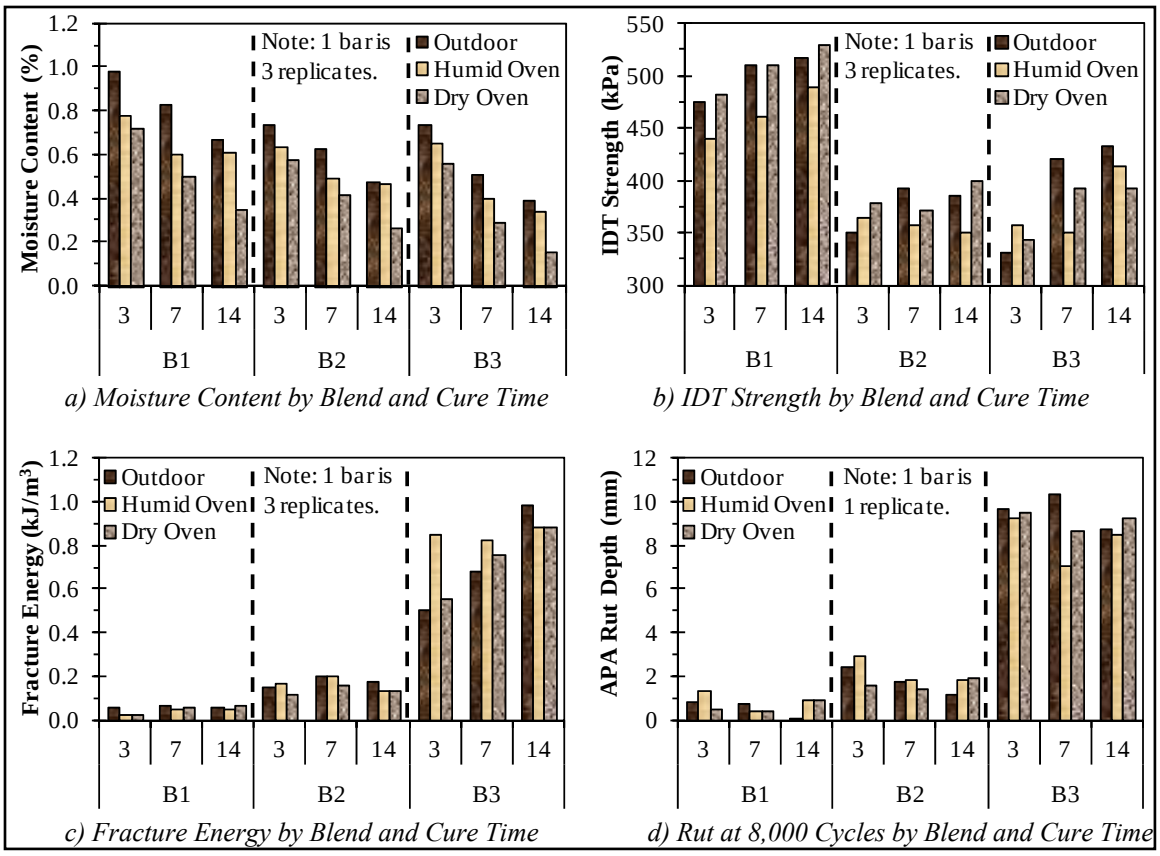

Figure 5.7 *Hwy 49* Laboratory Curing Experiment Results

Two-factor randomized complete bock ANOVAs were conducted for all Figure 5.8 data except CR data. Data was blocked by cure time since results were expected to vary by cure time; curing method and binder blend were the two factors studied for each response variable (e.g. *MC*, S_t). ANOVAs were significant (*p-value* < 0.05) in all cases; curing method and binder blend did not interact except in Figure 8*c* data.

Multiple comparisons rankings of curing methods (shown in Figure 5.8) were conducted using the LSMEANS statement in PROC GLM in SAS 9.3. Curing methods are ranked by response variable mean values (in parentheses) and are assigned *t*-Group letters. Curing methods assigned different letters are significantly different while those

with identical letters are not. Where interaction was encountered (Figure 5.8c), mean *MC* values for each blend are shown. While *t*-Group letters are not applicable in Figure 5.8c, curing methods did significantly rank in the order presented.

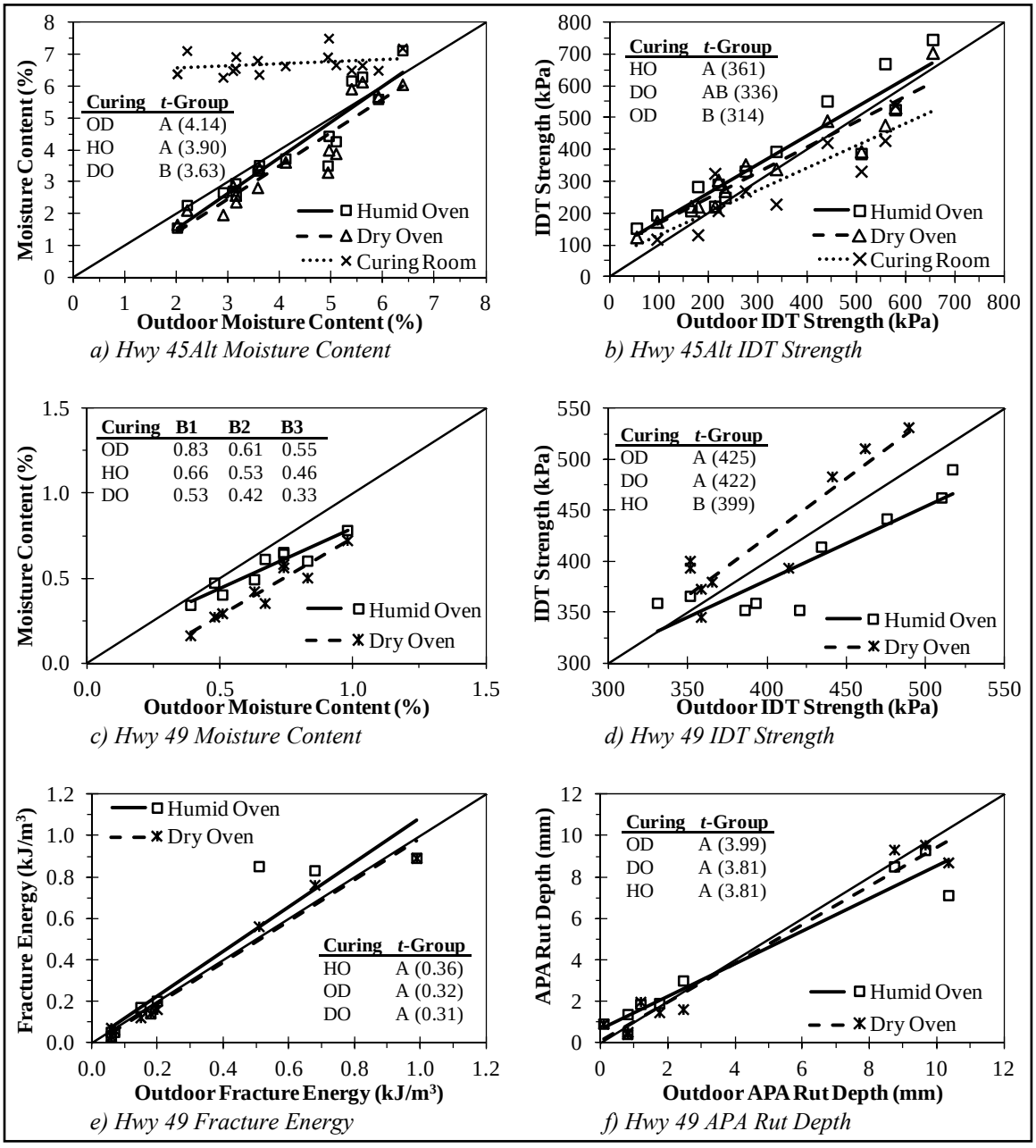

Figure 5.8 Comparison of Various Curing Methods to Outdoor Curing

OD curing always ranked highest with respect to *MC*. With respect to S_t, curing method rankings changed between *Hwy 45Alt* and *Hwy 49*. In both cases, DO and OD curing were not significantly different from each other. Curing methods were not significantly different with respect to FE and APA results. Overall, statistical analysis did not identify a single curing method which best represents outdoor curing in all categories studied, implying humid and dry oven curing are both options worth considering.

5.6 Summary and Conclusions

Field testing and instrumentation of a cement CIR project was used in conjunction with laboratory testing to investigate two aspects of CIR design and construction which involve moisture: compaction and curing. Special consideration was given to moisture as it would relate to either cementitious or bituminous SCB systems as well as cementitious and bituminous MCB systems. Key conclusions are:

- Moisture sensors were successfully installed in a field CIR project and were able to obtain data not only during curing but also during compaction.
- *Hwy 45Alt* field *MC*s (directly-measured and GS3-measured) support previous laboratory findings that unnecessary excess water is expelled early during compaction. Volumetric calculations agree and suggest excess moisture, if not able to escape, could hinder compaction. Results herein affirm the recommended 6% maximum *MC* in Chapter 2. As in Chapter 2, Proctor-based *MC* determination for CIR is discouraged. Use of a fixed CIR *MC* appears reasonable and would allow laboratory design efforts to primarily focus on selection of appropriate binder blends.

- Humid oven curing (40 °C and 35 to 50% humidity) and dry oven curing (40 °C) appear to reasonably represent outdoor curing conditions in the Mississippi summer and were not greatly different from each other. Either humid or dry oven curing are candidates for universal design; however, given field conditions (specifically in the southeast US) are humid (Table 5.2), the humid oven appears a more logical choice at present for use in a universal CIR design framework.

CHAPTER 6

A CASE STUDY OF HIGH-TRAFFIC IN-PLACE RECYCLING ON US HIGHWAY 49: MULTI-YEAR PERFORMANCE ASSESSMENT

This chapter has been submitted as a case study paper to a peer-reviewed journal. At the time of writing of this dissertation, the paper is in peer review.

6.1 Introduction

The American Society of Civil Engineers (ASCE) has recently promoted a sustainability triple bottom line encompassing economics, environment, and social well-being. In-service performance of highways certainly affects all triple bottom line aspects. In-place recycling of existing pavements is one rehabilitation technique with potential to positively impact the triple bottom line. Relative to traditional construction, recycling pavements in place usually reduces emissions and costs since fewer virgin materials are used and transported. Likewise, social benefits often include shorter construction delays relative to traditional reconstruction and extended performance relative to other rehabilitation techniques (e.g. overlay, mill-and-fill).

Cold in-place recycling (CIR) and full-depth reclamation (FDR) are the focus of this chapter. Herein, CIR is defined as the recycling of asphalt concrete layers only, while FDR involves recycling underlying layers as well. Both are mature concepts which have existed for decades. While mature, however, in-place recycling should not be mistaken

for a fully-developed technology, especially since in-place recycling markets have been expanding in recent years to include higher-traffic routes. Hansen (2015) discusses the state of the $425 billion (2006 dollars) US highway system stating, among other details, that 14% of major US roads are in poor condition. With the highway system operating in this context, it is reasonable to expect in-place recycling markets to continue expanding.

In 2010, the Mississippi Department of Transportation (MDOT) conducted FDR, CIR, and traditional construction on high-traffic (average annual daily traffic (AADT) of 12,000) US Highway 49 (US-49) in Madison County, MS. All FDR was cement-stabilized while some CIR sections were cement-stabilized and others were emulsion-stabilized. Full-depth hot-mix asphalt (HMA) and composite HMA over jointed concrete pavement (JCP) (further denoted composite) structures were present prior to rehabilitation, resulting in various as-constructed cross-sections and recycling depths.

Given the variations present, US-49 provided a unique opportunity to evaluate in-place recycling in the context of the issues described in previous paragraphs. To this end, the primary objective of this chapter is to present a case study of US-49 construction and performance through 53 months of service (nominally 4.5 years). US-49 performance is characterized herein using road profiler distress survey data, pavement core properties, and falling weight deflectometer (FWD) data. Note that core properties and FWD data for FDR portions of US-49 are provided in Howard and Cox (2016) and reference is made to this document where pertinent.

A secondary objective is to provide a path forward for in-place recycling using lessons learned from US-49. Specifically, guidance is presented in the context of improving the triple bottom line by better optimizing in-place recycling binders,

especially for CIR which should not be mistaken for a fully-optimized technology in regards to economics and performance. Traditionally, two binder types, cementitious and bituminous, are used for in-place recycling. Cementitious binders are mostly used for FDR but have been used for CIR in some cases (e.g. US-49), and bituminous binders are most commonly used for CIR (Cox and Howard 2013).

Generally, most CIR design methods are binder-type-specific, resulting in designs which utilize only one binder type (in some cases a small amount of a secondary binder type is used but is generally not fully represented during design). This practice may result in unbalanced designs with respect to expected distresses (or individual components of the triple bottom line). For example, a cement CIR design may have excess rutting resistance but insufficient capacity with respect to cracking. Practically, there is little need for reserve capacity of one distress when other distresses are well past capacity (e.g. no rutting but cracking which exceeds design criteria).

Ideally, a CIR design with just enough capacity within each distress type to satisfy design criteria would yield a more economical and optimized design with respect to overall performance and the triple bottom line. This result could be achievable with more balanced blending of binder types (e.g. 2.5% portland cement with 2% emulsion), though this is largely neglected in practice due to the current lack of universal design protocols which accommodate both binder types. The US-49 case study, having both cement and emulsion CIR sections, provides field data useful in considering the MCB design approach and its potential regarding CIR cost and performance optimization.

6.2 Literature Review

6.2.1 Traffic Levels

Figure 6.1 presents traffic level histograms for CIR and FDR projects using data reported in Cox and Howard (2013). Considerably more CIR values were available than FDR values, but observed trends are similar. Nearly all in-place recycling projects were conducted on routes with daily traffic levels of 6,000 or less (i.e. half that of US-49 or less).

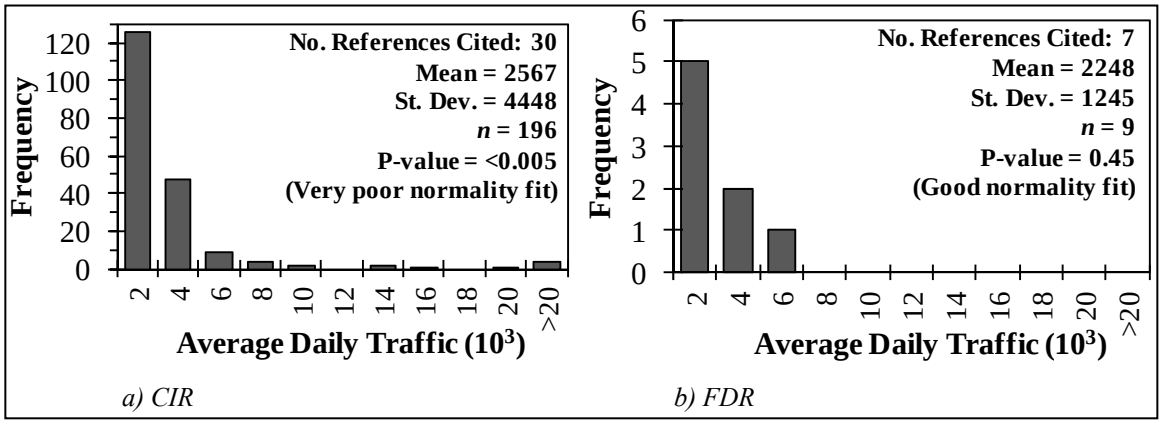

Figure 6.1 Traffic Distribution on CIR and FDR Projects

Several CIR projects were documented at very high traffic levels relative to the average (approximately 2,500). While definitions vary, Mamlouk (1991) referred to low-volume roads as those with 400 AADT or less; similarly, Kim et al (2010) considered any route over 800 AADT to be high-traffic. At 12,000 AADT, US-49 is among a small sect of high-traffic projects.

6.2.2 Distress Surveys

Kim et al. (2010) conducted short-term and long-term (average ages of 4.6 and 14.5 years, respectively) distress surveys on 26 CIR pavements in Iowa. Average pavement condition indices (PCIs) were 91 and 74, respectively, which typically rate as good and satisfactory (e.g. Shahin 2006). Approximately 60% of short-term PCIs were between 90 and 100, followed by 27% between 80 and 90 (satisfactory to good rating). Long-term PCIs were fairly evenly dispersed from 48 to 98 (poor to good rating).

6.2.3 Falling Weight Deflectometer Testing

Table 6.1 presents FWD data (ranked by effective structural number (SN_{eff}) as defined in AASHTO (1993)) obtained from literature to provide a frame of reference for FWD data presented herein. Multiple route types (e.g. county road, interstate) and structures (e.g. composite, FDR) were included to provide a relatively broad data set; however, specific details relating to each Table 1 entry are largely omitted as they are not the focus.

Efforts were made to ensure values were consistently reported (e.g. deflection under the center of loading (d_0) normalized to 40 kN and corrected to 20 °C), though this was not possible in some cases. For example, Kim et al. (2010) and Noureldin et al. (2005) reported FWD data for 18 CIR projects and 5 interstates, respectively. For brevity, only minimum (min), maximum (max), and average (avg) or median values were shown for these references. Overall, SN_{eff} and d_0 values range from 1.1 to 8.9 and 2.0 to 48 mils, respectively. While approximate when multiple studies are coupled together and some

details are not always uniformly handled or available, the general relationship between SN_{eff} and d_0 is reasonable for purposes of this chapter's evaluation.

Table 6.1 FWD Literature Summary

Source	State	Route Type and Description	D_{HMA} (cm)	D_p (cm)	M_R (MPa)	d_0 (mils)	SN_{eff}
Howard and Warren (2009)	AR	Frontage road	6	22	77	48	1.1[c]
Howard and Warren (2009)	AR	Frontage road	6	32	77	34	1.8[c]
Noureldin et al. (2005)	IN	State route	20	37	28	14	2.9
Noureldin et al. (2005)	IN	State route	28	48	42	10	5.0
Kim et al. (2010)	IA	Low-volume road, emulsion CIR (max)	5	37	17	22	5.2[c]
Chen et al. (2011)	TX	State route, CTB, Un-cracked	8	56	154	7.9	5.2[c]
Noureldin et al. (2005)	IN	Multiple interstates (min)	20	49	42	4.8	5.5
Smith et al. (2008)	GA	County road, Lime-stabilized FDR	8	44	251[c]	3.8	6.1[c]
Kim et al. (2010)	IA	Low-volume road, emulsion CIR (median)	5	36	27	13	6.3[c]
Chen et al. (2011)	TX	State route, CTB, Cracked	8	56	154	5.4	6.5[c]
Noureldin et al. (2005)	IN	US Highway	25	60	63	4.0	6.5
Noureldin et al. (2005)	IN	Multiple interstates (avg)	28	62	63	3.1	6.9
Zhang et al. (2008)	LA	Multiple HMA pavements	*n/a*	*n/a*	47	7.0	7.3
Chen (2007)	TX	Farm to Market, Lime-stabilized base	4	55	105[a]	6.0	7.3[c]
Howard and Cox (2016)	MS	US Highway, cement FDR (avg)	11	52	216	3.4	7.8
Zhang et al. (2008)	LA	Multiple composite pavements	*n/a*	*n/a*	45	5.3	8.2
Noureldin et al. (2005)	IN	Multiple interstates (max)	38	76	77	2.0	8.5
Kim et al. (2010)	IA	Low-volume road, emulsion CIR (min)	11	72	65	6.5	8.9[c]

a) M_R was not provided in Chen (2007); default value of 105 MPa was used to calculate SN_{eff}.
b) Chen (2007) reported d_0 for a 44.5 kN (10 kip) loading; therefore, SN_{eff} calculations use 44.5 kN as well.
c) Values calculated according to AASHTO (1993) Appendix L5 by the author of this dissertation.
-- D_{HMA} = asphalt concrete thickness -- D_p = total pavement thickness
-- M_R = subgrade resilient modulus -- d_0 = deflection under center of loading
-- SN_{eff} = effective structural number -- CTB = cement-treated base

6.3 US-49 Construction

6.3.1 Project and Site Information

Since CIR and FDR were largely untested by MDOT prior to US-49, construction details of US-49 (Federal Aid Project number NH-008-03(032)) were documented by MDOT in Strickland (2010). The US-49 project was constructed on a 14.8 km section of four-lane divided highway where AADT was 12,000 at time of construction. The

approximate bid price and final project cost were around $15 and $16.5 million, respectively.

Pre-existing pavement cross-sections were full-depth HMA and composite HMA over JCP. Original concrete slabs and full-depth HMA sections were constructed in 1959 and 1980, respectively. Distresses such as longitudinal cracking, transverse cracking with spalling, rutting, potholes, and patching were present on US-49 prior to recycling. In MDOT's assessment, US-49 was a viable candidate for in-place recycling because the distresses present were numerous and severe enough that milling and overlaying was not a practical long-term solution.

6.3.2 Original Construction Plan

A three-stage approach was taken to US-49 construction to accommodate removal and replacement of two northbound bridges. In stage 1, southbound lanes near the two bridges were recycled and overlaid with a nominal 7.6 cm lift of HMA base course (19 mm nominal maximum aggregate size (NMAS) PG 76-22). Stage 1 was performed so all traffic could be diverted to southbound lanes in a head-to-head fashion, allowing construction traffic to use northbound lanes during the bridge replacements. In stage 2, the bridges were replaced, and all other in-place recycling was conducted followed by the HMA base course overlay. Most US-49 construction took place in stage 2. In stage 3, areas adjacent to the replaced bridges were rebuilt with a traditional construction approach (HMA over crushed stone), and the entire project was overlaid with a nominal 3.8 cm lift of HMA surface course (9.5 mm NMAS PG 76-22).

Aside from the traditional construction near the replaced northbound bridges, original plans were to conduct emulsion-stabilized CIR in the northbound lanes and cement-stabilized CIR in the southbound lanes. Recycling depths targeted 23 cm in full-depth HMA sections and 15 cm in composite sections. FDR was not originally planned.

6.3.3 Construction Plan Modifications

Issues arose during stage 2 construction in some full-depth HMA sections where the weight of recycling equipment overstressed the existing subgrade. To compensate for the subgrade structural deficiencies, a supplemental agreement was developed to conduct cement-stabilized FDR instead of CIR in most full-depth HMA sections where concrete was not present. Note that some full-depth HMA sections (concrete not present) proceeded with CIR as originally planned. FDR stabilization was nominally 41 cm deep with 4.8% cement by mass; FDR construction details are provided in Howard and Cox (2016).

6.3.4 Construction Processes

CIR binder dosages by mass were 4.4% for cement-stabilized CIR and 4% engineered emulsion plus 1% hydrated lime for emulsion-stabilized CIR. Chapter 2 provides information regarding mix design procedures in which those binder dosages were determined. All CIR construction processes were essentially identical except for binder incorporation.

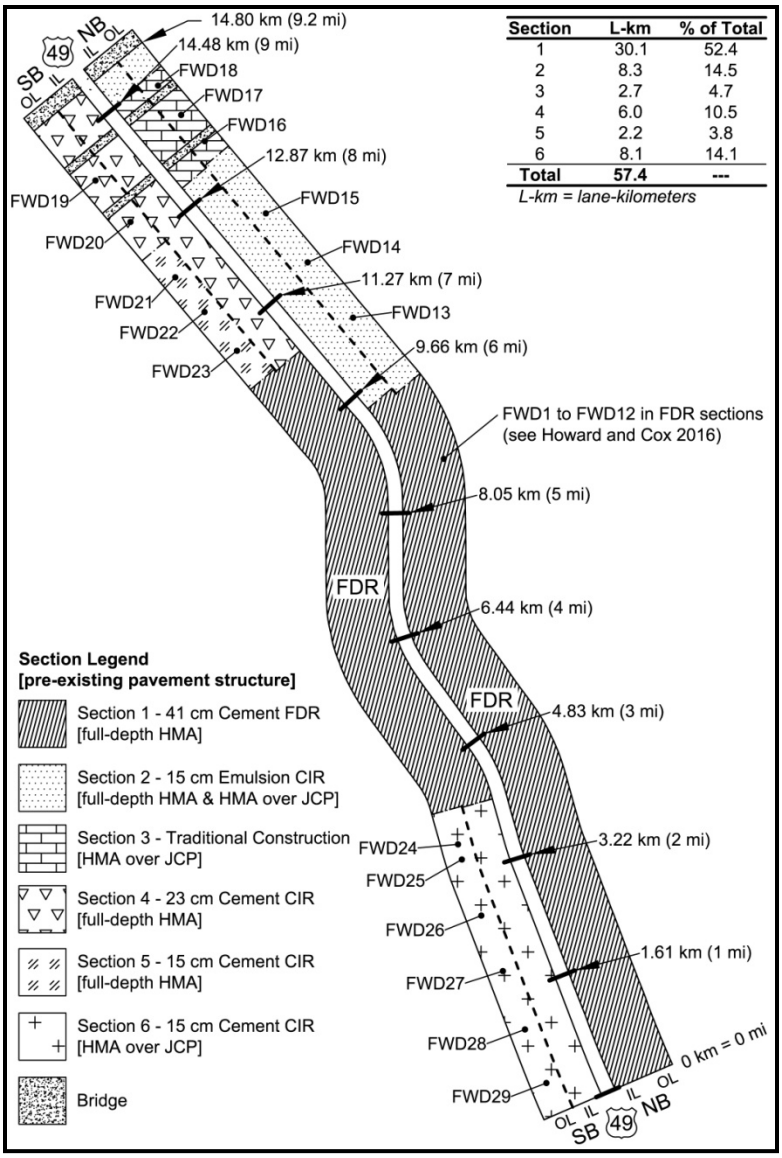

Figure 6.2 US-49 Map

Hall Brothers Recycling & Reclamation, Inc. performed all US-49 recycling procedures. Figure 6.2 shows the as-constructed layout of US-49, which was divided into six sections as discussed further in the next subsection. Figure 6.3 provides photographs of major CIR construction processes. First (not shown in Figure 6.3), the top 7.6 cm of existing asphalt pavement was milled and taken off site to establish a uniform grade.

Second, hydraulic binders (cement or hydrated lime) were spread onto the milled surface with an auger system (Figure 6.3b). Next, a Caterpillar PR-1000 cold planing unit pulverized and reclaimed the existing pavement to 15 or 23 cm (Figure 6.3c). Reclaimed material was conveyed to a screening and crushing unit (Figure 6.3d) which fed into a pugmill (Figure 6.3e). Emulsion was stored in a tank and, where needed, was metered into the pugmill and mixed with reclaimed material.

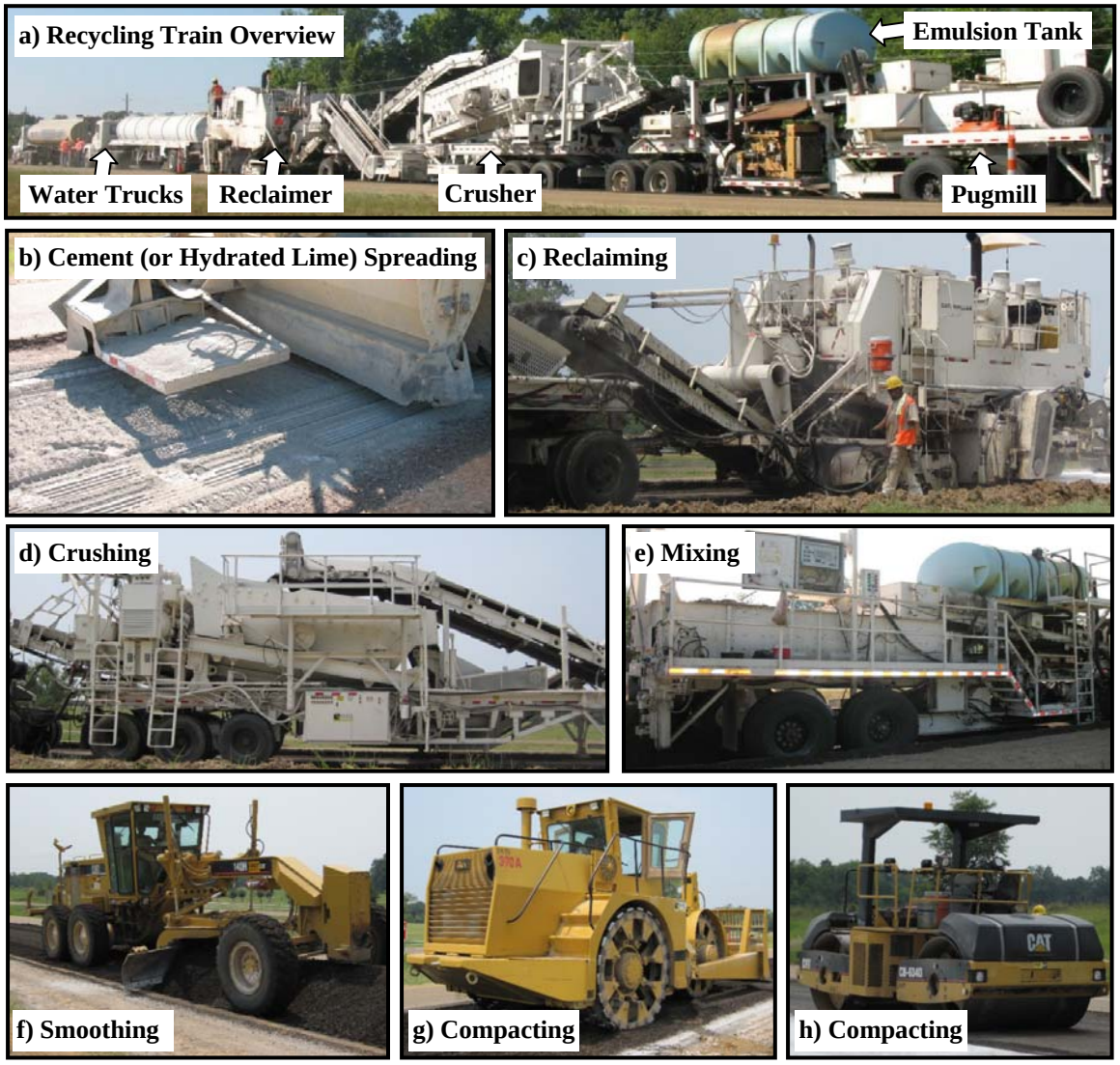

Figure 6.3 US-49 CIR Construction Photos

The pugmill deposited material into a windrow which was smoothed with a Caterpillar 140H motor grader (Figure 6.3f). Smoothed material was compacted with a Rex® 3-70A compactor with steel wheels fitted with rectangular steel pads (Figure 6.3g). The 140H motor grader then smoothed the material a second time, and final compaction was performed with a Caterpillar CB-634D vibratory steel wheel roller (Figure 3h). For full pay, 97% of standard Proctor density was required.

Curing specifications prior to HMA overlay varied by binder type. Emulsion CIR cured until the moisture content was less than 2.5%. Cement CIR and FDR was sealed with a tack coat to minimize moisture loss and was cured for 7 days. CIR construction began in June 2010, and all CIR, FDR, and HMA base course was placed by November 2010. Public traffic was allowed on the entire route around November 2010 with only the HMA base course placed. The final HMA surface course (stage 3) was placed between July and August of 2011.

6.3.5 Final US-49 Section Details

Figure 6.2 presents the 6 as-built sections of US-49 and their locations. Section 1 is the cement FDR section which is primarily documented in Howard and Cox (2016).

Section 2 is emulsion CIR targeting a 15 cm thickness since concrete slabs were present. At least one area was encountered within Section 2 where concrete slabs were not present; the history of this area was unknown but was likely the result of previous rehabilitation efforts which called for slab removal and replacement with full-depth HMA. Where full-depth HMA was encountered in this section, CIR continued as

originally planned as if concrete slabs were present (i.e. recycling depths were 15 cm not 23 cm).

Section 3 is traditional construction. Existing HMA materials were removed down to existing concrete slabs. Serving as a crack mitigation layer, 15 cm of crushed stone base was placed on top of the concrete slabs. A total of 19 cm of 19 mm NMAS HMA was placed in three lifts where the first 6.3 cm lift had PG 67-22 binder and the top two 6.3 cm lifts had PG 76-22 binder. The surface was the same as that used in stage 3 construction.

Sections 4, 5, and 6 are cement-stabilized CIR. Section 4 CIR thicknesses targeted 23 cm since no concrete slabs were present. No concrete slabs were present in Section 5; however, the target thickness was 15 cm instead of 23 cm. The reason for this deviation from original construction plans is unknown to the author. Lastly, Section 6 CIR thicknesses targeted 15 cm since concrete slabs were present. Discussion with MDOT engineers indicated there was a tack coat (curing-related) application delay on the north end of the project, which would correspond most likely with Section 4 but possibly Section 5 as well. Exact records regarding location and length of delay were not kept, but it is believed that tack coat was applied the following day. By the time of application, MDOT engineers noted transverse shrinkage cracks were visible in the CIR layer, which should be considered when evaluating performance results.

6.4 Field and Laboratory Test Methods

Three data sets are presented in this chapter: pavement distress survey, laboratory-measured properties of in-place cores, and FWD data. The majority of the data was

obtained in late April to early June of 2015, which was the fifth construction season since US-49 was built. Nominally, this data is referred to herein as 53-month data, measured from the time US-49 was fully opened to traffic.

6.4.1 Pavement Distress Survey

The 53-month pavement distress survey was conducted on April 23, 2015, using MDOT's Pathrunner™ profiler, which is equipped with several computers for distress measurement. Data was collected in 152 m long units which were later merged to produce results by test section. Parameters reported were MDOT's pavement condition rating (PCR), mean roughness index (MRI), rutting, fatigue cracking, block cracking, longitudinal cracking, and transverse cracking. Each distress was quantified by severity level based on the Federal Highway Administration publication RD-03-031 (Miller and Bellinger 2003). MDOT's profiler was capable of measuring other distresses (e.g. edge cracking), but these were not reported since they were not observed.

PCR values are reported on a 0 to 100 scale where the thresholds for various condition ratings vary depending on route type. PCR is a composite index which combines roughness and distress into a single index and is calculated using an algorithm defined by MDOT.

6.4.2 Coring

The cutting of 62 total cores (100 or 150 mm diameter) was attempted from US-49. Cores were taken from all four lanes at locations which were spread longitudinally and distributed spatially in attempts to fully represent US-49. Cores up to 61 cm long

were obtained using coring bit sleeve extensions. Most cores were cut to the depth where the entire recycled layer could be retrieved, while cores obtained at FWD locations were cut to the subgrade. Of the 62 cores, 12 were FDR, and 50 were CIR.

Cores were visually examined, logged, and then sliced to individual test specimens. Bulk and maximum specific gravities (G_{mb} and G_{mm}, respectively) were measured as per Chapter 4 for air void (V_a) determination. Specimens were tested for multiple properties: indirect tensile (IDT) strength (S_t) (100 and 150 mm diameter), ASTM D7369 IDT resilient modulus (M_r), fracture energy (FE), AASHTO T340 Asphalt Pavement Analyzer (APA) rut depth, and unconfined compressive strength (UCS). Six replicates were tested at a minimum except for APA testing of cement CIR where two replicates were tested and UCS testing where three replicates were tested. Coring continued until minimum replication targets could be met, which required varying numbers of cores to be cut per section due to varying thicknesses and some cores being damaged or cracked.

For this chapter, coring and subsequent testing prioritized Sections 2, 5, and 6, as well as the HMA base and surface mixtures. Section 1 cores and results are discussed in Howard and Cox (2016). Section 3 was not cored. As it related to material properties measured on cores, Sections 4 and 5 were expected to be similar since the only meaningful difference between the two sections was layer thickness (23 cm compared to 15 cm). Two cores were cut from Section 4 for an estimate of as-built layer thickness. However, most coring was performed in Section 5 since its 15 cm thickness aligned more closely with typical CIR thicknesses (Cox and Howard 2013) and also provided more direct comparison to Section 6.

S_t and FE tests were conducted at 50 mm/min on specimens with target sliced thicknesses of 50 mm for both 100 and 150 mm diameters. M_r testing was conducted on 150 mm diameter specimens prior to determining S_t and FE. UCS tests were conducted at 0.13 mm/min on 100 mm diameter specimens nominally sliced to 115 mm.

6.4.3 Falling Weight Deflectometer

MDOT collected FWD data when possible throughout the first 53 months of US-49's service life, with the final test date coinciding with the 53-month coring. Testing occurred at 24, 28, 34, 40, and 53 months. A total of 29 FWD locations were tested on US-49 (denoted FWD1 to FWD29 in Figure 6.2). In Sections 2, 5, and 6, at least three FWD locations were cored directly at the FWD drop location to assist FWD analysis.

FWD testing was conducted at multiple loadings, and all deflections were adjusted linearly to a 40 kN (9 kip) loading. Deflections under the center of loading (d_0) were corrected to 20 °C ($d_{0\text{-}20}$) using Figure L5.5 of the 1993 Pavement Design Guide (AASHTO 1993).

6.5 Results

6.5.1 Pavement Distress Survey Results

Table 6.2 presents distress survey results for all six sections. All sections are rated "good" according to PCR values and MDOT's rating categories for four-lane routes. PCR values were not meaningfully different between sections. Practically, all six sections are similar with respect to average MRI and all severity levels. Section 4 (23 cm cement CIR over full-depth HMA) MRI is very slightly better than that of other sections. The average

MRI for each section is well below the 2.37 mm/m threshold separating low and medium severity levels.

MDOT also measured MRI in September of 2011 (after 10 months of service); however, much of the northern portion of the project was not surveyed. Section 3 was not surveyed, and approximately 30, 75, and 30% of Sections 2, 4, and 5 were not surveyed. Average MRI where measured ranged from 0.87 to 1.04 mm/m. Differences between 10- and 53-month MRI values (in cases where both were measured) ranged from 0.05 to 0.32 mm/m, resulting in a 5 to 31% increase within 43 months.

Table 6.2 Summary of US-49 Distress Survey at 53 Months

	Avg or	Highway 49 Section					
Distress	**Severity**	**1**	**2**	**3**	**4**	**5**	**6**
PCR	Avg	87	86	85	86	86	87
MRI	Avg (mm/m)	1.09	1.06	1.06	0.95	1.06	1.15
	L (%)	83.7	84.5	83.6	89.1	85.5	80.5
	M (%)	15.1	14.4	15.6	9.8	12.0	17.6
	H (%)	1.1	1.2	0.8	1.0	2.3	1.8
Rutting	Avg (mm)	1.3	2.0	2.4	2.0	1.8	1.0
	L (%)	97.1	86.1	76.3	78.2	86.8	97.7
	M (%)	2.5	13.3	23.7	20.7	12.3	2.1
	H (%)	0.4	0.6	0.0	1.1	0.6	0.2
Fatigue Cracking	L (%)	0.4	0.2	0.3	0.4	0.3	0.4
	M or H (%)	0.0	0.0	0.0	0.0	0.0	0.0
Block Cracking	L (%)	2.8	0.0	0.0	2.3	4.5	0.9
	M or H (%)	0.0	0.0	0.0	0.0	0.0	0.0
Longitudinal Cracking	L (%)	29.7	37.8	53.6	40.4	55.9	30.6
	M (%)	1.8	2.7	0.9	5.4	3.0	2.8
	H (%)	0.3	0.1	0.0	0.5	0.2	0.0
Transverse Cracking	L (%)	20.6	11.5	8.1	20.4	13.4	27.5
	M (%)	2.4	1.5	1.5	2.2	0.7	2.9
	H (%)	0.2	0.1	0.0	0.2	0.0	0.4

-- L = low, M = medium, H = high
-- For PCR, Very Good ≥ 89, 82 ≤ Good < 89, 73 ≤ Fair < 82, 63 ≤ Poor < 73, Very Poor < 63
-- For MRI, L: MRI < 2.37 mm/m, M: 2.37 < MRI < 4.74 m/m, H: MRI > 4.74 mm/m
-- For rutting, L: 1.6 < Rut < 3.2 mm, M: 3.2 < Rut < 6.4 mm, H: Rut > 6.4 mm
-- Fatigue and block cracking values were figured using 3.66 m lane widths
-- Edge cracking, patching, potholes, raveling, and bleeding were not detected

Rutting was manageable for each section. On average, Sections 1 and 6 exhibit slightly less rutting (i.e. classifying in the "null" rating), while all other sections are in the "low" rating on average. Based on severity level percentages, Sections 1 and 6 appear to have less rutting than Sections 2, 4, and 5, which have less than Section 3. It is interesting that the traditionally-constructed Section 3 exhibits the highest rutting with nearly 25% of the section classifying as medium severity. Overall, however, rutting in any section does not appear to be of concern.

All observed fatigue cracking classifies as low severity. Section 2 (emulsion CIR) appears slightly better than all cement-stabilized sections. Overall, some trends are observed, but differences are slight. Block and fatigue cracking results are similar. All block cracking observed is low severity, and there is a gap between Sections 2 and 3 (emulsion CIR and traditional construction) and all cement-stabilized sections. This gap is slightly wider for block cracking than fatigue cracking as no block cracking was observed in Sections 2 and 3 while a modest amount was observed in cement-stabilized sections.

Longitudinal cracking results are less straightforward than other distresses. Three general groups are observed. Sections 1 and 6 exhibit around 30% low severity cracking, Sections 2 and 4 exhibit around 40%, and Sections 3 and 5 exhibited more than 50%. Cement-stabilized sections were observed in all three groups, and Sections 2 and 3 fell in the middle and worst groups. Overall, Sections 1 and 6 exhibit the least amount of longitudinal cracking.

Transverse cracking results appear as expected, especially when all caveats of US-49 are considered. Sections 2 and 3 exhibit the least amount of low-severity cracking

while more cracking is generally observed in cement-stabilized sections. Recall that Sections 2 and 6 have concrete slabs underneath the CIR layers; therefore, at least some of the observed transverse cracking is likely attributed to reflective cracking at slab joints. Section 6, which is the worst section, would likely be closer to other cement CIR sections if reflective cracking from underlying concrete was not present. Likewise, Section 2 would likely exhibit less transverse cracking than Section 3 if reflective cracking could be factored out of the final results.

Recall that Section 4 is where tack coat application delays were likely experienced, resulting in shrinkage cracking tendencies. It is likely that the high amount of transverse cracking at 53 months is a factor of shrinkage cracking occurring immediately after construction. If Section 4 shrinkage cracking and Section 6 reflective cracking could be factored out of transverse cracking results, it is possible Sections 4, 5, and 6 would converge somewhat relative to their actual observed differences. Overall, cement stabilization appears to yield noticeably more transverse cracking than emulsion stabilization, which is neither an unexpected nor unreasonable finding.

When considering survey results as a whole, all sections appear to be performing satisfactorily. Performance of Sections 1 and 2 is slightly better than other sections. Section 1 exhibits less rutting, but more cracking, than Section 2, and vice versa.

6.5.2 Core Properties

6.5.2.1 Layer Thicknesses

Figure 6.4 provides representative photos of US-49 cores with arrows indicating layer interfaces. Section 1 is shown for reference (Figure 6.4a), and two cores from

Section 2 (Figures 6.4b and 6.4c) are presented showing the differences between when concrete was and was not present.

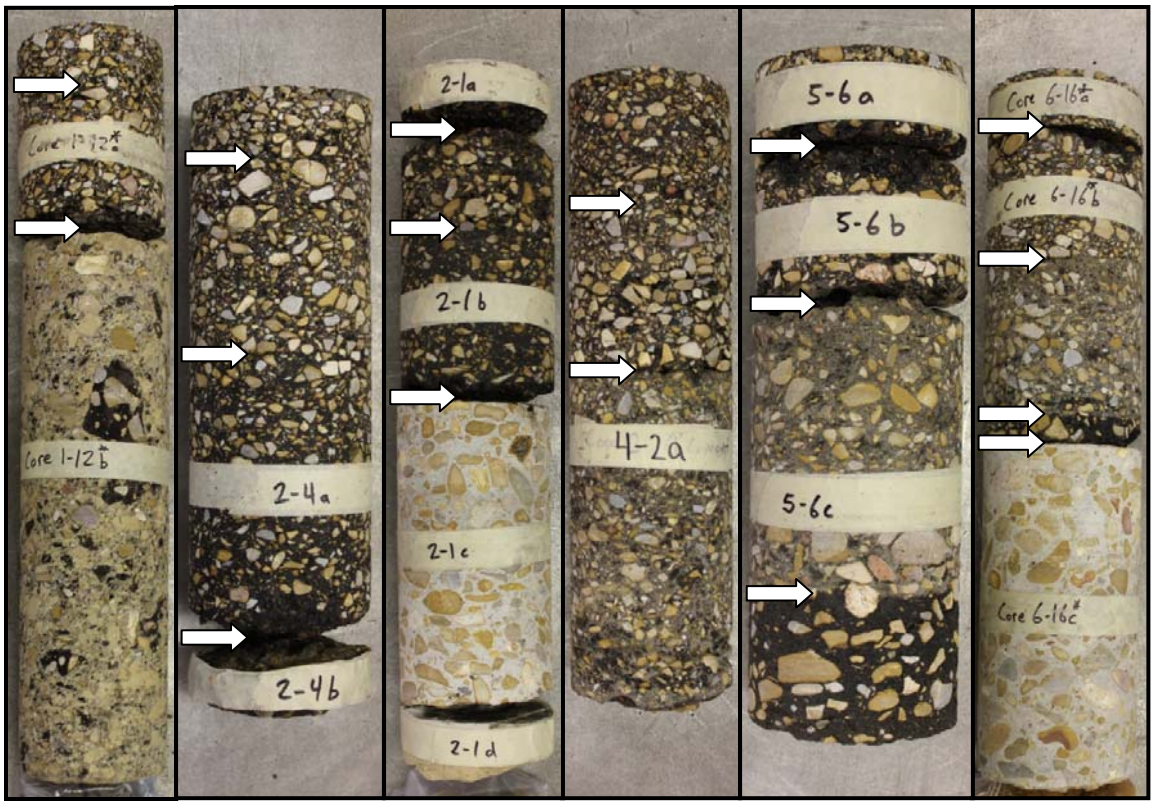

a) Section 1 *b) Section 2* *c) Section 2* *d) Section 4* *e) Section 5* *f) Section 6*

Figure 6.4 Representative Photos of 100 mm Diameter US-49 Cores

Figures 6.4b and 6.4e show pre-existing asphalt materials remaining underneath CIR layers, which appear to be bituminous materials originally serving as a base. Figure 6.4c and 6.4f show CIR above concrete. Figure 6.4c shows recycling depths extending to the top of the concrete while Figure 6.4f shows recycling depths which did not reach the top of the concrete. This type of layer thickness variability was very common within each

section and across US-49 (Figure 6.4 provides photos of the most representative core from each section).

Table 6.3 summarizes layer thicknesses by section to provide an understanding of the variability present. Note that all layers, specifically those underneath recycled layers, were not retrieved for all cores since the main goal was to retrieve the HMA and CIR/FDR layers unless the core was taken at an FWD location. For example, concrete was only retrieved for 4 of the 17 Section 6 cores; concrete thickness statistics for Section 6 are of all concrete cores retrieved. Also note that Section 4 variability appears very low, which is primarily because only two cores were cut in Section 4 and were cut in close proximity to each other.

Aside from Section 4, thickness of the HMA surface course was, on average, close to the targeted 3.8 cm thickness; however, thicknesses still varied considerably from 3.2 to 7.0 cm (not including Section 4). In Section 4, HMA surface course thicknesses were nearly double the target. Overall, 57% of all cores exhibited HMA surface thicknesses within 0.5 cm of the target thickness. Similarly, 61% were between 3 and 4 cm, 28% were between 4 and 5 cm, and 11% were greater than 5 cm.

Aside from Section 4, HMA base course thicknesses were also, on average, close to the targeted thickness (7.6 cm); however, thicknesses still varied considerably from 5.7 to 10.2 cm (not including Section 4). In Section 4, HMA base course thicknesses were greater than the target as with the HMA surface course although the difference was not as great. Overall, 30% of all cores exhibited HMA base thicknesses within 0.5 cm of the target thickness. Further, 28% were between 6 and 7 cm, 30% were between 7 and 8 cm, and 32% were greater than 8 cm.

Table 6.3 US-49 Cored Layer Thicknesses

Section	Statistic	HMA Surface	HMA Base	CIR or FDR	Underlying Layers Asphalt[a]	Underlying Layers Concrete
1	Avg (cm)	4.0	7.1	39.0	---	---
	Min (cm)	3.2	6.4	30.5	---	---
	Max (cm)	5.1	8.6	49.5	---	---
	COV (%)	16	11	14	---	---
2	Avg (cm)	4.1	9.2	13.1	7.6	20.3
	Min (cm)	3.2	7.0	9.5	2.5	19.1
	Max (cm)	7.0	10.2	15.9	16.5	22.9
	COV (%)	25	14	19	101	11
4	Avg (cm)	7.5	10.0	19.4	---	---
	Min (cm)	7.3	9.5	19.1	---	---
	Max (cm)	7.6	10.5	19.7	---	---
	COV (%)	3	7	2	---	---
5	Avg (cm)	3.6	7.9	12.7	8.5	---
	Min (cm)	3.2	5.7	8.9	7.6	---
	Max (cm)	4.8	10.2	14.0	8.9	---
	COV (%)	13	23	11	9	---
6	Avg (cm)	4.1	7.6	8.4	3.1	20.8
	Min (cm)	3.8	6.4	4.4	1.3	20.3
	Max (cm)	5.1	8.3	12.7	6.4	21.6
	COV (%)	9	6	31	59	3

a) may be bituminous base or hot mix asphalt, primarily depending on whether concrete slabs were or were not present

-- COV = coefficient of variation (standard deviation divided by average)

Section 1 FDR layers were close to the 41 cm target thickness on average but exhibited a fairly wide range of thicknesses overall, from 30.5 to 49.5 cm. Sections 2, 5, and 6 target thicknesses were 15 cm, but average as-built thicknesses were 13.1, 12.7, and 8.4 cm, respectively. Section 6 thicknesses were considerably lower than the target and, as shown in Figure 6.4f, could have been modestly greater before reaching underlying concrete.

Thicknesses varied considerably from 4.4 to 15.9 cm for all three 15 cm targeted sections. For Sections 2, 5, and 6 combined, 29% of CIR thicknesses were less than 10

cm, 21% were between 10 and 12 cm, 31% were between 12 and 14 cm, and 19% were greater than 14 cm. Section 4 CIR, at 19.4 cm on average, was also slightly less than its 23 cm target thickness.

Table 6.3 illustrates considerable construction variability with respect to layer thicknesses. As recommended in Strickland (2010), more extensive pre-construction coring could be beneficial towards reducing thickness variability. However, distress survey results presented in the previous section indicate US-49 is performing well despite this variability.

6.5.2.2 Air Voids

Table 6.4 summarizes US-49 CIR air voids for Sections 2, 5, and 6. Results shown are for all test specimens sliced from cores. In addition to analyzing all specimens simultaneously, top and bottom pairs are compared to investigate density gradients where cores were thick enough to obtain two test specimens from a single core. Paired *t*-tests were conducted to investigate statistical differences between top and bottom layer air voids at a 5% significance level.

Table 6.4 shows Section 2 V_a's were 10.0% on average compared to Section 5 and 6 V_a's of 13.8 and 15.3%, respectively. Trends between emulsion and cement CIR are similar to laboratory-compacted specimens fabricated by the author. They appear reasonable primarily because emulsion is likely to facilitate compaction more so than cement and because emulsion fills more volume than cement due to specific gravity differences (1.03 versus 3.15) (i.e. emulsion occupies more voids in mineral aggregate than cement for similar dosages by mass).

Top and bottom layers were significantly different with respect to V_a for all three sections. Section 2 V_a's were significantly lower at the top of the layer than the bottom, while the opposite was true for Sections 5 and 6. Material segregation may have led to the observed Section 5 and 6 density gradients, though the cause is unknown. Note that for Section 6, only 3 pairs were available primarily because the Section 6 CIR was fairly thin and typically only yielded one test specimen per core.

Table 6.4 Summary of US-49 CIR Air Voids

	All Specimens			Top- and Bottom-Layer Paired Specimens				
Section	***n***	**Avg V_a (%)**	**COV (%)**	**n_{pairs}**	**Avg $V_{a,top}$ (%)**	**Avg $V_{a,bottom}$ (%)**	***p-value***	**Sig Diff?**
2	18	10.0	20	8	8.6	11.7	<0.001	Yes
5	19	13.8	9	7	14.8	12.9	0.008	Yes
6	18	15.3	7	3	16.7	15.0	0.033	Yes

-- Air void (V_a) values were calculated using G_{mm} values of 2.366 (Section 2) and 2.455 (Sections 5 and 6), which were obtained following protocols of Chapter 4. This approach calculates CIR G_{mm} based on RAP G_{mm} and individual binder specific gravities and dosages. G_{mm} values measured on cored materials obtained during a 41-month pilot investigation were 2.335 (Section 2) and 2.376 (Sections 5 and 6). Internal investigation to date has led the author to the perspective that field G_{mm} values measured on compacted and broken up materials after several years of service may not be as reliable as values measured according to Chapter 4, especially for cement CIR sections where cement hydration over time likely affects G_{mm} measurement ability (lower values expected from broken up cores). A considerable amount of effort was put forth to develop the CIR protocols in Chapter 4, and, until more information is available, the author recommends use of this method to determine CIR G_{mm} when possible.

6.5.2.3 Strength and Performance Properties

Table 6.5 presents laboratory-measured properties for the HMA surface course, HMA base course, and CIR materials from Sections 2, 5, and 6. Properties tested for Section 1 (FDR) are summarized herein for comparison but differed slightly from those in this chapter. Howard and Cox (2016) presented properties from Section 1 cores: elastic modulus (ASTM C469) was approximately 1.4 GPa (200 ksi), UCS was approximately

2.8 MPa (400 psi), $S_{t,100\ mm}$ was approximately 0.5 MPa (75 psi), and APA rut depths were less than 1 mm.

Table 6.5 Summary of US-49 Properties Measured on Cores at 53 Months

Property		HMA Surface Course	HMA Base Course	CIR Section No. 2	5	6
$M_{r,total}$ (GPa)	$Avg_{T(10\%)}$	7.6	7.4	3.2	13.9	11.8
	n	6	6	6	6	6
	COV (%)	23	23	10	17	20
	Avg V_a (%)	6.3	6.6	9.2	14.1	15.6
$S_{t,\ 100\ mm}$ (MPa)	Avg	1.39	0.95	0.65	1.14	1.02
	n	16	8	6	8	7
	COV (%)	17	34	14	13	21
	Avg V_a (%)	7.1	7.0	10.1	14.0	15.1
$S_{t,\ 150\ mm}$ (MPa)	Avg	1.41	1.20	0.62	1.04	1.10
	n	6	6	6	6	6
	COV (%)	19	38	18	22	20
	Avg V_a (%)	6.3	6.6	9.2	14.1	15.6
FE (kJ/m^3)	$Avg_{POR,T(10\%)}$	2.72	0.65	1.29	0.11	0.09
	n	6	6	6	6	6
	COV (%)	53	34	26	58	33
	Avg V_a (%)	6.3	6.6	9.2	14.1	15.6
APA Rut Depth (mm)	Avg	2.2	4.0	11.8	0.9	1.2
	n	6	6	6	2	2
	COV (%)	20	3	3	---	---
	Avg V_a (%)	6.4	7.6	10.8	12.8	14.9
UCS (MPa)	Avg	---	---	---	3.70	3.80
	n	---	---	---	3	3
	COV (%)	---	---	---	13	10
	Avg V_a (%)	---	---	---	13.4	15.4

-- Total M_r ($M_{r,total}$) is reported rather than instantaneous M_r. Six replicates yields 24 $M_{r,total}$ values (two faces, two axes per replicate). Trimming 10% removes the highest and lowest 10% of values (3 readings in this case).

-- For fracture energy, 6 replicates yields 12 FE values (two faces per replicate). Of the 12 values, probable outliers were removed and then the highest and lowest 10% of values were trimmed (2 readings in this case).

-- $Avg_{T(10\%)}$ =trimmed average (10% trimmed)

-- $Avg_{POR,T(10\%)}$ = trimmed average (10% trimmed) after probable outlier removal

-- Average $M_{r,total}$ and S_t of underlying asphalt was 6.1 GPa and 0.68 MPa, respectively.

-- Average elastic modulus and UCS of underlying concrete was 43.7 GPa and 84.7 MPa, respectively.

HMA mixture properties are presented first for comparison with other CIR properties. $M_{r,total}$ for both HMA mixtures is similar at approximately 7.5 GPa. Tensile strengths for 100 mm and 150 mm diameter specimens ($S_{t,\ 100\ mm}$ and $S_{t,\ 150\ mm}$, respectively) are relatively similar for either diameter. S_t values for surface and base courses are approximately 1.4 and 1.1 MPa, respectively. Mixture cracking susceptibility is characterized via FE (larger FE suggests better cracking resistance), which is 2.72 and 0.65 kJ/m^3 for surface and base courses, respectively. The surface FE appears reasonable, but the base FE is of concern. Although no errors were found in data files, the 0.65 kJ/m^3 FE is not believed to be correct and should be interpreted accordingly. APA rut depths for surface and base courses are 2.2 and 4.0 mm, respectively.

Section 2 emulsion CIR properties are considerably different from that of the HMA mixtures, which is reasonable. $M_{r,total}$, S_t, and FE are approximately 3.2 GPa, 0.6 MPa, and 1.3 kJ/m^3, respectively; all of which are slightly less than half of corresponding HMA properties. At 11.8 mm, APA rut depths are approximately 3 to 5 times greater than that of HMA mixtures. Overall, the comparison between emulsion CIR and HMA is reasonable in that $M_{r,total}$, S_t, and FE are all lower while APA rut depth is greater.

Sections 5 and 6 cement CIR properties demonstrate clear contrasts with emulsion CIR properties. $M_{r,total}$ is approximately 13 GPa on average, which is nearly two and four times greater than HMA and emulsion CIR $M_{r,total}$, respectively. S_t is approximately 1.1 MPa, which is approaching that of HMA S_t but is approximately twice that of the emulsion CIR. FE is approximately 0.10 kJ/m^3, which, at 10% and 5% of emulsion CIR and HMA FE values, is considerably lower. APA rut depths, at approximately 1 mm, are almost negligible relative to HMA and emulsion CIR rut depths. UCS was determined for

cement CIR only and is approximately 3.75 MPa, which is reasonable considering the US-49 cement CIR design required 2.1 MPa after 7 days of moist curing. Overall, cement CIR properties are effectively opposite of emulsion CIR properties in that cement CIR provides higher $M_{r,total}$ and S_t, considerably greater rutting resistance, but considerably less fracture resistance.

As suggested by pavement distress survey results presented previously, all US-49 sections are performing satisfactorily though slight distinctions can be observed between sections (e.g. more cracking in cement CIR sections than emulsion CIR). Properties measured on cores support distinctions observed in the distress survey, particularly regarding cement versus emulsion. Trends observed in strength and performance properties may serve as a foretelling of the expected progression of distresses on US-49. For example, the gap between cracking distresses in cement-stabilized and emulsion-stabilized sections will likely grow, and the gap between rutting distresses may grow slightly.

6.5.3 Falling Weight Deflectometer Results

Figure 6.5 presents FWD $d_{0\text{-}20}$ deflections with time for all FWD locations tested by MDOT through the first 53 months of service. Plots in Figure 6.5 also show $d_{0\text{-}20}$ data for locations which were not tested by MDOT over time but were added during the 53-month investigation for various reasons, mainly to collect more data in sections where there were less than three FWD locations. No FWD testing was conducted in Section 4 prior to the 53-month investigation; therefore, Section 4 data was included in Figure 5c with Section 5 since the two were similar other than layer thickness.

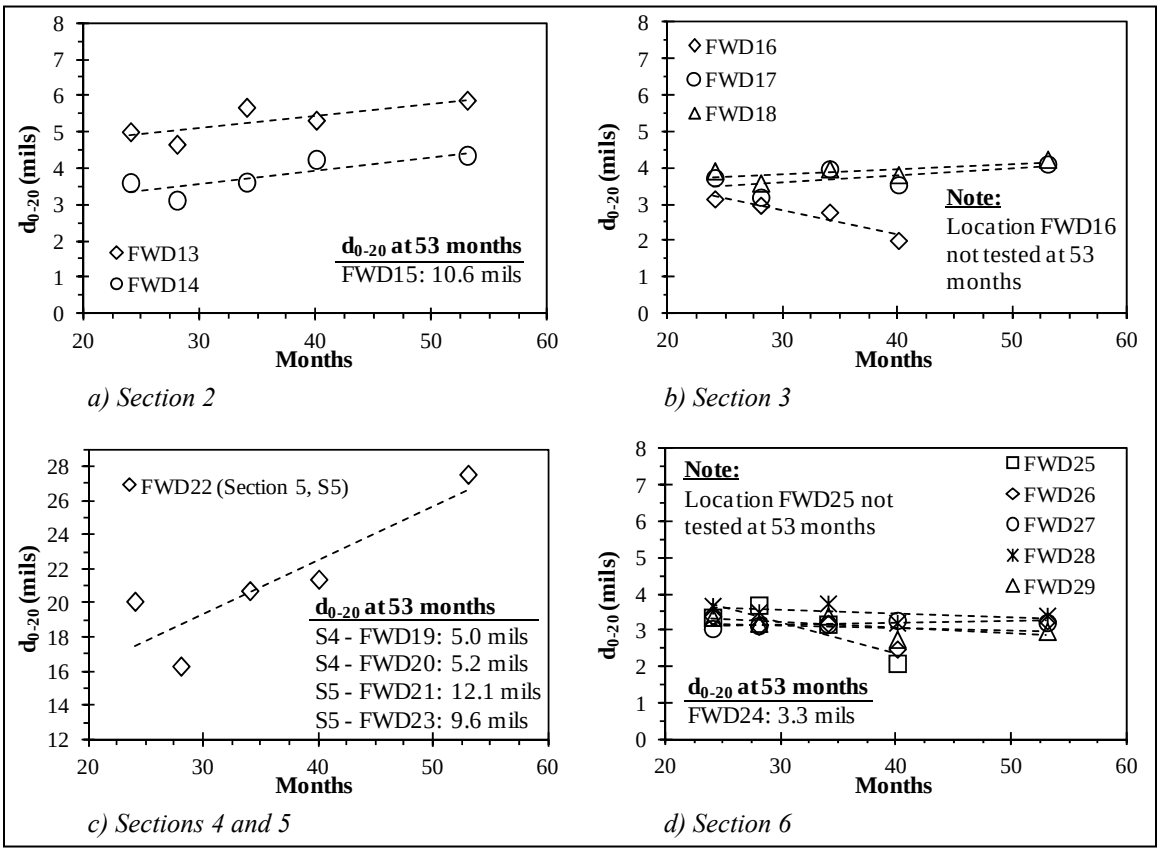

Figure 6.5 FWD Deflection Data

Figure 6.5 shows deflections generally ranging from 3 to 6 mils, with several locations around 10 to 12 mils. FWD22 (Figure 6.5c) deflections are considerably higher because FWD22 was located in an area of localized severe rutting and wheel path cracking (Figure 6.6). The cause of this distress is unknown, but it was limited to an area approximately 15 m long and is not representative of Section 5 as a whole.

Initially, a more involved FWD analysis was considered herein, such as the one used in Howard and Cox (2016). However, when all available FWD data was processed, Howard and Cox (2016) data (Section 1) was fairly symmetrical and suitable for the

AASHTO (1993) analysis, while all other data was less symmetrical and less conducive to a detailed (yet reliable) analysis. For example, Section 1 was effectively a two-layer pavement structure with a high-modulus material over a low-modulus material, which yields a fairly straightforward analysis. In contrast, other sections consisted of up to four layers (Table 6.3) with the highest-modulus material encountered on US-49 (i.e. concrete) comprising the lowest layer. The types of pavement structures encountered in Sections 2 through 6 complicate analysis considerably relative to Section 1. When layer properties were coupled with the high layer thickness variability observed, the suitability of a sophisticated FWD analysis to meet this dissertation's needs was questioned, and it was decided that a more approximate analysis approach would be utilized.

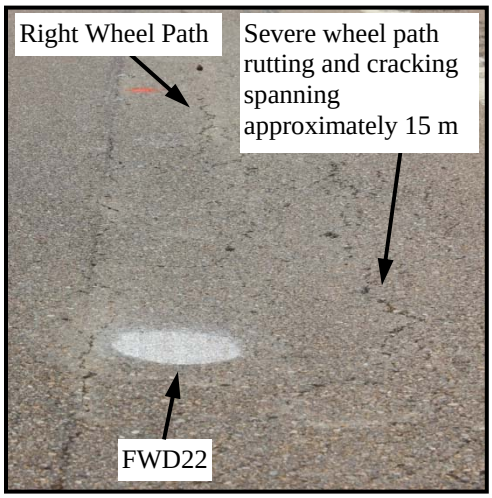

Figure 6.6 Distresses at FWD22 Location

As an initial reasonableness assessment, layer thicknesses and material modulus values were input into the multi-layer linear elastic analysis KENLAYER program to calculate pavement surface deflections at the center of loading. Generally, KENLAYER

parameters were set to the default, idealized case (e.g. fully-bonded layers). Calculated deflections for Sections 2 to 6 ranged from 4.4 to 7.2 mils, which support FWD-measured deflections as generally in line with expected deflections calculated with these layer properties and thicknesses.

It is important to note that the Section 5 KENLAYER deflection was 6.6 mils, whereas the average FWD $d_{0\text{-}20}$ was 10.9 mils (excluding FWD22). This discrepancy is likely due to two issues. First, linear elastic calculations provide an ideal result; second, calculations are dependent on material properties. In coring Section 5, one out of every three cores, on average, was cracked. However, only intact cores were tested, meaning laboratory test results were the best possible representation of Section 5. Therefore, Table 5 properties may not necessarily align with Section 5 FWD deflections. Likewise, KENLAYER cannot appropriately consider this issue.

A second FWD assessment was conducted by comparing Table 6.1 literature values to US-49 FWD data in Figure 6.7 where deflection is plotted against SN_{eff}. For US-49 data, approximate SN_{eff} values were calculated by summing layer thicknesses multiplied by corresponding layer coefficients (AASHTO 1993). Table 6.3 layer thicknesses were used, and layer coefficients were assigned as follows: 0.44 (HMA), 0.30 (CIR and FDR), and 0.20 (all underlying layers). Layer coefficients are undoubtedly approximate but were considered sufficient given the analysis was intended to show trends from many studies in several states over time. Figure 6.7 shows that US-49 and literature trends are relatively similar.

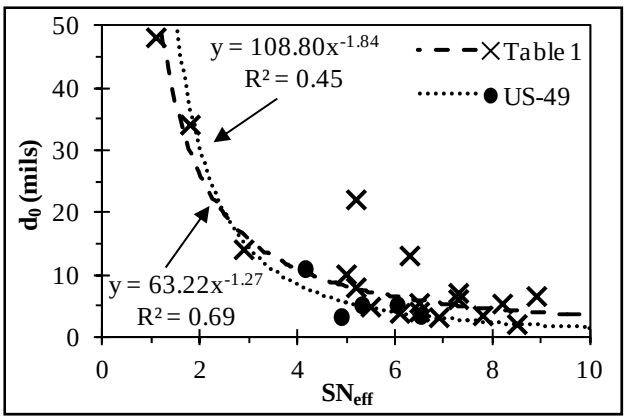

Figure 6.7 d_0 versus SN_{eff} for Literature and US-49

Figure 6.7 also assists in identifying Section 5 as the most structurally deficient. Compared to Section 4, the CIR layer is thinner, and compared to Section 6, underlying layers are considerably less stiff (i.e. no concrete is present). Therefore, it is likely that Section 5 has accumulated greater fatigue damage than Sections 4 and 6. This could support the high coring failure rate as well as the higher FWD deflections. It also suggests Section 5 performance may begin to deteriorate at a faster rate relative to other US-49 sections.

Overall, though an approximate analysis was conducted, FWD testing generally concluded that US-49 is performing well from a structural capacity perspective. However, Section 5 is the one notable exception and, structurally, is of greater concern than other sections. This finding generally agrees with the distress survey. Core testing does not support this finding, yet that is likely because only intact (i.e. un-cracked) cores were tested.

6.6 Discussion of Results and Path Forward

Essentially all findings within this chapter support the notion that US-49 is performing well regardless of the section considered. Further, the performance of recycled sections is comparable to or slightly better than that of the traditionally constructed section after 53 months of service. Differences between the properties of cement-stabilized and emulsion-stabilized cores are distinct when directly measured, but based on distress survey and FWD results, those differences have not yet meaningfully manifested themselves within overall pavement performance as of 53 months in service (note some differences have been observed, such as with Section 5 structural capacity).

Given the current, relatively satisfactory performance of all US-49 sections, discussion focuses primarily on concepts which could be taken from this study and applied to future in-place recycling projects to better the triple-bottom line (i.e. economics, environment, and social well-being). Several of the immediate benefits, such as fewer costs and emissions due to fewer virgin materials needed or shorter construction delays, have already been discussed. However, US-49 results provide evidence that economics and performance, which ultimately affect social wellbeing, can be further optimized.

With regard to economics, Table 6.6 presents US-49 cost information by section. Costs per lane-km were calculated two ways: for only the base layer and for the base layer and HMA overlay. The term base layer refers to cement FDR (Section 1), emulsion CIR (Section 2), crushed stone (Section 3), and cement CIR (Sections 4, 5, and 6).

When comparing only base layers, Table 6.6 shows that emulsion CIR was around twice the cost of cement CIR. Cement FDR was only slightly more cost effective

than emulsion CIR, mainly due to the greater recycling depth. The crushed stone base layer used in Section 3 was nearly 1.5 times the cost of emulsion CIR (both targeted 15 cm depths). As an aside, Table 6.6 illustrates the potential economic benefit of CIR or FDR in general relative to crushed stone bases, specifically for Mississippi where crushed stone materials are typically transported from neighboring states. Regarding CIR, cement CIR demonstrates considerable economic benefits relative to emulsion CIR and would likely be preferred if only economics were considered.

Table 6.6 US-49 Cost Information

		Cost per lane-km	
Section	**Description**	**Base**	**Base & HMA**
1	Cement FDR (41 cm)	$39,000	$114,000
2	Emulsion CIR (15 cm)	$44,000	$119,000
3	Traditional Construction	$62,000	$200,000
4	Cement CIR (23 cm)	$25,000	$99,000
5 or 6	Cement CIR (15 cm)	$22,000	$97,000

-- Costs calculated using bid unit prices for applicable pay items.
-- Emulsion cost = $0.64 per liter ($2.42 per gallon)
-- Hydrated lime cost = $201 per metric ton ($182 per ton)
-- Cement cost = $114 per metric ton ($103 per ton)

Cement stabilization in general was also preferred by MDOT engineers during US-49 construction. MDOT engineers felt that cement was easier to work with than emulsion in that mix designs were easier to obtain, early-age properties were more predictable, and traffic could be returned to the pavement in less time. For example, during a 2012 cement FDR project on State Route 14 in Issaquena County, MS, MDOT allowed traffic on the FDR layer within three hours of compaction (project details: 23 cm recycling depth (18 cm HMA plus 5 cm cement-treated base), 5% cement by volume, 700

AADT, $19,000 per lane-km FDR cost, double chip seal surfaced). These characteristics could be considered to positively impact social well-being.

Pavement performance also impacts social well-being, and recycling techniques which prolong pavement life would have a considerable positive impact on social well-being. Results in this chapter indicate cement FDR and emulsion CIR have slightly outperformed cement CIR sections up to 53 months, and based on core properties, it would not be surprising for the performance gap to increase over time. Cement FDR and emulsion CIR may provide better long-term performance, which justifies higher initial costs within a triple bottom line framework.

Results in this chapter suggest the idea of multiple component CIR binder systems has merit with respect to the triple bottom line. For US-49, emulsion CIR could be said to have sufficient rutting capacity and excess reserve cracking capacity, at a high cost relative to cement CIR. Cement CIR, however, is more economical, perhaps more convenient from a construction perspective, and could be said to have excess reserve rutting capacity but not excess cracking capacity. Utilizing a balanced binder blend of cement and emulsion could better optimize economics and distress capacities, in turn benefiting the triple bottom line. For example, 2.5% emulsion and 2% cement should be better balanced (i.e. adequate rutting resistance, adequate cracking resistance, sufficient constructability, and mid-range economics). To this end, Chapter 7 provides further guidance regarding cost and performance optimization using multiple component binder systems for CIR.

6.7 Conclusions

The objective of this chapter was to present a case study of US-49 which documented construction details, presented performance through the first 53 months in service, and provided discussion on implications of US-49 relating to better meeting the triple bottom line of economics, environment, and social well-being in future in-place recycling projects. US-49 consisted of six sections which were studied herein and can be largely grouped into four categories: traditional construction, cement-stabilized FDR, cement-stabilized CIR, and emulsion-stabilized CIR. Key findings are as follows:

- Pavement distress survey results at 53 months indicate all sections of US-49 are performing satisfactorily. Recycled sections are performing comparably to, or slightly better than, the completely reconstructed section. For specific distresses, slight differences can be observed, particularly between cement stabilization and emulsion stabilization. For example, emulsion CIR exhibited less cracking than cement-stabilized sections. Overall, the cement FDR and emulsion CIR sections are performing the best based on survey results.
- US-49 coring revealed considerable variation underneath the pavement surface. Layers varied considerably (e.g. concrete slabs were sometimes present in the emulsion CIR Section 2 and were sometimes not present). Layer thicknesses varied considerably. Density (or air void) gradients were significant within CIR layers. Despite these factors, US-49 is performing relatively well, which is encouraging.
- Properties of US-49 cores demonstrated distinct differences between cement and emulsion stabilization. Emulsion CIR exhibited greater cracking resistance, while

cement CIR exhibited greater modulus, strength, and rutting resistance. These trends have not yet manifested themselves meaningfully within the overall pavement performance (i.e. distress survey results) but are likely to become more apparent over time.

- FWD data demonstrated that most US-49 sections are structurally sound through 53 months. It did, however, suggest Section 5 (cement CIR) structural capacity is low relative to the rest of US-49. This is potentially an indication of fatigue damage that, relative to other sections, may result in more rapid performance deterioration.
- Cost data and overall performance findings from US-49 suggest the triple bottom line could be positively impacted relative to current CIR practices by exploring more balanced multiple component binder blends (e.g. balanced amounts of cement and emulsion). Generally, single component binder blends often result in excess reserve capacity with respect to one or more distresses while perhaps resulting in insufficient capacity with respect to another distress. Multiple component binder systems could potentially address this issue as well as provide economically-competitive alternatives.

CHAPTER 7

COLD IN-PLACE RECYCLING CHARACTERIZATION FOR SINGLE OR MULTIPLE COMPONENT BINDER SYSTEMS

This chapter has been submitted as a paper to a peer-reviewed journal. At the time of writing of this dissertation, the paper is in peer review.

7.1 Introduction

Cold in-place recycling (CIR) is a pavement rehabilitation technique that has been used for decades. During this time, single component binder (SCB) systems have governed the CIR market. SCB systems, as defined herein, are those with one binder (or two if the secondary binder dosage is 1% or less). Two SCB examples are 4% portland cement or 3% asphalt emulsion with 1% hydrated lime. In contrast, this chapter focuses efforts on multiple component binder (MCB) systems. An MCB example is 2.5% emulsion with 2% cement.

CIR, in general, is of interest with respect to the sustainability triple bottom line, which has been recently promoted by the American Society of Civil Engineers (ASCE) and focuses on economics, environment, and social well-being. While traditional CIR mixtures with SCB systems have demonstrated positive impacts on the triple bottom line (e.g. fewer required virgin materials reduce emissions and costs relative to traditional reconstruction), CIR mixtures with MCB systems exhibit the potential for even greater

triple bottom line impacts. To this end, this chapter aims to contribute to the CIR knowledge base in three key areas (KA):

KA1. Universal Design Framework: Present a CIR specimen preparation, curing, and testing framework which can be universally applied to any mixture irrespective of the bituminous or cementitious stabilization materials. This type of framework is needed for unbiased side-by-side comparisons of various binder types and does not currently exist. Further, this type of framework could offer agencies (e.g. departments of transportation, DOTs) flexibility to continue SCB use or consider MCB use.

KA2. MCB Sustainability Advantages: Provide evidence within a universal design framework that CIR incorporating MCB systems, when conditions warrant, is more likely to positively affect the triple bottom line than almost exclusive reliance on SCB systems, which is the current state of practice. Specifically, MCB systems could optimize economics and performance on a project-by-project basis. For example, Chapter 6 documents a high-traffic CIR project on US-49 in Mississippi where emulsion and cement SCB sections were built. Economic and field performance data indicated emulsion SCB portions were less economical and rut resistant, but more crack resistant, than cement SCB portions. A balanced MCB system is believed to be able to provide adequate cracking and rutting resistance with mid-range economics.

KA3. Extensive SCB and MCB Characterization: Present data for a broad spectrum of SCB and MCB binder blends. Specifically, incremental adjustments in MCB emulsion and cement contents herein provide resolution

regarding MCB trends. In contrast, current literature typically compares limited numbers of binder blends for a given highway's exiting materials.

Data presented in this chapter is the culmination of all previous chapters. For this reason, components of the presented design framework discussed in previous chapters are summarized herein. Chapters prior to this one focused on foundational aspects (e.g. curing protocols) which were applicable to SCB or MCB systems. They stopped short of presenting suitable performance tests for a universal framework or fully characterizing advantages of MCB systems. Both are presented in this chapter.

Literature review was performed on the state of CIR design practice, previous SCB and MCB comparisons, and the cracking characterization tests utilized herein. Thereafter, companion research is presented on the universal design framework. Finally, test results are presented and discussed in the context of the aforementioned key contributions.

7.2 Literature Review

7.2.1 State of Practice

As it relates to a universal design framework (KA1), the state of practice for CIR laboratory design (focusing on DOT requirements) is presented to contrast existing emulsion and cement SCB protocols. Nine emulsion and five cement design methods were reviewed; for cement methods, one CIR and four full-depth reclamation (FDR) methods were reviewed and considered similar for purposes of this discussion.

Methods were summarized collectively by binder type (Table 7.1) since methods were similar for a given binder type. Emulsion designs almost always utilized tests 1 to 3,

frequently utilized test 4, and occasionally utilized tests 5 and 6. The key Table 7.1 observation is that emulsion and cement design methods do not overlap..

Table 7.1 Summary of Existing Mix Design Methods

Mix Design Component	Emulsion Methods	Cement Methods
Mixing & Compaction *MC*	Expected *MC* to be added at the milling head in construction, typically 1.5 to 2.5%, few use Proctor-determined *OMC*	*OMC* determined by Proctor compaction
Compaction	30-gyration Superpave Gyratory Compactor (SGC), some still alternatively allow 75-blow Marshall	Standard or modified Proctor
Curing	Oven curing at 60 °C to constant mass (0.05% mass change in 2 hrs) but within 16 to 48 hrs	Moist curing, generally in sealed bag for 7 days at room temperature
Density	Specimen V_a reported using T209 and T166 (or equivalents) G_{mm} and G_{mb} (T166 submerged mass recorded at 1 min)	Specimen densities not reported
Design Binder Content Selection Tests (most common AASHTO or ASTM specifications are provided) [test criteria in brackets]	1) T245 Marshall stability [5.56 kN min. at 40 °C] 2) T245 retained stability [70% min. at 40 °C after vacuum saturation and 24 hr soak] 3) D7196 raveling test [2% mass loss max.] 4) T322 critical cracking temperature [T_{crit} < LTPP Bind 98% reliability low PG temperature at depth corresponding to top of CIR layer] 5) IDT S_t [276 to 310 kPa min.] 6) Hamburg LWT [5,000 to 15,000 passes to 12.5 mm rut]	1) D1633 unconfined compressive strength (UCS) [2,086 kPa min.; max. ranges from 2,758 to 5,516 kPa]

-- *MC* and *OMC = moisture content and optimum MC*
-- G_{mm} *and* G_{mb} *= maximum and bulk specific gravity*
-- *PG = performance grade*
-- S_t *= IDT tensile strength*
-- V_a *= air voids*
-- T_{crit} *= critical cracking temperature*
-- M_r *= resilient modulus*
-- *LWT = loaded wheel tester*

7.2.2 Multiple Component Binder Systems

This section focuses on MCB investigations found in literature (Table 7.2) as it relates to KA2. Table 7.2 demonstrates the ability of cementitious binders to improve modulus, strength, moisture resistance, and rutting, as well as worsen fatigue and thermal cracking characteristics.

Table 7.2 Multiple Component Binder Review Summary

Reference	RAP/Agg	Binders Studied	Findings
Terrel and Wang (1971)	0/100	7e; 7e with 0.5, 1, 1.5, & 3c	-- Ultimate M_r (triaxial) was increased up to 200% with increasing cement content -- Cement accelerated curing
Schmidt et al. (1973)	0/100	7.5e; 7.5e with 1.3 & 3c	-- Cement increased M_r -- Increasing cement decreased fatigue resistance -- Cement accelerated curing and improved moisture resistance
Head (1974)	0/100	7e; 7e with 1 & 2c	-- 1c increased Marshall stability ~2 to 3 times -- 2c increased Marshall stability ~3 to 4 times
Brown and Needham (2000)	0/100	8e; 8e with 1, 2, 3, & 4c	-- Above 200 initial με, cement decreased fatigue life; below 200 initial με, cement (up to 3%) increased fatigue life -- Cement improved moisture resistance
Zawadzki (2000)	~30/70	3e with 2, 3, & 4c; 4e with 2, 3, & 4c; 5e with 2, 3, & 4c	-- M_r (23 °C) increased considerably with cement and decreased slightly with increasing emulsion; total range was ~7 Gpa (2c5e) to 20 Gpa (4c3e) -- Stability (60 °C) increased with increasing cement and/or decreasing emulsion; total range was ~13 kN (2c5e) to 45 kN (4c3e) -- S_t (23 °C) increased with increasing cement and/or decreasing emulsion; total range was ~400 kPa (2c5e) to 1125 kPa (4c3e)
Thomas et al. (2000)	100/0	1.5e1.5HLS; 10FA	-- T_{crit} values were -27 °C (1.5e1.5HLS) and -12 °C (10FA)
Du and Cross (2006)	100/0	1.5e; 1.5e with 1.5HL & 1.14QL	-- APA rut depths were 6.5 mm (1.5e) versus 4.5 mm (1.5e1.5HL) and 3.8 mm (1.5e1.14QL)
Niazi and Jalili (2009)	80/20	3.5e; 3.5e with 2c, 2HLS, & 2HL	-- M_r increased 175% (2c) and 130% (2HLS, 2HL) from 1190 MPa (3.5e) -- S_t increased 170% (2c), 140% (2HLS), and 100% (2HL) from 245 kPa (3.5e) -- Stability increased 150% (2c) and 140% (2HLS, 2HL) from 8.3 kN (3.5e) -- Cementitious binders greatly increased retained stability and tensile strength ratio -- Wheel-tracking rut depths decreased 60% (2c), 50% (2HLS), and 40% (2HL) from 12.5 mm
Kavussi and Modarres (2010)	100/0	4e; 4e with 1, 2, & 3c	-- Fatigue life increased with increasing cement content below 250 με and decreased with increasing cement content above 250 με

-- RAP/Agg refers to relative amounts of RAP and aggregate utilized (e.g. 0/100 is an aggregate-only mixture, 80/20 is 80% RAP and 20% aggregate).

-- Binder blends identified by number (dosage percentage) and letter (binder type) designations for emulsion (e), cement (c), hydrated lime (HL), hydrated lime slurry (HLS), quick lime (QL), and fly ash (FA). For example, 1.5e1.5HLS is 1.5% emulsion with 1.5% hydrated lime slurry.

-- HLS dosages refer to the effective lime dosage (e.g. 1.5% HLS implies 1.5 grams of lime in dry form per 100 grams of RAP).

A key observation is that MCB behavior has been documented. Most studies primarily considered cement as an additive to emulsion-stabilized mixtures. Efforts focused on improving emulsion's properties with cement as long as effects were not adverse (likely leading to the common practice of 1 or 1.5% (but rarely more) cement or hydrated lime addition to mixtures (Cox and Howard 2013)). Table 7.2 does not fully consider symmetrical comparisons of cementitious and bituminous binders, an area this chapter seeks to address (KA3).

Thomas et al. (2000) states Kansas utilized emulsion CIR for many years, but due to rutting and stripping problems on some projects, the Kansas DOT discontinued emulsion CIR use in 1992 and specified Class C fly ash as the only approved CIR binder. Though fly ash alleviated rutting and stripping, premature cracking problems were encountered.

Mallick et al. (2002) documents an FDR project in Maine where four sections were built with three SCB systems (7% water, 5% cement, and 3.4% emulsion) and one MCB system (3.4% emulsion with 2% hydrated lime). A structural evaluation was conducted one year after construction, and sections were ranked by unit cost (cost per mile) and effective unit cost (cost per mile per 1,000 equivalent single axle load (ESAL) increase in life relative to pre-construction). The emulsion with lime section had the highest unit cost ($45,000 per mile), but it had the lowest effective unit cost ($1.80) (compared to $2.90 for the cement section and $4.00 for the emulsion section) and was recommended for consideration in future recycling projects.

7.2.3 Cracking Characterization

In this chapter, the two distresses of greatest interest to CIR in the context of cementitious and bituminous binders are rutting and cracking. Relative to rutting characterization, CIR cracking characterization has been studied to a lesser extent; therefore, literature was reviewed in search of a suitable test for use in the universal framework presented in this chapter. Key criteria were that the test has shown promise for asphalt concrete testing and that test specimens could be reasonably fabricated for any SCB or MCB system without excessive labor or specimen damage.

Four tests were considered: the single-edge notched beam test (SENB), the disc-shaped compact tension test (DCT), the semi-circular bend test (SCBend), and the instrumented IDT test. SENB was removed since its specimen size was less practical (30 by 5 by 6.5 cm beams). DCT and SCBend were also removed since they required extensive sawing and drilling to produce specimens. Based on previous attempts by the author to saw CIR specimens, sawing is prohibited by some SCB or MCB systems.

Instrumented IDT testing appeared most promising since test specimens could be produced without sawing. The University of Florida has conducted extensive research on IDT cracking tests and was consulted by the author for guidance. The IDT test is relatively simple and produces stress states in the center of the specimen which resemble that of a field pavement (horizontal tension combined with vertical compression), two factors which have led to fairly widespread use of the test (Roque and Buttlar 1992). IDT strength ($S_{t,ult}$) is the most common parameter derived from IDT testing; however, $S_{t,ult}$ alone is not a reliable indicator of cracking performance (Kim and Wen 2002, Marasteanu et al. 2007).

Roque and Buttlar (1992) first proposed the use of gage-point-mounted extensometers for IDT deformation measurements and recommended a 38 mm gage length for 150 mm diameter specimens. Roque and Buttlar (1992) also developed correction factors to account for errors associated with applying 2-D plane stress calculations to 3-D specimens. Kim and Wen (2002) used 3-D finite element analysis to determine errors incorporated with 2-D calculations were approximately 2.5% (the author did not use correction factors for CIR later in this dissertation).

Kim and Wen (2002) observed that neither $S_{t,ult}$ nor horizontal strain at peak stress (ε_{ult}) correlated well to fatigue cracking for WesTrack mixtures. However, fracture energy (FE), defined as the area under an IDT stress-strain curve up to the point of fracture, correlated well with field cracking (Kim and Wen 2002, Zhang et al. 2001). The point of fracture occurs when a specimen's deformation differential curve (vertical minus horizontal deformations) peaks, which should occur prior to the peak load (Koh and Roque 2010, Buttlar et al. 1996, Roque et al. 1997). Koh and Roque (2010) found a one-to-one correlation between FE determined by dog-bone direct tension and IDT tests, supporting FE as a fundamental property independent of specimen geometry and loading mode and rate. Birgisson et al. (2003, 2007) reported asphalt concrete FE values ranging from 0.8 to 1.4 kJ/m^3 and 2.0 to 7.4 kJ/m^3, respectively.

Zhang et al. (2001) and Roque et al. (2002) presented a cracking threshold concept which uses FE to obtain dissipated creep strain energy (DCSE) by subtracting elastic energy (EE) from FE. Figure 7.1 illustrates a typical stress-strain curve (CIR) showing DCSE and EE (calculated using fracture strength, $S_{t,f}$, and resilient modulus, M_r). FE represents the cracking failure threshold for single, critical load applications,

while DCSE, also shown to be a fundamental property, represents the threshold for continuous repeated loading (Zhang et al. 2001).

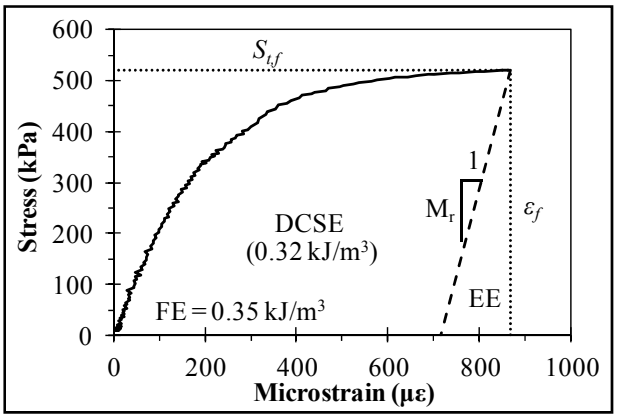

Figure 7.1 IDT Stress-Strain Curve Illustration for CIR

Roque et al. (2004) developed the energy ratio (ER) concept, which is the ratio of a mixture's DCSE to a minimum required DCSE ($DCSE_{min}$). The $DCSE_{min}$ is an empirically-determined value that accounts for a mixture's creep compliance, tensile strength, and pavement structure. Field results indicated ER's greater than 1 coupled with DCSE between 0.75 and 2.5 kJ/m^3 at 10 °C exhibited satisfactory cracking performance.

7.3 Review of Universal Design Framework Components

Work towards components of the universal design method presented in previous chapters is summarized in this section. Together, components presented comprise the mix design approach that was used throughout this chapter.

7.3.1 Moisture in Compaction

Chapter 2 and Chapter 5 evaluated moisture's role during compaction and its effect on compacted density. Motivation for this research was a result of the many documented means for determining mixing and compaction moisture contents (*MC*s). These range from using standardized *MC*s (generally ranging from 2 to 5%) to Marshall methods (i.e. density- and strength-optimized *MC*s) to Proctor moisture-density relationships. These methods yielded *MC*s from less than 1 to 8%. *MC*s greater than 4% (usually Proctor-determined) were of particular interest since water was typically expelled during SGC compaction at these *MC*s, bringing its necessity into question.

Chapter 2 studied specimens compacted at 6 to 10% *MC* and 5 to 150 gyrations. SGC dry densities were indifferent to *MC* between 6 and 10%, and *MC*s were around 6% by 30 gyrations regardless of initial *MC*. A 6% maximum *MC* was recommended. Chapter 5 sought to validate Chapter 2 findings with an MDOT field CIR project where pre-compaction *MC* was 8.2% (Proctor-determined). Directly-measured *MC* immediately after compaction was 5.8%, suggesting trends observed in Chapter 2 are also applicable to field compaction. This was supported by volumetric calculations which showed that, in order to reach the average achieved air voids (V_a) of 15.5%, some moisture must be expelled. Overall, Chapter 5 affirmed the 6% maximum *MC*.

7.3.2 Moisture during Curing

Chapter 5 also addressed moisture as it relates to curing in a universal design protocol since existing curing protocols are considerably different for bituminous and cementitious binders. Bituminous-stabilized mixtures are typically dry oven cured at 60

(most common) or 40 °C while cementitious-stabilized mixtures are usually moist cured at 23 °C. Essentially, a given protocol represents a favorable environment for one binder and an unfavorable for the other, and neither represents curing on an actual field project.

Four curing methods for SCB and MCB mixtures were compared: 40 °C oven at approximately 35 to 50% humidity, 40 °C dry oven, 23 °C moist curing room, and outdoors exposed to sunlight but not rain. *MC*, S_t, FE, and asphalt pavement analyzer (APA) rut depth were evaluated after 1, 3, 7, and 14 days of curing. Outdoor curing (the reference) was reasonably represented by humid oven or dry oven curing but not the moist curing room. Overall, Chapter 5 concluded either humid or dry oven curing are candidates for a universal design method although the humid oven appears to be a more logical choice at present, at least in Mississippi and much of the southeast US where field conditions are humid.

7.3.3 Density and Air Voids

Chapter 4 sought after more reliable maximum and bulk specific gravity (G_{mm} and G_{mb}) measurement for V_a determination. Motivation for doing so stemmed from variability within CIR density measurement methods and reported densities (V_a's from multiple sources ranged from 2 to 23%). The traditional G_{mb} approach (AASHTO T166) was discouraged since most CIR V_a's were above 8 to 9% where T166's 2% water absorption limit is typically exceeded. Alternatively, vacuum sealing (CoreLok®) was used to measure G_{mm} (ASTM D6857) and G_{mb} (T331) in comparison with T209 (Rice gravity) and T269 (dimensional measurement).

For G_{mm}, D6857 was compared to T209 for multiple reclaimed asphalt pavement (RAP) materials. D6857 provided at least as reliable RAP G_{mm} measurements as T209 but with greater efficiency. To provide a convenient means to obtain CIR G_{mm}, Equation 4.3 was developed to estimate CIR G_{mm} using D6857 RAP G_{mm} and known binder dosages and gravities. Estimated and D6857-measured CIR G_{mm}'s correlated well (R^2 of 0.99).

For G_{mb}, wet (since specimens contained some moisture) G_{mb} was measured via T269 and T331 then converted to dry G_{mb} using specimen *MC*. T269 yielded V_a's consistently 1.1% greater on average. T331 was most accurate, but, given the consistent offset, the more cost-effective T269 could also be used. Overall, Chapter 4 recommended CIR G_{mm} be calculated with the estimation equation and D6857-measured RAP G_{mm} and CIR G_{mb} be obtained via T331.

7.3.4 Performance Characterization Tests

Chapter 3 performed an initial assessment of performance tests available for AC and with potential to characterize CIR for a diverse array of binding agents. For example, the predominant tests used in traditional SCB design methods (i.e. unconfined compressive strength (UCS) for cementitious binders and Marshall stability for bituminous binders) only reasonably characterize one binder type, not both. Evaluated tests were the Cantabro durability test, the bending beam rheometer (BBR) flexural stiffness test for mixture beams, wheel tracking with the Hamburg Loaded Wheel Tester (HLWT) and APA, a loaded wheel fatigue test, and an IDT cracking characterization test.

Findings were APA wheel tracking following traditional protocols was informative, and IDT testing (S_t and FE) appeared promising.

Research in Chapters 2 through 5 established key aspects of a universal design framework: mixing and compaction moisture recommendations (6% maximum *MC*), curing recommendations (40 °C at 35 to 50% humidity), a method to measure G_{mm}, G_{mb}, and V_a, and a screening of various performance tests. However, Chapter 2 through 5 did not fully evaluate performance characteristics of SCB and MCB systems. This chapter builds on others by addressing this issue.

7.4 Experimental Program

7.4.1 Materials Tested

Table 7.3 presents properties of asphalt materials tested herein. One RAP material, sampled from US-49 during construction, was utilized in CIR mixtures. RAP was dry sieved into multiple size fractions, and test specimens were batched from these fractions to the as-received bulk gradation.

Multiple asphalt concrete (AC) mixtures were tested to provide a reference data set for CIR data presented herein. Four airfield mixtures were studied in a full-scale comparison of hot mix and warm mix asphalt (HMA and WMA) at the Engineering Research and Development Center (ERDC). Loose mixture was paver-sampled and reheated to compact test specimens. All four mix designs were identical except for WMA technologies and compaction temperatures. Table 7.3 presents one set of properties common to all four mixtures. HMA was compacted at a target temperature of 146 °C, had no warm mix additives, and is further denoted HMA. All other mixtures had a target

compaction temperature of 116 °C and employed the following warm mix technologies that are used hereafter for identification: Sasobit®, Evotherm™, and foam.

Table 7.3 Materials Tested

Material		RAP	AC
Source		US-49	ERDC
Percent Passing	**25.0 mm**	100	100
	19.0 mm	100	100
	12.5 mm	94	96
	9.5 mm	85	85
	4.75 mm	55	68
	2.36 mm	38	54
	1.18 mm	29	38
	0.60 mm	20	28
	0.30 mm	8	15
	0.15 mm	3	7
	0.075 mm	1.5	4.9
Total P_b (%)		5.1	5.3
PG Grade		---	67-22
Continuous Grade		94-14	---
G_{mm}		2.447	2.461
G_{se}		2.642	2.668
$P_{ba,mix}$		1.1	0.8
P_{be}		4.0	4.5
VMA		---	14.3
VFA		---	72
Agg G_{sb}		2.567	2.609
Agg G_{sa}		2.627	2.688
Agg *Abs* (%)		0.8	1.2
Agg *FAA* (%)		41	---

-- AC properties were obtained from the mix design.
-- RAP gradation is for bulk RAP (not extracted aggregate).
-- RAP P_b obtained via AASHTO T308 (ignition oven). No aggregate correction factor was used.
-- RAP PG grade is true grade measured on extracted and recovered asphalt.
-- RAP G_{mm} measured as per Chapter 4.
-- RAP aggregate properties tested on extracted aggregates.
-- Aggregate Bulk and apparent specific gravities (G_{sb} and G_{sa}) and absorption (Abs) determined via ASTM C127 and C128.
-- Fine aggregate angularity (FAA) determined via ASTM C1252 Method C.

Table 7.4 presents the nine CIR binder combinations tested herein. Each is denoted by the dosage of cement (c), emulsion (e), and hydrated lime (HL) present (e.g.

2.5c2e is 2.5% cement with 2% emulsion). The 4.4c and 4e1HL blends were the US-49 CIR design blends and, thus, were the initial SCBs considered. Three cement and three emulsion SCB blends were tested. Emulsion SCBs always included 1% hydrated lime as in the US-49 design. Cement and emulsion were adjusted in 1% increments to produce all other blends. Three cement-emulsion MCB blends were tested to provide a symmetrical progression between US-49 SCB design blends.

Table 7.4 Binder Combinations Tested

	Cement SCB			Cement/Emulsion MCB			Emulsion SCB		
Blend ID	**2.5c**	**3.5c**	**4.4c**	**3.5c1e**	**2.5c2e**	**1.5c3e**	**4e1HL**	**3e1HL**	**2e1HL**
Cement (%)	2.5	3.5	4.4	3.5	2.5	1.5	0	0	0
Emulsion (%)	0	0	0	1	2	3	4	3	2
Hydrated Lime (%)	0	0	0	0	0	0	1	1	1

-- Binders dosed as a percentage of dry RAP mass.
-- Cement is Type I portland cement; emulsion is an engineered emulsion classifying as CSS-1h (63.5% residue).
-- Note 3.5c1e is, by definition, an SCB; however, it was used herein as an MCB for a more symmetrical matrix of MCB binder blends.

7.4.2 Specimen Preparation

7.4.2.1 Compaction

Most CIR specimens were SGC-compacted (150 mm diameter) to 30 gyrations which is the predominant CIR gyration level (e.g. Cross 2003). Slabs (7.5 by 29.3 by 62.4 cm) were also compacted in the Linear Asphalt Compactor (LAC) (Doyle and Howard 2014) with 30 roller passes at a 2930 kPa hydraulic system pressure. Immediately prior to compaction, RAP, mixing water (6% as per Chapter 2), and binders were uniformly mixed at room temperature (emulsion was heated to 60 °C). In all, 279 SGC and 12 LAC specimens were tested. SGC asphalt concrete specimens (150 mm diameter) were

compacted to fixed heights and target air void (V_a) levels. LAC asphalt concrete slabs were compacted 18 passes at a 2413 kPa hydraulic pressure. In all, 288 SGC and 8 LAC asphalt concrete specimens were tested.

7.4.2.2 Curing and Aging

CIR specimens were cured in a 40 °C oven at 35 to 50% relative humidity. Several 4.4c specimens were also traditionally cured (23 °C moist curing room). Multiple cure times were evaluated (3, 7, 14, 28, 56, 90, and 180 days). Half of the SGC-compacted AC specimens were outdoor-aged (exposed to rain and sunlight) for two years in PVC sleeves (i.e. only the top face was exposed to direct sunlight). Aged and un-aged specimens are denoted 2-yr and 0-yr, respectively. LAC slabs were not aged.

7.4.2.3 Air Voids

CIR V_a's were measured as per Chapter 4 protocols discussed previously. *MC*'s for calculating dry G_{mb} were not measured on SGC specimens tested in this chapter since Chapter 5 found that *MC* was very low after 14 days of humid oven curing. Instead, power fits for 4.4c, 2.5c2e, and 4e1HL data from Chapter 5 were developed to estimate *MC* at a given cure time. *MC* for 3.5c1e and 1.5c3e blends was interpolated, and *MC* for SCB blends was taken as the same as 4.4c or 4e1HL *MC*. Estimated *MC*'s ranged from 0.7% (4.4c at 3 days) to 0.1% (4e1HL at 180 days). The 95% confidence intervals for all SGC V_a's were 16.3 to 18.4% (cement SCBs), 13.6 to 17.2% (emulsion SCBs), and 14.9 to 17.7% (MCBs). LAC slab V_a's were determined after 3 days of curing, at which point they were sawn in half for later testing and a 2.5 cm slice was removed from one side to

obtain *MC* for dry G_{mb} calculation. SGC-compacted AC specimens targeted 4.0 to 4.5% or 7.5 to 8.5% V_a via AASHTO T331, which is approximately 4% and 7% V_a via T166. AC V_a levels are hereafter denoted 4% and 7%. LAC slabs targeted 7.5 ± 1% V_a by T331 (approximately 6 to 8% V_a by T166).

7.4.2.4 Instrumentation

Most SGC specimens (CIR and AC) were prepared for IDT instrumentation (Figure 7.2). To attach extensometers, steel gage points were mounted on specimen faces using rapid-set two-part epoxy (38 mm gage length). Preparation of the faces varied between CIR and AC.

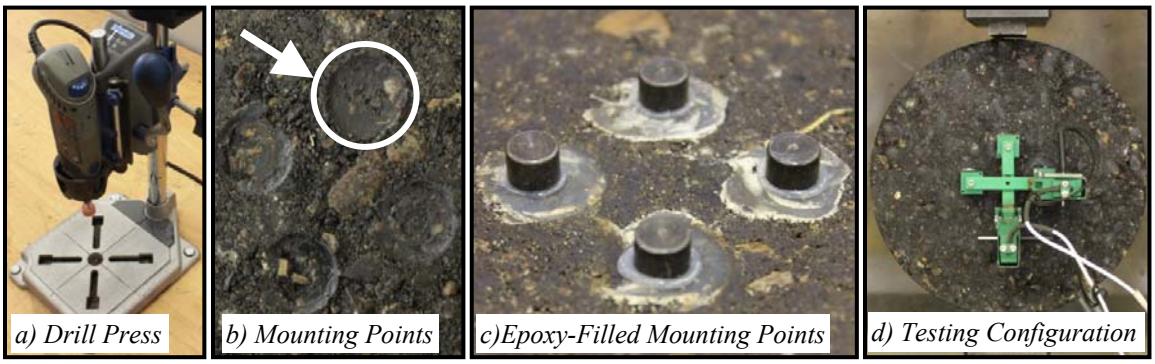

Figure 7.2 Instrumented Specimen Preparation

Instrumented CIR specimens were compacted to a target thickness of 63 mm. AC specimen faces are typically sliced to produce smooth surfaces for gage point mounting. As in Chapter 3, CIR specimens were not sawn; instead, a high-speed drill press (Figure 7.2a) and 16 mm diameter grinding stone attachment were used to polish mounting surfaces (Figure 7.2b). With this method, it was common for gage points to be easily

dislodged due to particles flaking off the surface, especially with cement-dominated blends. Therefore, additional steps were added where epoxy was applied to polished surfaces, spread to lock surface particles in place, and then sanded flush with the grinding stone (Figure 7.2c). This provided a more stable base and decreased the percentage of gage points which had to be re-glued. Though this may affect measurements slightly, overall trends did not appear meaningfully affected.

Instrumented AC specimens were also compacted to 63 mm; however, AC specimens were sliced as usual. AC slicing procedures were identical for all specimens. A 12.5 mm slice was removed from the top of the specimen, and then the test specimen (target thickness of 31 mm) was sliced from the center of the original SGC specimen. Gage points were mounted directly to sliced faces with no intermediate steps such as polishing.

7.4.3 Test Methods

7.4.3.1 Wheel Tracking

APA rut testing was conducted according to T340 (6 hour conditioning, 445 N wheel load, 690 kPa hose pressure, 8,000 cycles) at 64 °C. For CIR, 90-day humid-oven cured specimens were tested; one replicate (one track) was tested per binder blend. Three AC replicates were tested per V_a and aging combination (e.g. 7% V_a, 2 yr).

Wheel tracking was also performed with the PURWheel laboratory wheel tracker (denoted PW) described in Howard et al. (2010). Figure 7.3 shows key PW components. Two independent loaded wheel carriages mounted with pneumatic rubber tires track LAC slabs 20,000 passes (10,000 cycles) per test. Note that some CIR slabs were exposed to

multiple tests (i.e. tracked more than 20,000 passes). Standard PW parameters are 862 kPa tire pressure, 1750 N wheel load, and 33 ± 2 cm/sec wheel speed. Figure 7.3b shows one wheel carriage and its tire print which results in contact pressures of approximately 630 kPa (gross) and 850 kPa (net) at the beginning of a test. The PW collects continuous rut measurements throughout testing.

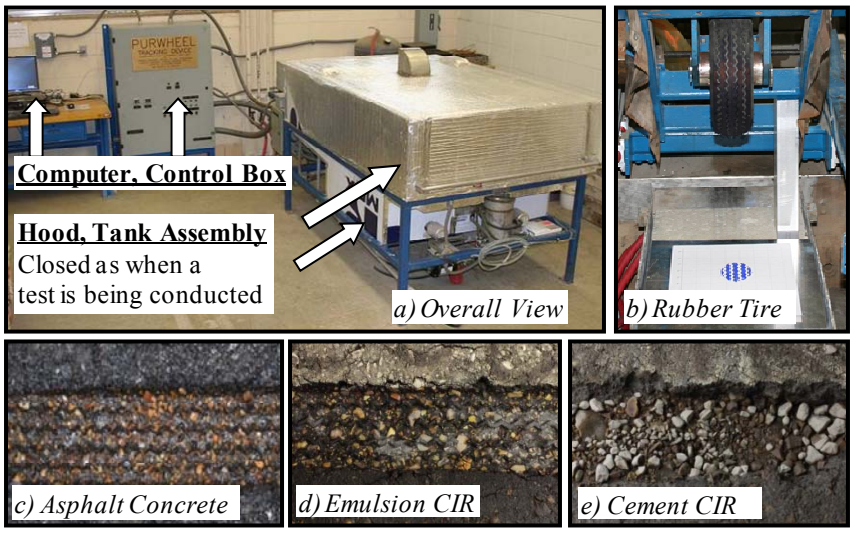

Figure 7.3 PURWheel Laboratory Wheel Tracker

PW testing is conducted at 64 °C (high temperature binder grading requirement for much of the southeast US) and can be conducted dry or submerged in 64 °C water (i.e. wet). Wet tests were conducted herein to evaluate wheel tracking in the presence of moisture. Dry PW testing was not utilized since it correlates reasonably well with the APA (Doyle and Howard 2013).

Figures 7.3c to 7.3e show distresses for various representative mixtures after wet PW testing. The number of passes to 12.5 mm of rutting ($P_{12.5}$) was the primary test result

reported. Note that moisture damage mechanisms likely differ between emulsion CIR and cement CIR. Emulsion CIR damage mechanisms are similar to that of AC (i.e. stripping, mixture shear failure); whereas, cement CIR damage mechanisms are likely more related to pore pressure stresses caused when saturated specimens are loaded.

CIR slabs for PW testing were 90-day humid oven cured as with APA specimens (one 4.4c slab was tested at 28 days as well). Most testing was conducted at the standard PW load (1750 kN); however, 4.4c and 4e1HL testing also included 50% and 80% test loads. Two replicates (one slab sawn into two halves) were tested per binder blend, cure time, and test load. Immediately prior to testing, CIR slab permeability was measured with the MSP-L_L permeameter (Cox et al. 2015b) in multiple locations, and average infiltration (cm/min) was reported. AC slabs were tested according to the standard PW protocol (4 replicates, 1750 kN load).

7.4.3.2 Modulus and Compliance

IDT resilient modulus (M_r) testing and data analysis was performed according to ASTM D7369. Testing was performed in a servo-hydraulic universal testing machine with an environmental chamber (further denoted UTM). Total M_r ($M_{r,total}$) is reported herein and is calculated using total deformations (instantaneous recoverable plus time-dependent recoverable deformations).

D7369 standard test parameters require application of 100 loading cycles (data recorded over the last 5) where each cycle consists of a 0.1 sec haversine load pulse with a 0.9 sec rest at a small contact load ($P_{contact}$). D7369 requires $P_{contact}$ to be 4% of the maximum load (P_{max}) so long as it is between 22 and 89 N. Note that the UTM control

software utilized was not able to meet this criteria as $P_{contact}$ which was pre-programmed to be 10% of P_{max}.

For all mixtures, three replicates were tested to obtain a single M_r value. Specimens were tested along two axes, rotated 90° from each other, and vertical and horizontal deformations were recorded on both faces for a total of 12 M_r values (3 replicates, 2 axes, 2 faces) from which a 10% trimmed average was reported. Tests were conducted at 20, 0, -10, and -20 °C. For CIR, only 14-day humid oven cured specimens were tested at temperatures other than 20 °C.

IDT creep compliance (D(t)) testing was conducted according to AASHTO T322 and analyzed using "LTSTRESS.xls" developed by Christensen (1998) for T322 data analysis. LTSTRESS both reduces raw D(t) data and calculates a thermal stress curve for critical cracking temperature (T_{crit}) determination (i.e. point at which thermal stresses exceed mixture strength). Creep tests were conducted for 1,000 seconds, which is permitted by T322 but is longer than the standard 100 second test. LTSTRESS was developed to analyze 100-second tests and was modified by the author to accommodate 1,000-second tests. Test loads for a mixture were selected to produce horizontal deformations between 1.25 and 19 μm at 1,000 seconds. Replication and test temperatures were identical to M_r testing except only one axis was tested. CIR creep testing was only conducted on 14-day humid oven cured specimens.

7.4.3.3 Strength and Fracture Energy

Instrumented IDT tests were performed at 50 mm/min (20 °C) and 12.5 mm/min (0, -10, -20 °C) according to T322. Ultimate IDT strength ($S_{t,ult}$), fracture IDT strength

($S_{t,f}$), and fracture energy (FE) were calculated from load and deformation measurements. Tests were conducted at 20, 0, -10, and -20 °C, with three replicates (six faces) comprising one test. For the six FE results obtained, probable outliers were removed then the highest and lowest values were trimmed as long as at least three values remained. For example, if two outliers were removed, the two extremes would not be trimmed as this would leave only two values to be averaged.

The author developed an IDT data analysis Excel worksheet in which all results were calculated. The point of fracture for each face was determined using the deformation differential curve (DDC) approach discussed previously. The desired case (defined in T322) is when the DDC is positive and peaks prior to the ultimate load (denoted Case 1). The least desirable case (defined in T322) is when the DDC is never positive, in which case the test is invalid and no result is produced (denoted Case 4).

The author often observed two cases in addition to those defined in T322. First, the DDC peaked after the ultimate load was reached (Case 2). When Case 2 was encountered, the stress-strain curve was truncated at the point of ultimate load. Case 2 was considered undesirable but manageable by the author. The second scenario encountered was slightly more complex. In some cases, strain during loading would increase, peak, and then decrease, as if the extensometer slipped (Case 3). When Case 3 was encountered, unreasonable data was removed, and the stress-strain plot was forecasted to the fracture stress using remaining deformation data. Since Case 3 results were expected to be less reliable, a limitation was put in place that no more than half of the final data values (after outlier removal and trimming of extremes) could be Case 3 values. If that limitation was exceeded, replacement specimens were made and tested.

More in-depth description of FE data analysis can be found in the sponsor report (Cox and Howard 2015a). DCSE and ER were also considered; DCSE trends were similar to FE trends and are omitted for brevity, while ER, as calculated in Roque et al. (2004), was not appropriate for CIR since $DCSE_{min}$ was developed empirically for asphalt concrete.

7.5 Results

7.5.1 Asphalt Concrete

Figure 7.4 plots $M_{r,total}$ results. Additional plots are omitted for brevity, but all results are provided in Table 7.5. Asphalt properties were used to provide a reference data set for comparison to CIR.

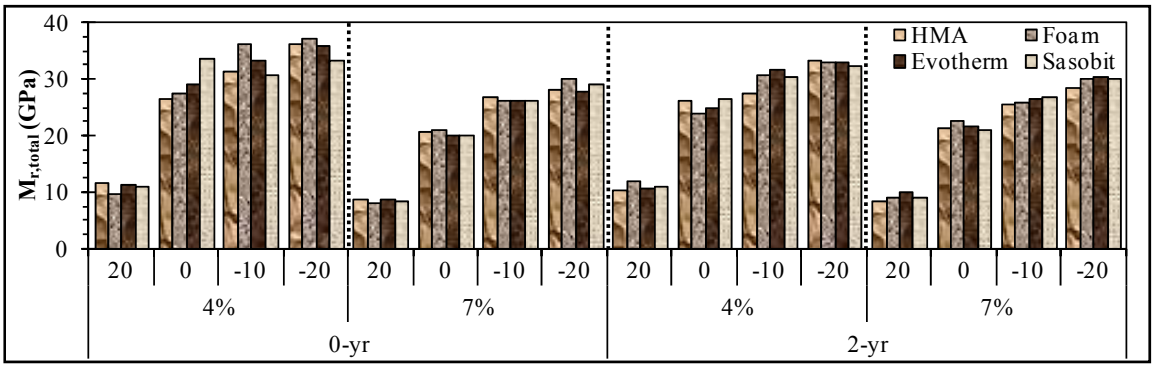

Figure 7.4 Asphalt Concrete Resilient Modulus

Table 7.5 Asphalt Concrete Properties

	HMA				Foam				Evotherm				Sasobit					
	0-yr		2-yr		0-yr		2-yr		0-yr		2-yr		0-yr		2-yr		0-yr	2-yr
Property	**4%**	**7%**	**4%**	**7%**	**4%**	**7%**	**4%**	**7%**	**4%**	**7%**	**4%**	**7%**	**4%**	**7%**	**4%**	**7%**	**Avg**	**Avg**
RD_{APA}	5.3	4.9	6.1	8.4	3.0	5.6	4.7	6.0	6.1	8.8	6.8	8.8	3.9	4.6	3.2	4.7	5.3	6.1
PW $P_{12.5}$	---	7550	---	---	---	5525	---	---	---	5925	---	---	---	7867	---	---	6717	---
$M_{r(20C)}$	11.7	8.9	10.3	8.4	9.7	8.2	11.9	9.1	11.3	8.8	10.7	10.0	11.1	8.5	11.2	9.0	9.8	10.1
$M_{r(0C)}$	26.6	20.7	26.4	21.6	27.6	21.1	24.2	22.9	29.1	20.0	25.1	21.6	33.6	20.2	26.6	21.2	24.9	23.7
$M_{r(-10C)}$	31.6	26.9	27.6	25.6	36.5	26.3	30.7	26.0	33.3	26.3	31.8	26.7	30.8	26.4	30.4	27.0	29.8	28.2
$M_{r(-20C)}$	36.4	28.3	33.5	28.5	37.2	30.3	33.1	30.1	35.9	27.9	33.1	30.3	33.5	29.1	32.4	30.3	32.3	31.4
T_{crit}	-17.4	-19.8	-16.2	-15.5	-15.2	-18.8	-17.1	-15.3	-16.5	-20.9	-17.1	-15.0	-14.4	-16.4	-12.0	-14.5	-17.4	-15.3
$S_{t(20C)}$	1979	1476	1330	1600	1792	1369	1658	1591	1897	1541	1714	1669	1794	1461	1176	1311	1664	1506
$S_{t(0C)}$	3809	2984	4002	2866	3731	2884	4031	2898	3660	3068	4335	2959	3814	2506	3881	2899	3307	3484
$S_{t(-10C)}$	4846	3939	4618	3736	4890	4135	5106	4233	5584	3725	4412	3665	4511	3229	4481	3750	4357	4250
$S_{t(-20C)}$	4917	4216	5264	3232	3653	3756	5228	3750	4890	4495	5575	4341	4585	3142	4449	3538	4207	4422
$FE_{(20C)}$	2.73	3.49	0.88	3.62	4.64	3.83	1.17	2.61	4.61	4.11	1.92	2.13	2.76	1.78	0.35	1.34	3.5	1.8
$FE_{(0C)}$	0.97	1.18	1.29	0.85	1.21	0.85	1.02	0.54	1.12	1.02	1.68	0.80	1.13	0.79	0.89	0.92	1.0	1.0
$FE_{(-10C)}$	0.95	0.68	0.62	0.65	0.86	0.86	0.83	0.96	0.96	0.69	0.54	0.60	0.68	0.47	0.70	0.68	0.8	0.7
$FE_{(-20C)}$	0.56	0.58	0.72	0.31	0.34	0.48	0.82	0.34	0.61	0.77	0.96	0.59	0.48	0.31	0.56	0.37	0.5	0.6

-- RD_{APA} = APA rut depth at 8,000 cycles -- $P_{12.5}$ = passes to 12.5 mm rut -- T_{crit} = critical cracking temp

-- M_r (GPa), S_t (kPa), and FE (kJ/m^3) denoted with subscripts indicating test temperature of 20, 0, -10, or -20 °C

7.5.2 Cold In-Place Recycling

7.5.2.1 Wheel Tracking

Figure 7.5 presents APA, PW, and infiltration results. Cement SCB APA rut depths (RD_{APA}'s), at approximately 1 mm, are practically negligible. RD_{APA} ever so slightly decreases as cement content increases. Chapter 3 cites various RD_{APA} threshold criteria of 4 to 6 and 12 mm for high-traffic and standard- and medium-traffic routes in MS as well as 8 mm. Cement SCB RD_{APA}'s are well below both these thresholds and Table 7.5 AC values. Emulsion SCB RD_{APA}'s fall among Table 7.5 AC values but also among cited thresholds, indicating discretion is warranted regarding emulsion SCB rutting.

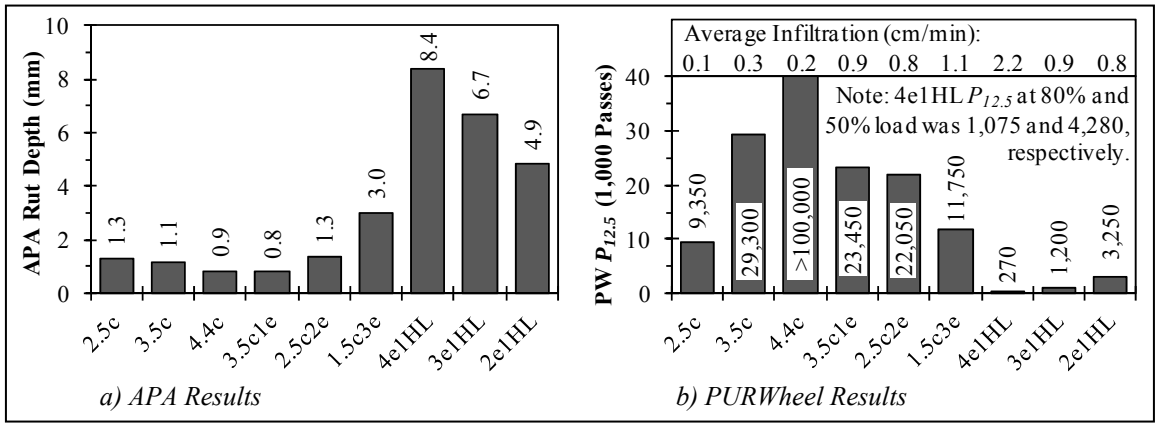

Figure 7.5 Wheel Tracking

MCB results demonstrate an exponential trend from insignificant (4.4c) to considerable (4e1HL) rutting. Relative to 4e1HL, 1.5c3e exhibits a considerable RD_{APA} decrease; 2.5c2e exhibits another noticeable decrease at which point RD_{APA} is similar to all other blends including cement. APA results indicate rutting concerns with emulsion

SCBs are completely eased with cement SCBs or can be comfortably managed with emulsion-dominated MCBs.

PW results are slightly more pronounced than APA results due to the presence of moisture. Table 7.5 AC $P_{12.5}$'s range from approximately 5,500 to 8,000 passes, and all cement SCB $P_{12.5}$'s exceed AC values. The 4.4c blend did not meaningfully degrade through 100,000 passes where testing was eventually terminated ($P_{12.5}$ for 4.4c at 28 days was also >100,000). The 2.5c and 3.5c blends experienced degradation (rather than densification or shear failure). Emulsion SCB $P_{12.5}$'s are well below AC values and decrease with increasing emulsion content. As with the APA, MCBs demonstrate ability to balance wheel tracking performance.

Permeability, as characterized by infiltration (*Inf*), was measured as a durability index. *Inf* ranges from 0.1 to 2.2 cm/min with cement SCB *Inf*'s being distinctly lower than emulsion SCB or MCB *Inf*'s. Cox et al. (2015b) reports average *Inf*'s for field-compacted asphalt concrete ranging from 0.5 to 4.2 cm/min. CIR *Inf* values appear reasonable if not lower than expected given its high V_a's (the LAC may produce relatively sealed slab surfaces). Based on results presented, permeability does not seem to be of greater concern than for typical asphalt concrete.

7.5.2.2 Modulus and Compliance

Figure 7.6a presents M_r results for 14-day humid oven cured specimens, which are generally 20 to 30% of Table 7.5 AC M_r results. Cement SCB M_r, ranging from approximately 3 to 9 GPa, generally increases with cement content and is relatively insensitive to temperature. Emulsion SCB M_r is considerably temperature-dependent. At

20 °C, M_r is approximately 1.8 GPa for all emulsion contents. At lower temperatures, differences between emulsion contents are more apparent. MCB M_r exponentially decreases and becomes increasingly temperature-dependent when progressing from 4.4c to 4e1HL. MCB results illustrate ability to affect M_r; however, 2.5c2e is the only MCB blend that, at 20 °C, yields an M_r which meaningfully balances cement and emulsion SCB M_r's (i.e. 4.4c and 3.5c1e or 1.5c3e and 4e1HL are not practically different).

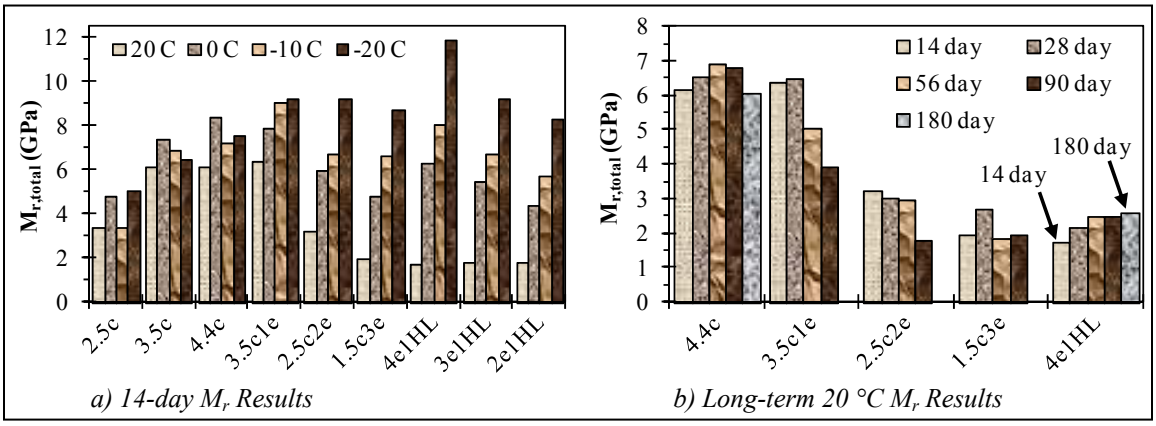

Figure 7.6 Resilient Modulus

Variability was investigated at 20 °C and 14 days of curing for 4.4c, 2.5c2e, and 4e1HL. Five tests (15 specimens) were conducted for each blend yielding between-test coefficients of variation (COVs) of 3.4, 11.7, and 5.7%, respectively. This degree of variability is very manageable for CIR (D7369 within-laboratory repeatability 1s (i.e. COV) is 7% for AC).

Figure 7.6b presents M_r results at 20 °C for 14 to 180 days of humid oven curing. In this case, only 4.4c, 4e1HL, and MCB blends were tested. Aside from 180-day M_r, 4.4c M_r generally increased with time, likely due to cement hydration. Similarly, 4e1HL

M_r increased over time, likely due to a combined effect of emulsion curing at early ages and aging at later ages. M_r for 3.5c1e and 2.5c2e decreases over time. This trend is questionable since cement hydration and emulsion aging would be expected to increase M_r; at present, this behavior is not understood.

Figure 7.7 presents T_{crit} results derived from creep compliance testing. LTSTRESS calculates $S_{t,f}$ for T_{crit} determination as 78% of $S_{t,ult}$, which is based on a relationship presented in NCHRP Report 530 (Christensen and Bonaquist 2004). Figure 7.7 results used the 78% relationship, but results (in brackets) were also calculated using the directly-measured $S_{t,f}$ to $S_{t,ult}$ relationship for CIR, which was 89% on average. Though this shifts T_{crit} results slightly, overall trends are not affected, and results are discussed in terms of LTSTRESS calculated values.

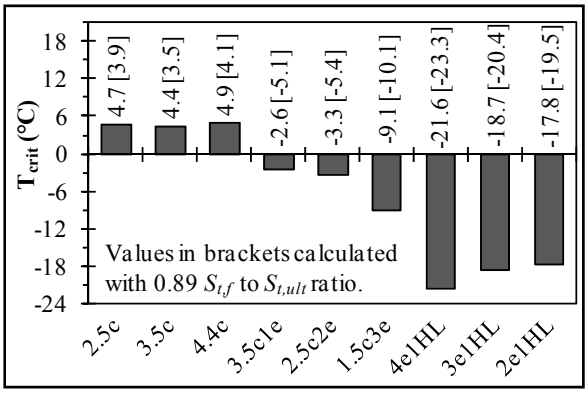

Figure 7.7 Critical Cracking Temperature

At between 4 and 5 °C, cement SCB T_{crit} values are similar for all cement contents. Emulsion SCB T_{crit} values, ranging from -21.6 to -17.8 °C, are considerably lower and vary by emulsion content. MCB T_{crit} values fall in between SCB values and

improve as MCB blends progress from 4.4c to 4e1HL. MCBs demonstrate ability to improve thermal cracking performance relative to cement SCBs, which typically are of greater concern regarding cracking.

7.5.2.3 Strength and Fracture Energy

Figure 7.8a presents $S_{t,ult}$ results for 14-day humid oven cured specimens, which are on average 15 to 25% of Table 7.5 AC $S_{t,ult}$ results depending on temperature. As with M_r, Figure 7.8a results increase as temperature decreases. The low-temperature (0 °C and below) $S_{t,ult}$'s, however, were primarily used for calculation of T_{crit} values discussed in the previous section. When used in mix design methods or for mixture characterization, intermediate-temperature (e.g. 20 °C) $S_{t,ult}$'s are primarily used and are the focus of remaining discussion.

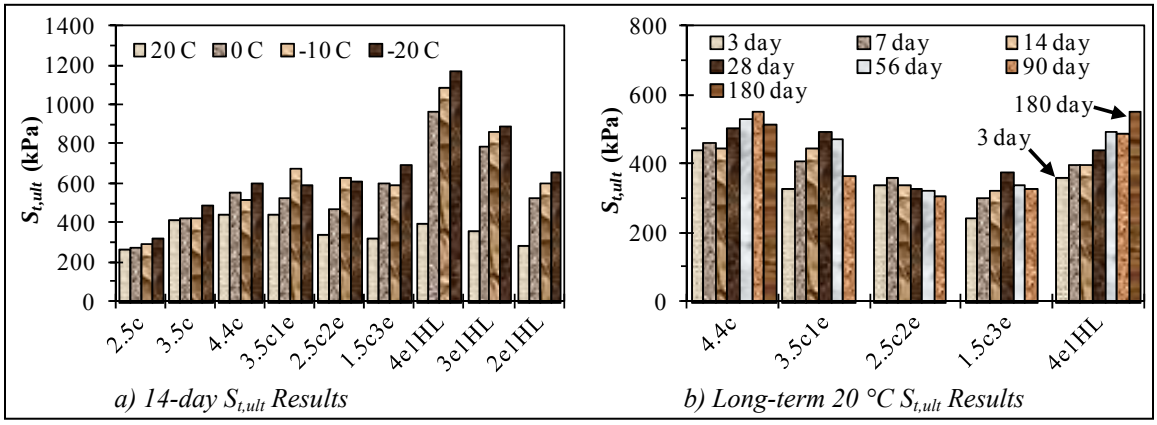

Figure 7.8 Indirect Tensile Strength

For 20 °C results, trends among SCBs and MCBs are less distinct than for other properties (e.g. T_{crit}). Consequently, $S_{t,ult}$'s are alternatively discussed in reference to the

Table 7.1 criteria of 276 to 310 kPa minimum. All binder systems except 2.5c and 2e1HL yield $S_{t,ult}$'s greater than 310 kPa. At 269 and 283 kPa, 2.5c and 2e1HL $S_{t,ult}$'s are concerning but are also reasonable given these blends have the lowest binder dosages. MCB $S_{t,ult}$'s, namely for 2.5c2e and 1.5c3e, are approximately 20% lower than for the US-49 design SCB blends (4.4c and 4e1HL). This result seems counterintuitive and perhaps could be further investigated in future research efforts, but these $S_{t,ult}$'s are slightly above Table 7.1 thresholds nonetheless.

Variability was investigated at 20 °C and 14 days of curing for 4.4c, 2.5c2e, and 4e1HL. Five tests (15 specimens) were conducted for each blend yielding between-test COVs of 5.1, 3.4, and 3.0%, respectively. This degree of variability is very manageable for CIR (at 25 °C, ASTM D6931 suggests a single-laboratory standard deviation of 80 kPa for AC, corresponding to approximately 20% COV in this case).

Figure 7.8b presents $S_{t,ult}$ results at 20 °C for 3 to 180 days of humid oven curing. As with M_r, only 4.4c, 4e1HL, and MCB blends were tested. $S_{t,ult}$ increased over time for both 4.4c and 4e1HL SCBs. Generally, $S_{t,ult}$ over time increased for MCBs with the exception of 2.5c2e.

Figure 7.9a presents FE results for 14-day humid oven cured specimens. Cement SCB FE values are low, ranging from 0.03 to 0.07 kJ/m^3 for all cement contents and temperatures. In contrast, emulsion SCB FE values decrease considerably with temperature and vary by emulsion content. At 20 °C, FE ranges from 0.87 kJ/m^3 with 4e1HL to 0.29 kJ/m^3 with 2e1HL (AC FE values were 2.6 kJ/m^3 on average). Overall, 4e1HL FE values at 20 °C are more than an order of magnitude greater than for 4.4c.

MCB FE values exponentially increase from 4.4c to 4e1HL and also increase in temperature dependence.

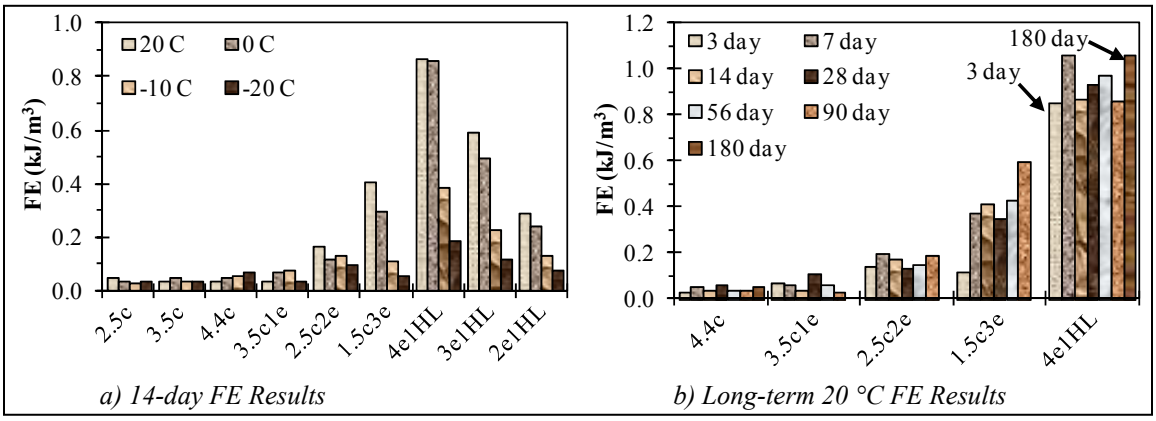

Figure 7.9 Fracture Energy

Variability was investigated at 20 °C and 14 days of curing for 4.4c, 2.5c2e, and 4e1HL. Five tests (15 specimens) were conducted for each blend yielding between-test COVs of 22.0, 26.3, and 8.8%, respectively. Though this variability is greater than for M_r and S_t, it could still be considered manageable for CIR. Figure 7.9b presents FE results at 20 °C for 3 to 180 days of humid oven curing. Overall, FE appears relatively constant over time though some variability is present and the 1.5c3e FE seems to increase.

For the 4.4c blend, a small set of tests were performed on specimens cured in a traditional curing room (CR) for comparison to humid oven (HO) curing. Figure 7.10 presents $S_{t,ult}$ and FE results from 3 to 56 days of curing. At 56 days, CR $S_{t,ult}$ is approximately 1.5 times greater than HO $S_{t,ult}$ and exhibits an increasing trend; whereas, HO strength gain seems relatively constant in comparison. FE results are similar. Figure 7.10 highlights noticeable differences between CR and HO curing. Specifically, it

demonstrates the usefulness of a universal design framework to treat various binder systems identically for direct comparisons. Without a universal framework, direct comparisons of cement SCB and emulsion SCB properties are not possible.

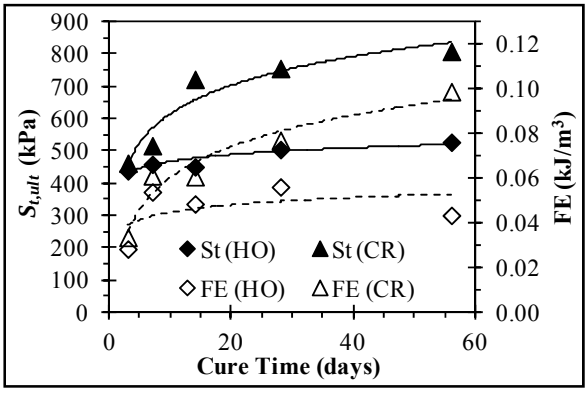

Figure 7.10 Humid Oven versus Curing Room for 4.4c

7.6 Discussion of Results

Perhaps with the exception of $S_{t,ult}$, differences between cement SCB and emulsion SCB systems were distinct for all performance properties presented. Cement SCB systems offered superior wheel tracking performance and higher M_r values, while emulsion SCB systems offered superior critical cracking temperatures and greater FE values. CIR wheel tracking results were comparable to AC results; however, CIR M_r, $S_{t,ult}$, and FE results were considerably lower than AC results. MCB results demonstrated promise in that MCBs were able to bridge the gap between cement and emulsion SCBs and balance rutting and cracking properties.

With regard to the three key contribution areas, the tests evaluated herein were informative within a universal design framework (KA1) in that most tests were able to

differentiate cement and emulsion binders and dosages. APA wheel tracking was insightful, and results were supported by additional, and arguably more severe, PURWheel testing. The APA, being a common test, could be incorporated into agency design methods for rutting characterization with relative ease. M_r and T_{crit} results were informative and could be used in universal design as they already are by some agencies.

Though $S_{t,ult}$ was not greatly informative in terms of distinguishing binder systems, minimum strength requirements could still be useful in a design method. FE results were informative and capable of distinguishing binder blends. Further, T_{crit} and FE results supported each other, which is encouraging. Although FE is less practical for daily mix design operations than the commonly specified Marshall stability, FE data exhibits greater value and can be obtained with little additional effort when T_{crit} testing is required as is currently the case with several agency specifications.

Regarding MCB advantages (KA2), MCBs were able to balance desirable and less desirable traits of SCBs. As supported by the field study of US-49 cement and emulsion SCB sections presented in Chapter 6, SCB systems may result in excess reserve capacity for one distress and no reserve capacity of another. For example, the US-49 cement SCB section exhibits no rutting concerns (greater reserve capacity) but is showing modest cracking distresses at 4.5 years of service (lesser reserve capacity). Based on results herein, MCB systems could offer a more balanced solution to this issue, positively impacting ASCE's triple bottom line. Given the differences in emulsion and cement costs, MCB economic impacts could also be significant.

Figure 7.11 uses FE and APA data from this chapter, as well as cost data from Chapter 6, to illustrate an example mix design plot and evaluate optimization abilities

with MCBs. Note that other results (e.g. T_{crit}) could have been shown with similar implications. Rutting and cracking are best balanced around 1.5c3e (i.e. a small dosage of cement can considerably improve rutting while a larger dosage of emulsion is needed to maintain cracking resistance). This finding alone is not necessarily unique as many agencies already incorporate a small amount of cement or hydrated lime. However, the Figure 7.11 concept is unique with respect to its potential value, partly due to the symmetrical distribution of MCBs tested (KA3). The following paragraph discusses examples in which Figure 7.11 provides flexibility for an agency (KA1).

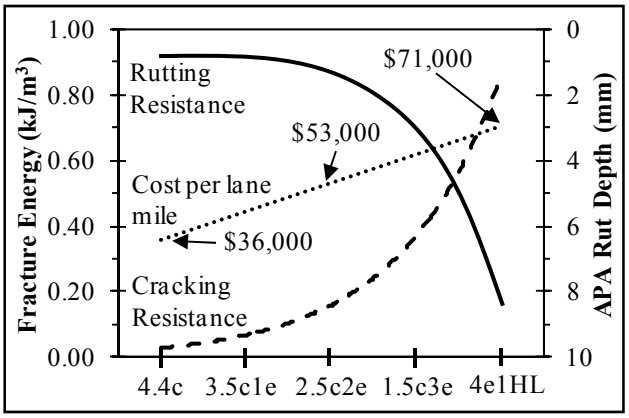

Figure 7.11 CIR Optimization with Multiple Component Binder Systems

Since Figure 7.11 incorporates cracking, rutting, and cost data, multiple parameters can be considered on a project-by-project basis, taking into account route type, traffic level, anticipated surface treatment, and current material costs. In one case, an agency may have many routes in need of repair and might opt for cement-dominated binders so that a fixed budget can repair more lane miles. In another case, an agency may opt for reserve rutting capacity (cement-dominated) and tolerate more cracking so that a

chip seal surface can be used without major rutting concerns since it is typically a greater safety concern than cracking. Lastly, for a lightly-trafficked route where rutting distresses would take longer to develop, an agency may elect to spend more for reserve cracking capacity (emulsion-dominated) in hopes of a longer service life.

In all cases, Figure 7.11 could likely be used to make more informative decisions. Additionally, agencies could continue using current design blends (e.g. emulsion SCB) but would also have the flexibility to explore other options if desired. Lastly, the Figure 7.11 approach could prevent repeat occurrences such as the one documented by Thomas et al. (2000) in Kansas and would more effectively promote a fair and competitive bidding process. Rather than having to predetermine binder type in order to specify a design method, agencies could establish and specify performance criteria and allow bidders to bid any binder combination, SCB or MCB, they choose as long as it satisfies the criteria. This would be conceptually similar to some agencies allowing hot and warm mix asphalt to be bid interchangeably.

7.7 Conclusions

A major goal of this chapter was to present a universal design framework for CIR that is indifferent to binder type and can accommodate cementitious and bituminous binder types either individually (SCB) or collectively (MCB). By studying a broad range of cement SCB, emulsion SCB, and cement-emulsion MCB systems, this chapter demonstrated potential advantages of MCB systems. Key findings from this chapter are as follows:

- A universal CIR design framework is capable of providing direct comparisons between cement and emulsion SCB systems and accommodating MCB systems, offering increased flexibility to agencies.
- The framework presented entails SGC compaction (30 gyrations) of CIR materials at 6% *MC* followed by curing in a 40 °C oven at 35 to 50% humidity for an established cure time (14 days was the predominant cure time herein). Specimen V_a is determined by the vacuum sealing method (both G_{mm} and G_{mb}), which is capable of interfacing with construction. Design binder blends are determined based on several parameters: rutting, cracking, and cost.
- For SCB systems, cement blends offered low cracking resistance, high rutting resistance, and lower costs. Emulsion blends yielded the opposite. Both were similar regarding $S_{t,ult}$.
- For MCB systems, rutting, cracking, and cost can be balanced by proportioning cementitious and bituminous binders, which can positively impact the triple bottom line. Overall, the 1.5c3e blend, while not the most economical blend tested, appeared to offer the best balance between rutting and cracking.

CHAPTER 8

CONCLUSIONS AND RECOMMENDATIONS

8.1 Conclusions

The overall goal of this dissertation was to present: 1) a universal design framework for CIR which is capable of considering SCB and MCB systems; and 2) a detailed characterization of SCB and MCB systems. Throughout the dissertation, other conclusions were made which could be useful in other manners related to CIR. Key conclusions are as follows:

- Though Proctor compaction resulted in high *OMC*s (from 6 to 10%), SGC compaction was indifferent to *MC* in this range. More than 6% *MC* added no value in terms of SGC density gain. Proctor compaction does not appear as informative for CIR as for other materials such as soil.
- Field moisture data, alongside volumetric analysis, validated laboratory moisture findings in that more than 6% *MC* did not benefit field compaction. Excess moisture will likely be expelled rather than aid compaction.
- SGC compaction at 30 gyrations produced laboratory-compacted V_a's which were reasonable in comparison to those measured on US-49 field cores.
- Mississippi summer outdoor curing conditions seem to be reasonably represented by humid oven curing (40 °C and 35 to 50% humidity) or dry oven curing (40 °C) based on work to date.

- CIR practices could benefit from using G_{mm}, rather than Proctor $\gamma_{d,max}$, as a reference density. For CIR with 100% RAP, ASTM D6857 vacuum sealing G_{mm} can be determined as reliably as with AASHTO T209 but with greater ease.
- CIR G_{mm} can be directly measured on loose mixtures (as opposed to compacted then broken up mixtures), which is likely the most reliable approach; however, it can also be reasonably and efficiently estimated using Equation 4.3.
- CIR G_{mb} measured with AASHTO T331 is the most accurate approach. AASHTO T269 G_{mb}'s consistently yield V_a's that are 1.1% greater on average, which can be reasonably accounted for in the event T269 is used.
- Cantabro, BBR, and HLWT tests were not practical for CIR across SCB and MCB systems. Loaded wheel fatigue testing was resource intensive and produced only modest results. APA and instrumented IDT testing were informative.
- US-49 exhibits considerable layer thickness and density variability but is performing well overall at approximately 4.5 years of age. The distress survey, core properties, and FWD results collectively indicate cement SCB sections are more crack susceptible while emulsion SCB sections are more rut prone. Coupled with US-49 cost data, findings suggest MCBs are worth considering.
- The universal design framework presented in this dissertation is likely to offer increased flexibility to agencies during bidding, designing, and building.
- Cement SCBs yielded low cracking resistance, high rutting resistance, and lower costs. Emulsion SCBs yielded the opposite.
- MCBs demonstrated ability to balance rutting, cracking, and economics. Overall, 1.5c3e provided the best balance between rutting and cracking.

8.2 Recommendations

In the US-49 case study, the emulsion SCB blend was approximately double the cost of the cement SCB blend; however, cement SCB sections exhibited more extensive cracking and potential fatigue-related structural concerns. Based on these findings, MCB consideration for future CIR projects is warranted since MCB systems demonstrated the ability to balance rutting, cracking, and economics, directly addressing several key concerns with US-49.

The following list describes key components recommended from this study for a universal design framework that would accommodate MCBs while also allowing SCB usage to continue in manners similar to current practice:

- Mixing and Compaction *MC*: Overall, rather than devoting testing efforts to *OMC* determination attempts, a fixed *MC* no greater than 6% is recommended, allowing testing efforts to focus on binder blend selection. It is believed that *MC*'s lower than 6% (e.g. 4 to 5%) may also be adequate but should first be evaluated across several SCB and MCB systems since they were not studied herein.
- Compaction: SGC compaction at 30 gyrations is recommended.
- Curing: Humid oven curing (40 °C and 35 to 50% humidity) is recommended as it reasonably represented outdoor curing. A 14-day cure time was predominantly used in this study, though it did not yield greatly different properties from 7-day curing. Either 7-day or 14-day curing appear to be reasonable options.
- Density Measurement: Three recommendations are provided to calculate V_a. First, measure RAP G_{mm} using D6857 vacuum sealing. Second, calculate CIR G_{mm} using Equation 4.3. Third, measure CIR G_{mb} using T331 vacuum sealing.

- Binder Blend Selection: Determine a design blend based on several parameters; rutting, cracking, and cost (e.g. Figure 7.11) are parameters recommended from this study. This approach would offer considerable flexibility as it provides the user with data necessary to make informed decisions on a project-by-project basis. Of the tests evaluated in this study, APA rut depth and IDT FE are recommended for rutting and cracking characterization (it is likely that other informative characterization tests also exist and could be considered). This study did not evaluate thresholds for characterization tests; threshold criteria could be an avenue for future research studies. Full scale test section should be constructed with MCB systems and monitored over time to establish characterization test thresholds.

REFERENCES

AASHTO (1993). *Guide for Design of Pavement Structures*, Washington, D.C.

AI (2001). *Superpave Mix Design: Superpave Series No. 2 (SP-2)*. 3rd Edition. Asphalt Institute, Lexington, KY.

Aschenbrener, T. (1995). "Evaluation of the Hamburg Wheel-Tracking Device to Predict Moisture Damage in Hot Mix Asphalt," *Transportation Research Record: Journal of the Transportation Research Board*, 1492, pp 193-201.

Bang, S., Lein, W., Comes, B., Nehl, L., Anderson, J., Kraft, P., deStigter, M., Leibrock, C., Roberts, L., Sebaaly, P., Huft, D. (2011). *Quality Base Material Produced Using Full Depth Reclamation on Existing Asphalt Pavement Structure – Task 4: Development of FDR Mix Design Guide*. Final Report FHWA-HIF-12-015. U.S. Department of Transportation, Washington, D.C.

Berthelot, C., Haichert, R., Podborochynski, D., Wandzura, C., Taylor, B., Guenther, D. (2010). "Cement Stabilization of Reclaimed Asphalt Pavement Materials," CD-ROM, *Transportation Research Board 89th Annual Meeting*, Washington, D.C. Paper 10-1803.

Birgisson, B., Montepara, A., Romeo, E., Roque, R., Roncella, R., Tebaldi, G. (2007). "Determination of Fundamental Tensile Failure Limits of Mixtures," *Journal of the Association of Asphalt Paving Technologists*, 76, pp 303-344.

Birgisson, B., Soranakom, C., Napier, J.A.L., Roque, R. (2003). "Simulation of Fracture Initiation in Hot-Mix Asphalt Mixtures," *Transportation Research Record: Journal of the Transportation Research Board*, 1849, pp 183-190.

Braham, A., Howard, I.L., Barham, J., Cox, B.C. (2014). "Characterizing Emulsion Effects on Aged Asphalt Concrete Surfaces Using Bending Beam Rheometer Mixture Beams," *International Journal of Pavement Engineering*, 16(7), pp 620-631.

Brown, E.R., Kandhal, P.S., Zhang, J. (2001). *Performance Testing for Hot Mix Asphalt*. NCAT Report 01-05, National Center for Asphalt Technology, Auburn, AL.

Brown, S.F., Needham, D. (2000). "A Study of Cement Modified Bitumen Emulsion Mixtures." *Journal of the Association of Asphalt Paving Technologists*, 69, pp 92-121.

Buchanan, M.S., White, T.D., Smith, B.J. (2004). *Use of the Asphalt Pavement Analyzer to Study In-Service Asphalt Mixture Performance*. Report No. FHWA/MS-DOT-RD-04-155, Mississippi Department of Transportation, Jackson, MS.

Buttlar, W.G., Roque, R., Kim, N. (1996). "Accurate Asphalt Mixture Tensile Strength," *Proceedings of the 4th Materials Engineering Conference: Materials for a New Millennium*, Washington, D.C., pp 163-172.

Carter, A., Feisthauer, B., Lacroix, D., Perraton, D. (2010). "Comparison of Cold In-Place Recycling and Full-Depth Reclamation Materials," CD-ROM, *Transportation Research Board 89th Annual Meeting*, Washington, D.C., Paper 10-1325.

Chan, P., Tighe, S.L., Chan, S. (2010). "Exploring Sustainable Pavement Rehabilitation: Cold In-Place Recycling with Expanded Asphalt Mix," CD-ROM. *Transportation Research Board 89th Annual Meeting*, Washington, D.C., Paper 10-1542.

Chen, D.H. (2007). "Field and Lab Investigations of Prematurely Cracking Pavements." *Journal of Performance of Constructed Facilities*, 21(4), pp 293-301.

Chen, D.H., Hong, F., Zhou, F. (2011). "Premature Cracking from Cement-Treated Based and Treatment to Mitigate Its Effect." *Journal of Performance of Constructed Facilities*, 25(2), pp 113-120.

Christensen, D. (1998). "Analysis of Creep Data from Indirect Tension Test on Asphalt Concrete." *Journal of the Association of Asphalt Paving Technologists*, 67, pp 458-492.

Christensen, D.W., Bonaquist, R.F. (2004). *Evaluation of Indirect Tensile Test (IDT) Procedures for Low-Temperature Performance of Hot Mix Asphalt*. NCHRP Report 530.

Cox, B.C., Howard, I.L. (2013). *Cold In-Place Recycling and Full-Depth Reclamation Literature Review*. White Paper Number CMRC WP-13-1, Construction Materials Research Center, Mississippi State University, Starkville, MS. http://www.cee.msstate.edu/downloads/(2013)CoxandHoward-CMRCWP13-1-LitReviewofCIRandFDR.pdf

Cox, B.C., Howard, I.L. (2014). "Vacuum Sealing Based Volumetric Density Measurement Approach for Cold In-Place Recycling," *Transportation Research Record: Journal of the Transportation Research Board*, 2444, pp 11-19.

Cox, B.C., Howard, I.L. (2015a). *Cold In-Place Recycling Characterization Framework and Design Guidance for Single or Multiple Component Binder Systems*. Draft Final Report No. FHWA/MS-DOT-RD-15-250-Volume 2, Mississippi Department of Transportation, Jackson, MS, Anticipated Submission 2015. (In Preparation)

Cox, B.C., Howard, I.L. (2015b). "Merits of Asphalt Concrete Durability and Performance Tests When Applied to Cold In-Place Recycling," *Proceedings of IFCEE 2015* (GSP 256), San Antonio, TX, 2015, pp 369-379.

Cox, B.C., Howard, I.L., Battey, R. (2015a). "In-Place Recycling Moisture-Density Relationships for High-Traffic Applications," *Proceedings of IFCEE 2015* (GSP 256), San Antonio, TX, pp 349-358.

Cox, B.C., Howard, I.L., and Ivy, J. (2015b). "Evaluation of Approaches to Improve Longitudinal Joints in Mississippi Overlay Projects." Report FHWA/MS-DOT-RD-15-250-Volume 3, Mississippi Department of Transportation, In Sponsor Review.

Cross, S.A (2002). *Determination of N_{design} for CIR Mixtures Using the Superpave Gyratory Compactor*. Final Report FHWA Agreement No. DTFH61-98-X-00095, RMRC Research Project 15, Federal Highway Administration, Washington D.C.

Cross, S.A. (2003). "Determination of Superpave® Gyratory Compactor Design Compactive Effort for Cold In-Place Recycled Mixtures," *Transportation Research Record: Journal of the Transportation Research Board, No. 1819*, pp 152-160.

Doyle, J.D., Howard, I.L. (2011). "Evaluation of the Cantabro Durability Test for Dense Graded Asphalt," *Geotechnical Special Publication No. 211*, pp 4563-4572.

Doyle, J.D., Howard. I.L. (2013). "Rutting and Moisture Damage Resistance of High RAP Warm Mixed Asphalt: Loaded Wheel Tracking vs. Conventional Methods," *Road Materials and Pavement Design*, Special Issue from 88th Association of Asphalt Paving Technologists' Annual Meeting, 14(S2), pp 148-172.

Doyle, J.D., Howard, I.L. (2013). "Thermal Cracking Potential of High RAP-WMA Evaluated with Bending Beam Rheometer Mixture Beam Test," *Journal of Testing and Evaluation*, 41(2), pp 236-246.

Doyle, J.D., Howard, I.L. (2014). "Characterizing Dense-Graded Asphalt Concrete with the Cantabro Test," *Transportation Research Board 93rd Annual Meeting*, Washington, D.C., Paper 14-4013.

Doyle, J.D., Howard, I.L. (2014). *Linear Asphalt Compactor Operator's Manual*. Manual Number CMRC M 10-1, Version 2, Construction Materials Research Center, Mississippi State University, Starkville, MS.

Doyle, J.D., Howard, I.L., Robinson, W.J. (2012). "Prediction of Absorbed, Inert, and Effective Bituminous Quantities in Reclaimed Asphalt Pavement," *Journal of Materials in Civil Engineering*, 24(1), pp 102-112.

Du, J., Cross, S.A. (2006). "Rut Depth Prediction Model for Cold In-Place Recycled Mixtures by Gray System," *Transportation Research Board 85th Annual Meeting*, Washington, D.C., Paper 06-0281.

Du, J.C., Cross, S.A. (2007). "Cold In-Place Recycling Pavement Rutting Prediction Model Using Grey Modeling Method," *Construction and Building Materials.* 21(5), pp 921-927.

Feldman, R.F. (1972). "Density and Porosity Studies of Hydrated Portland Cement," *Cement Technology*, 3(1), pp 5-13.

FHWA. *Cold In-place Recycling (CIR) Survey Summary*. Office of Asset Management, Pavement, and Construction. Federal Highway Administration. https://www.fhwa.dot.gov/Pavement/recycling/cir/cir01.cfm. Accessed July 18, 2013.

Hansen, J. (2015). "Good Roads, Healthy America," *Asphalt Pavement Magazine*, 20(4), pp 47-51.

Head, R.W. (1974). "An Informal Report of Cold Mix Research Using Emulsified Asphalt as a Binder," *Journal of the Association of Asphalt Paving Technologists*, 43, pp 110-131.

Howard, I.L., Cox, B.C. (2016). "Multi-Year Laboratory and Field Performance Assessment of High-Traffic US Highway 49 Full-Depth Reclamation," *Submitted to the 95th Annual Meeting of the Transportation Research Board*, Paper 16-6963.

Howard, I.L., Doyle, J.D. (2014). "Investigating the Consistency of Asphalt Density Measurement Methods Over a Wide Range of Air Voids," *Journal of Testing and Evaluation*, 42(3), pp 1-12.

Howard, I. L., Doyle, J. D., Barham, J. M. (2012). "Uniformity, Repeatability, and Permanent Deformation Resistance of Slabs Produced with the Linear Asphalt Compactor," *Advances in Civil Engineering Materials*, 1(1), pp 1-17.

Howard, I.L., Doyle, J.D., Cox, B.C. (2013). "Merits of Reclaimed Asphalt Pavement-Dominated Warm Mixed Flexible Pavement Base Layers," *Road Materials and Pavement Design*, Special Issue from 88th Association of Asphalt Paving Technologists' Annual Meeting, 14(S2), pp 106-128.

Howard, I.L., Doyle, J.D., White, T.D., Ivy, J., Booth, O. (2010). *PURWheel Laboratory Wheel Tracker Operator's Manual*. Manual Number CMRC M 10-2, Version 1, Construction Materials Research Center, Mississippi State University, Starkville, MS.

Howard, I.L., Warren, K.A. (2009). "Finite Element Modeling of Instrumented Flexible Pavements under Stationary Transient Loading," *Journal of Transportation Engineering*, 135(2), pp 53-61.

Kandhal, P.S., Koehler, W.C. (1987). "Cold Recycling of Asphalt Pavements on Low-Volume Roads," *Transportation Research Record: Journal of the Transportation Research Board*, 1106, pp 156-163.

Kavussi, A., Modarres, A. (2010). "Laboratory Fatigue Models for Recycled Mixes with Bitumen Emulsion and Cement," *Construction and Building Materials*, 24, pp 1920-1927.

Kim, Y., Lee, H. (2006). "Development of Mix Design Procedure for Cold In-Place Recycling with Foamed Asphalt," *Journal of Materials in Civil Engineering*, 18(1), pp 116-124.

Kim, Y., Lee, H. (2008). "Influence of Reclaimed Asphalt Pavement Temperature on Mix Design Process of Cold In-Place Recycling Using Foamed Asphalt," CD-ROM, *Transportation Research Board 87th Annual Meeting*, Washington, D.C., Paper 08-3028.

Kim, Y., Lee, H. (2011). "Influence of Reclaimed Asphalt Pavement Temperature on Mix Design Process of Cold In-Place Recycling Using Foamed Asphalt," *Journal of Materials in Civil Engineering*, 23(7), pp 961-968.

Kim, Y., Lee, H. (2011). "Measurements of Moisture Conditions of Cold In-place Recycling Layer," CD-ROM, *Transportation Research Board 90th Annual Meeting*, Washington, D.C., Paper 11-3129.

Kim, Y., Lee, H., Heitzman, M. (2007). "Validation of New Mix Design Procedure for Cold In-Place Recycling with Foamed Asphalt," *Journal of Materials in Civil Engineering*, 19(11), pp 1000-1010.

Kim, Y., Lee, H., Heitzman, M. (2008). "Laboratory Evaluation of Cold In-place Recycling Mixtures using Foamed Asphalt Based on Dynamic Modulus and Repeated Dynamic Load Tests," CD-ROM, *Transportation Research Board 87th Annual Meeting*, Washington, D.C., Paper 08-2300.

Kim, Y., Lee, H., Heitzman, M. (2009). "Dynamic Modulus and Repeated Load Tests of Cold In-Place Recycling Mixtures Using Foamed Asphalt," *Journal of Materials in Civil Engineering*, 21(6), pp 279-285.

Kim, J., Lee, H.D., Jahren, C.T., Heitzman, M., Chen, D. (2010). "Long-Term Field Performance of Cold In-Place Recycled Roads in Iowa," *Journal of Performance of Constructed Facilities*, 24(3), pp 265-274.

Kim, Y., Im, S., Lee, H. (2011). "Impacts of Curing Time and Moisture Content on Engineering Properties of Cold In-Place Recycling Mixtures using Foamed or Emulsified Asphalt," *Journal of Materials in Civil Engineering*, 23(5), pp 542-553.

Kim, Y., and Wen, H. (2002) "Fracture Energy from Indirect Tension Testing," *Journal of the Association of Asphalt Paving Technologists*, 71, pp 779-793.

Kizito, F., Campbell, C.S., Campbell, G.S., Cobos, D.R., Teare, B.L., Carter, B., Hopmans, J.W., (2008). "Frequency, Electrical Conductivity and Temperature Analysis of a Low-Cost Capacitance Soil Moisture Sensor," *Journal of Hydrology*, 352, pp 367-378.

Khosla, N.P., Bienvenu, M.E. (1996). *Design and Evaluation of Cold In-Place Recycled Pavements*. Report No. FHWA/NC/97-006. North Carolina Department of Transportation, Raleigh, NC.

Koh, C., Roque, R. (2010). "Use of Nonuniform Stress-State Tests to Determine Fracture Energy of Asphalt Mixtures Accurately," *Transportation Research Record: Journal of the Transportation Research Board*, 2181, pp 55-66.

Lee, K.W., Brayton, T.E., Gress, D., Harrington, J. (2001). "A Performance-Based Mix-Design Method for Cold In-Place Recycling of Bituminous Pavements for Maintenance Management," *Proceedings of the 9th Maintenance Management Conference*, 23, pp 11-19.

Lee, H., Kim, Y. (2003). *Development of a Mix Design Process for Cold-In-Place Rehabilitation Using Foamed Asphalt*. Final Report for TR-474 Phase I, Iowa Department of Transportation, Ames, IA.

Lee, H., Kim Y., Hwang S. (2009). "Is 1.5% Moisture Content a Necessary Condition Before Overlaying the CIR Layer?" CD-ROM, *Proceedings of the 6th International Conference on Maintenance and Rehabilitation of Pavements and Technological Control*, Turin, Italy.

Leng, Z. (2011). *Prediction of In-Situ Asphalt Mixture Density Using Ground Penetrating Radar: Theoretical Development and Field Verification*. PhD Dissertation, University of Illinois at Urbana-Champaign, Urbana, Illinois.

Lewis, D.E., Jared, D.M., Torres, H., Matthews, M. (2006). "Georgia's Use of Cement-Stabilized Reclaimed Base in Full-Depth Reclamation," *Transportation Research Record: Journal of the Transportation Research Board*, 1952, pp 125-133.

Mallick, R.B., Bonner, D.S., Bradbury, R.L., Andrews, J.O., Kandhal, P.S., Kearney, E.J. (2002). "Evaluation of Performance of Full-Depth Reclamation Mixes." *Transportation Research Record: Journal of the Transportation Research Board*, 1809, pp 199-208.

Mallick, R.B., Kandhal, P.S., Brown, E.R., Bradbury, R.L., Kearney, E.J. (2002). *Development of a Rational and Practical Mix Design System for Full Depth Reclaimed (FDR) Mixes.* Final Report for Subcontract No. 00-373. The Recycled Materials Resource Center, Univ. of New Hampshire, Durham, NH.

Mamlouk, M.S. (1991). *Low-Volume Road Rehabilitation Strategies*. Report No. FHWA-AZ-91-840, Arizona Department of Transportation, Phoenix, AZ.

Mamlouk, M.S., Ayoub, N.F. (1983). "Evaluation of Long-Term Behavior of Cold Recycled Asphalt Mixture," *Transportation Research Record: Journal of the Transportation Research Board,* 911, pp 64-66.

Marasteanu, M.O., Velasquez, R., Falchetto, A.C., Zofka, A. (2009). *Development of a Simple Test to Determine the Low Temperature Creep Compliance of Asphalt Mixtures*. Final Report, Highway IDEA Project 133, Transportation Research Board, Washington, D.C.

Marasteanu, M., Zofka, A., Turos, M., Li, X., Velasquez, R., Li, X., Buttlar, W., Paulino, G., Braham, A., Dave, E., Ojo, J., Bahia, H., Williams, C., Bausano, J., Gallistel, A., McGraw, J. (2007). *Investigation of Low Temperature Cracking in Asphalt Pavements*. Report No. NM/RC 2007-43, Minnesota Department of Transportation, St. Paul, MN.

Martinez, A.H., Miró, R., Pérez-Jiménez, F. (2007). "Spanish Experience with Gyratory Compactor and Indirect Tensile Test in Design and Control of Cold Recycled Asphalt Pavement," *Transportation Research Record: Journal of the Transportation Research Board,* 2001, pp 163-168.

Miller, J.S., Bellinger, W.Y. (2003). *Distress Identification Manual for the Long-Term Pavement Performance Program (Fourth Revised Edition)*. Report No. FHWA-RD-03-031, Federal Highway Administration, McLean, VA.

Modarres, A., Nejad, F.M., Kavussi, A., Hassani, A., Shabanzadeh, E. (2011). "A Parametric Study on the Laboratory Fatigue Characteristics of Recycled Mixes," *Construction and Building Materials*, 25, pp 2085-2093.

Niazi, Y., Jalili, M. (2009). "Effect of Portland Cement and Lime Additives on Properties of Cold In-Place Recycled Mixtures with Emulsion," *Construction and Building Materials*, 23, pp 1338-1343.

Noureldin, S., Zhu, K., Harris, D., Li, S. (2005). *Non-Destructive Estimation of Pavement Thickness, Structural Number, and Subgrade Resilience Along INDOT Highways*. Report No. FHWA/IN/JTRP-2004/35, Indiana Department of Transportation, Indianapolis, IN.

Rajagopal, A., Crago, D. (2007). *A Comparative Evaluation of the CoreLok Device in Determining Reliable Bulk Specific Gravity and Maximum Specific Gravity Test Results*. Final Report FHWA/OH-2007/07, Columbus, OH.

Rand, D.A. (2006). *Hamburg Wheel Test*. Technical Advisory Dated August 16, 2006, Texas Department of Transportation Construction and Bridge Division.

Roque, R., Birgisson, B., Drakos, C., Dietrich, B. (2004). "Development and Field Evaluation of Energy-Based Criteria for Top-Down Cracking Performance of Hot Mix Asphalt," *Journal of the Association of Asphalt Paving Technologists*, 73, pp 229-260.

Roque, R., Birgisson, B., Sangpetngam, B., Zhang, Z. (2002). "Hot Mix Asphalt Fracture Mechanics: A Fundamental Crack Growth Law for Asphalt Mixtures," *Journal of the Association of Asphalt Paving Technologists*, 71, pp 816-827.

Roque, R., Buttlar, W.G. (1992). "The Development of a Measurement and Analysis System to Accurately Determine Asphalt Concrete Properties Using the Indirect Tensile Mode," *Journal of the Association of Asphalt Paving Technologists*, 61, pp 304-332.

Roque, R., Buttlar, W.G., Ruth, B.E., Tia, M., Dickson, S.W., Reid, B. (1997). *Evaluation of SHRP Indirect Tension Tester to Mitigate Cracking in Asphalt Pavements and Overlays*. Report No. B-9885, Florida Department of Transportation, Tallahassee, FL.

Salomon, A., Newcomb, D.E. (2000). *Cold In-Place Recycling Literature Review and Preliminary Mixture Design Procedure*. Final Report No. MN/RC-2000-21, Minnesota Department of Transportation, St. Paul, MN.

Santagata, E., Chiapinelli, G., Riviera, P.P., Baglieri, O. (2010). "Triaxial Testing for the Short-Term Evaluation of Cold-Recycled Bituminous Mixtures," *Road Materials and Pavement Design*, 11(1), pp 123-147.

Schmidt, R.J., Santucci, L.E., Coyne, L.D. (1973). "Performance Characteristics of Cement-Modified Asphalt Emulsion Mixtures," *Journal of the Association of Asphalt Paving Technologists*, 42, pp 300-319.

Schwartz, C.W., Khosravifar, S. (2013). *Design and Evaluation of Foamed Asphalt Base Materials*. Publication No. MD-13-SP909B4E. Maryland State Highway Administration, Baltimore, MD.

Shahin, M.Y. (2006). *Pavement Management for Airports, Roads, and Parking Lots*. 2nd ed., Springer, New York.

Sholar, G.A., Page, G.C., Musselman, J.A., Upshaw, P.B., Moseley, H.L. (2005). "Investigation of the CoreLok for Maximum, Aggregate, and Bulk Specific Gravity Tests," *Transportation Research Record: Journal of the Transportation Research Board*, 1907, pp 135-144.

Skok, G., Dai, S., Westover, T., Lukanen, E., Labuz, J. (2008). *Pavement Rehabilitation Selection*. Report No. MN/RC 2008-06. Minnesota Department of Transportation, St. Paul, MN.

Smith, C.R., Lewis, D.E., Turner, J., Jared, D.M. (2008). "Georgia's Use of Lime in Full-Depth Reclamation," *Transportation Research Record: Journal of the Transportation Research Board*, 2059, pp 89-94.

Strickland, M.J. (2010). *Construction monitoring of full-depth reclamation in madison count for MDOT Project No. NH-008-03(032)*. Report Number FHWA/MS-DOT-FDR, Mississippi Department of Transportation, Jackson, MS.

Stroup-Gardiner, M. (2011). *Recycling and Reclamation of Asphalt Pavements Using In-Place Methods: A Synthesis of Highway Practice*. NCHRP Synthesis 421, Transportation Research Board, Washington, D.C.

Terrel, R.L., and Wang, C.K. (1971). "Early Curing Behavior of Cement Modified Asphalt Emulsion Mixtures," *Journal of the Association of Asphalt Paving Technologists*, 40, pp 108-125.

Thomas, T., Kadrmas, A., Huffman, J. (2000). "Cold In-Place Recycling on US-283 in Kansas," *Transportation Research Record: Journal of the Transportation Research Board*, 1723, pp 53-56.

TRB Superpave Committee (2005). *Superior Performing Asphalt Pavement: Performance by Design*. Final Report of the Transportation Research Board of the National Academies, Washington, D.C.

Watson, D.E., Cooley Jr., L.A., Moore, K.A., Williams, K. (2004). "Laboratory Performance Testing of Open-Graded Friction Course Mixtures," *Transportation Research Record: Journal of the Transportation Research Board, No. 1891*, pp 40-47.

Woods, A., Kim, Y., Lee, H. (2012). "Determining Timing of Overlay on Cold In-Place Recycling Layer: Development of New Tool Based on Moisture Loss Index and In-Situ Stiffness," *Transportation Research Record: Journal of the Transportation Research Board*, 2306, pp 52-61.

Zawadzki, J. (2000). "Some Properties of the Mineral-Portland Cement-Emulsion Mix." *Proceedings of the 2nd Eurasphalt & Eurobitume Congress*, Barcelona, Spain, pp 678-685.

Zhang, Z., Roque R., Birgisson B., Sangpetngam B. (2001). "Identification and Verification of a Suitable Crack Growth Law," *Journal of the Association of Asphalt Paving Technologists,* 70, pp 206-241.

Zhang, Z., Wu, Z., Matinez, M., Gaspard, K. (2008). "Pavement Structures Damage Caused by Hurricane Katrina Flooding," *Journal of Geotechnical and Geoenvironmental Engineering*, 134(5), pp 633-643.

Zofka, A., Marasteanu, M., Li, X., Clyne, T., McGraw, J. (2005). "Simple Method to Obtain Asphalt Binders Low Temperature Properties from Asphalt Mixtures Properties," *Journal of the Association of Asphalt Paving Technologists*, 74, pp 255-282.